

POLITECNICO DI TORINO

Tesi di Laurea Magistrale in Ingegneria Biomedica

**Hydrodynamic characterization of a cystoperitoneal
shunt for the treatment of the arachnoid cyst**



Relatori: Prof. Umberto Morbiducci
Prof. Alberto Audenino
Ing. Davide Negro

Candidata: Chiara Sardone

Luglio 2019

Abstract

Arachnoid cysts are benign and usually asymptomatic cerebral lesions, that originate from an altered separation of the arachnoid membrane or, with lower incidence, develop after head injuries, tumors, meningitis.

Symptoms depend on their size and location and if they are not promptly treated, the arachnoid cysts could cause an excessive accumulation of CSF (event known as *hydrocephalus*) and provoke the ventricles expansion, the brain compression and an abnormal increase of ICP.

The arachnoid cysts can be detected through MRI or CT and can be treated through several procedures, including the surgical placement of a *shunting system*.

It is a passive derivation device that exploits the pressure difference ΔP between a cerebral CSF-filled compartment and a drainage site – for the cystoperitoneal shunt system, the arachnoid cyst and the peritoneal cavity respectively. It drains CSF in one direction and allows to reduce the resulting ICP increase.

Shunting systems are life-saving device but are negatively characterized by a high failure rate (40% of shunts fail within the first 2 years after the implantation and 98% within 10 years, according to scientific evidences), high morbidity rate, difficulty of diagnosing failure and limited control options. In fact, a shunt system does not include any type of feedback system that permits to control its functioning or to monitor important parameters like CSF's flow or the ICP's level, from the outside in a non-invasive way, excepting the telemetric device Miethke Sensor Reservoir. The shunt malfunctions are generally not detected before they manifest clinically and they are life-threatening, if not promptly discovered and treated.

Currently, shunt design has undergone few variations since their introduction in 1950s, thus a more technological and interactive shunting system would be necessary to improve the life quality of a shunted patient and to overcome the current device constraints. For several years researchers propose to develop a *smart shunt*, that could provide an advanced control, diagnostics and communication through sensors implanted within the brain, feedback systems and telemetry. However, there are no public evidence to date that a smart shunt has been developed and completely realized, thus it still remains a conceptual idea.

This thesis work was born as research of the state of the art of the shunting devices (from a collaboration between Polytechnic of Turin and the Pediatric Neurosurgery Department at Regina Margherita Hospital in Turin), with the aim to know the advantages and limitations of the device when it is used in the clinical practice.

Initially we wanted to find a solution to improve the device functioning and to implement a mechanical feedback system (without electronic components) in order

to monitor the ICP level developing in the brain or to understand if the device was working properly.

Before designing any type of feedback system, we decided to verify the functionality of a shunting device type, the Miethke proGAV 2.0 shunt system in order to highlight some possible engineering criticalities. Through the construction of a test rig and performing non-destructive tests, the device in horizontal position has been hydrodynamically characterized.

In horizontal position, the functioning range of the device, limited to the only opening pressure value of the adjustable DP unit equal to 0 cmH₂O, has been obtained in terms of flow-pressure curve. A peristaltic pump supplied flow-rates between 10.44 and 50 $\frac{ml}{hr}$ and the resulting pressure drop across the valve has been detected through two pressure sensors. Pressure signals have been filtered in order to remove the high frequency noise and the mains interference at 50 Hz.

The resulting flow-pressure curve, containing the mean, maximum and minimum differential pressure values, is comparable with the qualitative functioning range of the device provided by the manufacturer and curve trend is reflected in literature; testing the shunt valve in this orientation did not highlight any problems about its functionality.

Instead testing the device in vertical position has proved to be a challenge; reference was made to the testing procedures reported by a scientific article in literature in order to understand the functioning of the gravitational unit. Qualitative tests have been performed through a simplified test rig; the shunting device has undergone specific differential pressures from 0 to 80 cmH₂O to simulate the high CSF's flow conditions that occur when patient moves from a supine to an upright position because of gravity. The corresponding amount of fluid for each differential pressure applied has been measured. The resulting pressure-flow curves describe the dependence of the device, that in this position is governed by the gravitational unit, on the applied differential pressure.

Additionally, the device behavior has been evaluated both by changing the geodetic height of the reservoir upstream the device and by changing the geodetic height of the drainage reservoir, in order to generate different inflow and outflow pressures, respectively. It has been noted that device closes only when very negative inflow pressure were generated, confirming its role in a physiological condition, or when no siphoning effect was generated.

For future works an improved test bench, that does not influence testing device, should be designed in order to obtain a reliable functioning range of the valve in vertical position; in addition, exploiting the novel in vitro-test bench, the shunting system could be characterized, horizontally and vertically, at different opening pressure values of the adjustable DP unit (from 0 to 20 cmH₂O) or the single units could be divided and separately tested.

Contents

List of Figures	V
List of Tables	IX
1 The Arachnoid Cyst	1
1.1 General introduction about the arachnoid cyst	1
1.2 The arachnoid cysts treatments	4
2 Shunting system for the arachnoid cyst treatment	7
2.1 General description of the device	7
2.2 The <i>Codman Hakim Shunt</i> , a programmable differential pressure valve	14
2.2.1 The Codman Hakim Shunt programming	15
2.2.2 The Codman Hakim Shunt configurations	18
2.3 The <i>Miethke proGAV 2.0 Adjustable Shunt System</i>	21
2.3.1 The ProGAV 2.0 Adjustment	25
2.4 Problems and constraints of the shunting systems	29
2.5 The <i>Smart Shunt</i> concept	32
3 Intracranial Pressure Sensors	37
3.1 The Intracranial Pressure	37
3.2 The standard ICP measurement techniques	40
3.2.1 Invasive ICP measurement techniques	40
3.2.2 Non-invasive ICP measurement techniques	45
3.2.3 Telemetric Sensors	48
3.3 Some examples of alternative proposals of ICP measurement systems in literature	54
3.3.1 Intracranial Pressure Sensor	54
3.3.2 The Baric Probe	59
3.3.3 The snap valve cerebral shunt design	64
4 Evaluation of the hydrodynamic properties of the shunt system	69
4.1 The test method for determining pressure and flow characteristics .	70
4.1.1 Test Rig	70

4.2	Experimental tests of the shunting system in a horizontal position	81
4.2.1	Analysis of the pressure signals	86
4.3	Qualitative tests of the shunting system in vertical position	93
5	Discussions	101
6	Conclusions and Future Works	117
A	Numerical results of the shunting system test in a horizontal position	121
	References	133

List of Figures

1.1	Difference between a normal subject and a subject affected by hydrocephalus, with enlarged brain ventricles	2
1.2	MR image of an arachnoid cyst developed in the suprasellar region	3
2.1	Configuration of an implanted shunt system	8
2.2	Siphon resistive devices to prevent the overdrainage event due to the postural change	10
2.3	Two examples of shunt valve design: the spring ball and the diaphragm mechanism	12
2.4	List of the main fixed-pressure and flow-regulated valves commercially available and their features	13
2.5	List of the main programmable-pressure valves commercially available and their features	13
2.6	Design of the Codman Hakim valve	14
2.7	The inner mechanism of the Codman Hakim Shunt valve from the side view	15
2.8	The Codman Hakim Shunt equipment.	16
2.9	The radiographic elements positioned on the Codman Hakim Shunt that permit clinician to qualitatively determine the valve opening pressure	16
2.10	The X-ray image of the Codman Hakim Shunt	17
2.11	The eight configurations of the Codman Hakim Shunt	18
2.12	The Siphon-guard mechanism as a stand-alone unit or in line with the programmable DP valve	19
2.13	An inner view of the Codman Hakim Shunt with the Siphonguard mechanism	20
2.14	The Miethke ProGAV 2.0 Adjustable Shunt System design	21
2.15	The Miethke ProGav 2.0 Shunt System configuration	22
2.16	Functioning of the ProGAV 2.0 Shunt System when patient is lying down	23
2.17	Functioning of the fixed gravitational unit when patient moves in upright position	24

2.18	The ProGAV Tool set for the adjustment of the valve opening pressure	25
2.19	The radiographic visualization of the adjustable DP unit	27
2.20	The radiographic visualization of the fixed gravitational unit	28
2.21	The Smart Shunt concept	33
3.1	The Intracranial Pressure-Volume relationship.	38
3.2	Access points in the intracranial cavity for invasive ICP measurement techniques	40
3.3	The Raumedic Neurovent p-tel telemetric sensor for ICP monitoring.	49
3.4	X-ray image that shows the implantable probe P-tel on the left hemisphere of a shunted patient.	50
3.5	The Sensor Reservoir telemetric sensor for ICP monitoring.	51
3.6	Cross section of the Sensor Reservoir implantable unit.	52
3.7	Prototype of the intracranial pressure sensor	55
3.8	Some fabrication steps of the ICP sensor prototype	56
3.9	The linear relation between the pressure variations in mmHg and the distance of the fluid-air interface	57
3.10	The position of the fluid-air interface when pressure assumes the smallest value, 0 mmHg, and the greater value 22,5 mmHg regarding the pressure range tested	58
3.11	Prototype of the “baric probe”, a long-term implantable ICP monitoring device	59
3.12	Drawings of the baric probe design and functioning	60
3.13	The ultrasonographic image of the baric probe at different pressure levels obtained by modifying the height of the H ₂ O column	61
3.14	The graphic relation between change in pressure (ΔP in cmH ₂ O) and the change in position of the air-fluid interface (ΔL in mm)	62
3.15	The graphic relation between ICP (ΔP in cmH ₂ O) and the position of the air-fluid interface (ΔL in mm) after two weeks in situ	63
3.16	The valve snap design and its different configurations in response to the ICP or testing pressure levels	64
3.17	Schematic demonstration of the functioning and of the dynamic permeability of the STB device	65
3.18	The linear relationship between mass flow rate (in $\frac{g}{min}$) through a dome, characterized by 0.5 mm of thickness and 10 mm of radius, and pressure (in cmH ₂ O)	66
3.19	Ultrasound imaging of the STB valve achieved with a transducer marked with “T”	67
4.1	Test rig for testing the shunting device in a horizontal position	71
4.2	Schematic functioning of a peristaltic pump with a pump head (rotor) characterized by two rollers	72

4.3	The strain gage pressure transducer	76
4.4	Example of the Wheastone-bridge whit one strain gage activated[37]	77
4.5	The testing device, the Miethke ProGAV 2.0 Adjustable shunt system	80
4.6	Electronic Balance specifications supplied by the manufacturer . . .	80
4.7	Examples of pressure signals detected without the damping system	82
4.8	Graphs of pressure signals detected with the damping system in the test rig, for a flow-rate $Q=50 \frac{ml}{h}$	83
4.9	Example of a test rig, proposed by the Standard ISO 7197:1997, for determining the functioning range of a shunting device	84
4.10	Spectral analysis of the pressure signals detected upstream (P_1) and downstream (P_2) the shunt system at a flow-rate $Q= 50 \frac{ml}{h}$	88
4.11	Comparison between the original pressure signal (P_1) detected upstream the valve and the filtered pressure signal	89
4.12	Comparison between the original pressure signal(P_2) detected downstream the valve and the filtered pressure signal	89
4.13	Comparison between the original differential pressure signal $\Delta P = P_2 - P_1$ and the filtered differential pressure signal	90
4.14	Functioning range of the Miethke ProGAV 2.0 Adjustable Shunt System	92
4.15	Error bar representing the final mean pressure values and the standard deviation calculated for each flow-rate	92
4.16	Schematic drawing of the experimental set-up for testing the shunting device in a vertical position	94
4.17	Pressure-flowrate curves of the shunting system in vertical position, obtained at four different levels of outflow pressure	98
5.1	Pressures involved in the shunting system functioning when patient is in a recumbent position	103
5.2	Comparison between the functioning range obtained after the hydrodynamical characterization of the shunting system in horizontal position and the functioning range provided by the manufacturer within the device data-sheet	106
5.3	Least-squares line with the original differential pressure mean values from the functioning range	107
5.4	Graph of the total fluid dynamic resistance offered by the valve to fluid flow, against the flow-rate	108
5.5	Graph shows all the resistance calculated from differential pressure mean values and flow-rate values	109
5.6	Pressures involved in the shunting system functioning when patient is in an upright position	112

5.7	Comparison between the pressure-flow curves trend obtained by the reference article and the qualitative pressure-flow curves trend obtained by testing the device in vertical position	115
6.1	Schematic draw of a test bench to consider in future works, in order to improve the hydrodynamic characterization of the shunting device both in horizontal and vertical position.	118
A.1	Graph of the functioning range of the ProGav 2.0 Shunt System for the first testing day	123
A.2	Graph representing the differential pressure mean values and the corresponding standard deviations, calculated for each flow-rate, for the first day	123
A.3	Graph of the functioning range of the ProGav 2.0 Shunt System for the second day	125
A.4	Graph representing the differential pressure mean values and the corresponding standard deviations, calculated for each flow-rate, for the second day	126
A.5	Graph of the functioning range of the ProGav 2.0 Shunt System for the third day	128
A.6	Graph representing the differential pressure mean values and the corresponding standard deviations, calculated for each flow-rate, for the third day	128
A.7	Graph of the functioning range of the ProGav 2.0 Shunt System for the fourth day	130
A.8	Graph representing the differential pressure mean values and the corresponding standard deviations, calculated for each flow-rate, for the fourth day	131

List of Tables

2.1	Example of shunt devices depending on the positioning and pathway of their catheters	9
2.2	Different types of the ProGAV 2.0 gravitational unit and their features to identify the valve opening pressure through a X-ray image .	28
4.1	Features of the pressure sensors used in the test apparatus	77
4.2	Pressure Transducers specifications supplied by the manufacturer .	78
4.3	Differential Pressure data (P_2-P_1) for the final flow-rate/pressure curve, determining the functioning range of the shunting device . .	91
4.4	Qualitative data of the tests executed placing the shunting system is in a vertical position	97
4.5	“Semaphore test” to evaluate the open and closed configuration of the valve in vertical position, when different outflow pressures have been generated while maintaining the source reservoir at the same level of the device	99
4.6	“Semaphore test” to evaluate the open and closed configuration of the valve in vertical position, when different inflow pressures have been generated while maintaining the drainage reservoir at the same level of the device (even if this condition is not physiological)	99
A.1	Pressure mean values and standard deviations of the differential pressure signals detected at decreasing flow-rates ($\downarrow Q$) and increasing flow-rates ($\uparrow Q$) for each cycle respectively, during the first day . . .	121
A.2	The maximum and the minimum pressure values of the differential pressure signals detected at decreasing flow-rates ($\downarrow Q$) and increasing flow-rates ($\uparrow Q$) for each cycle respectively, during the first day	122
A.3	Average and standard deviation of the mean values of the differential pressure for evaluating the functioning range of the shunt device, for the first day	122
A.4	Pressure mean values and standard deviations of the differential pressure signals detected at decreasing flow-rates ($\downarrow Q$) and increasing flow-rates ($\uparrow Q$) for each cycle respectively, during the second day .	124

A.5	The maximum and the minimum pressure values of the differential pressure signals detected at decreasing flow-rates ($\downarrow Q$) and increasing flow-rates ($\uparrow Q$) for each cycle respectively, during the second day	124
A.6	Average and standard deviation of the mean values of the differential pressure for evaluating the functioning range of the shunt device, for second day	125
A.7	Pressure mean values and standard deviations of the differential pressure signals detected at decreasing flow-rates ($\downarrow Q$) and increasing flow-rates ($\uparrow Q$) for each cycle respectively, during the third day . .	126
A.8	The maximum and the minimum pressure values of the differential pressure signals detected at decreasing flow-rates ($\downarrow Q$) and increasing flow-rates ($\uparrow Q$) for each cycle respectively, during the third day	127
A.9	Average and standard deviation of the mean values of the differential pressure for evaluating the functioning range of the shunt device, for the third day	127
A.10	Pressure mean values and standard deviations of the differential pressure signals detected at decreasing flow-rates ($\downarrow Q$) and increasing flow-rates ($\uparrow Q$) for each cycle respectively, during the fourth day .	129
A.11	The maximum and the minimum pressure values of the differential pressure signals detected at decreasing flow-rates ($\downarrow Q$) and increasing flow-rates ($\uparrow Q$) for each cycle respectively, during the fourth day	129
A.12	Average and standard deviation of the mean values of the differential pressure for evaluating the functioning range of the shunt device, for the fourth day	130

Chapter 1

The Arachnoid Cyst

1.1 General introduction about the arachnoid cyst

Arachnoid cysts are benign and asymptomatic lesions that occur within the central nervous system, in particular in the intracranial space or in the spinal cord.

Nowadays arachnoid cysts are often discovered incidentally in the first few decades of life thanks to a more widespread use of imaging techniques like ultrasound, computed tomography (CT) and magnetic resonance (MR) by the clinicians [1].

They can be classified as primary cysts or secondary cysts: the primary arachnoid cysts are congenital anomalies that originate from an altered separation of the arachnoid membrane¹ and they reveal at birth and arise during the early weeks of gestation. The secondary arachnoid cysts instead are not as common as the primary cysts and they develop as a result of head injury, meningitis, tumors, or as a complication of a brain surgery [2].

Arachnoid cysts comprise 1% of all intracranial space-occupying lesions. The prevalence in adults is approximately 1.4% with a female preponderance, while the prevalence in children is 2.6% [3, p. 1].

The signs and symptoms of these intracranial lesions vary according to their size, large or small, and location, over the sylvian fissure (lateral sulcus), over

¹The *arachnoid mater* is one of the three meninges that covers and protects the brain and the spinal cord; it specifically is the intermediate membrane between the more superficial and much thicker *dura mater* and the deeper *pia mater*, from which it is separated by the subarachnoid space.

the cerebral convexity, within the lateral or fourth ventricle, in the middle cranial fossa, in the inter-hemispheric region, in the suprasellar region, around the optic nerve, the quadrigeminal plate, or the cerebellopontine angle, over the cerebellar hemisphere etc. [4].

Arachnoid cysts commonly remain stable in size and asymptomatic or occasionally regress and disappear entirely [3, p. 1]. The larger cysts can cause compression of the neurovascular structures leading neurological symptoms; so they are treated by a surgical approach. The smaller cysts are instead asymptomatic and they require a passive observation and follow up. The symptoms are several; the most common are: headache, dizziness, nausea, vomiting, ataxia, hearing loss, alterations in behavior, mental status changes, seizures.

Because of an altered separation of the arachnoid mater, some fluid-filled sacs develop; these sacs, whose wall is made of flattened arachnoid cells, include the Cerebrospinal Fluid (CSF). It is a clear, colorless body fluid produced by the specialized ependymal cells in the choroid plexuses of the brain ventricles and drained through the arachnoid granulations. CSF protects the human brain from physical injuries, keeps its tissue moist and transport the products of metabolism; its physiological flow-rate is approximately $20 \frac{ml}{h}$.

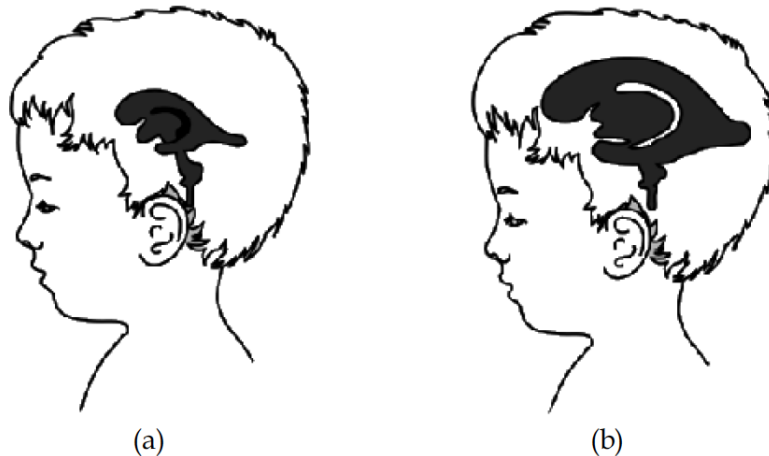


Figure 1.1: Difference between a normal subject (a) and a subject affected by hydrocephalus, with enlarged brain ventricles (b) [5]

CSF often creates a disturbance in intracranial dynamics: if, for different reasons, the rate of CSF absorption or drainage is consistently less than the rate of

production, the ventricles expand causing the brain compression. This event leads to the disorder known as *hydrocephalus*, as shown in Figure 1.1. Hydrocephalus causes an abnormal increase of Intracranial Pressure (ICP).

The arachnoid cysts are diagnosed by investigations with CT (Computerized Tomography) and MRI (Magnetic Resonance Imaging). MRI is the most used diagnostic procedure because of its ability to demonstrate the exact location, extent, and relationship of the arachnoid cyst to adjacent brain or spinal cord [6].

The Figure 1.2 depicts a MR image of a 35 year old female brain acquired in frontal (coronal) position, that reveals an example of arachnoid cyst in the suprasellar region, indicated in figure by a white arrow.

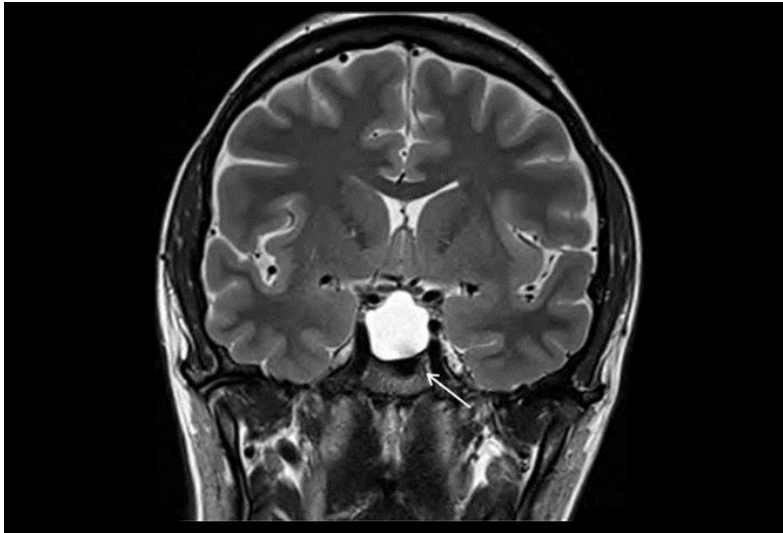


Figure 1.2: Coronal T2-weighted MRI images of a 35-years-old woman brain that shows an arachnoid cyst developed in the suprasellar region. The lesion is indicated by a white arrow [1].

Because arachnoid cysts develops through a process that acts as a growing space-occupying lesion, diagnosis and surgical treatment should be made early, before excessive cranial enlargement or irreparable brain damage occur.

1.2 The arachnoid cysts treatments

The treatments for the arachnoid cysts are different, disputed matter and they depend on their type, symptomatology, location and size; in fact most cysts are asymptomatic and, according to surgeons, they do not require treatments.

The cyst management, regardless of treatment type, is intended to remove the lesion pressure and to reduce the cyst dimensions, in order to allow maximal brain parenchyma expansion.

The most conventional methods used for the treatment of symptomatic arachnoid cyst are:

- capsular resection;
- drainage by needle aspiration or burr hole;
- fenestration via craniotomy with excision and marsupialization into the sub-arachnoid space, basal cisterns or ventricle;
- neuroendoscopic fenestration;
- shunting procedures, that include for example the cysto-peritoneal shunt and the ventriculo-peritoneal shunt when hydrocephalus occurs.

The first surgical option is a resection of the cyst wall with membrane opening; it reactivates the communication between cyst and the sub arachnoid space.

The first two procedures are simple and quick but they are characterized by infection, high rate of recurrence of the cyst and the risk of postoperative neurological deficits.

Instead the craniotomy with fenestration into the basal cisterns, allows a direct inspection and a total excising of the cyst wall and it appears to be the most rational treatment taking into account the secretory properties of the cyst membranes. It also treats located cysts effectively, allows visualization of bridging veins and it avoids a permanent shunt.

The endoscopic fenestration via craniotomy has some disadvantages like: the risk of occurrence of significant morbidity and mortality secondary to abrupt decompression; the incidence of blocking of the fenestration due to scarring phenomena, which may cause cyst regrowth and the CSF incapacity to flow through the sub arachnoid space, which may cause a postoperative shunt insertion [7, p. 171].

Through recent advances in the endoscopic field, another procedure is available to treat arachnoid cyst: the neuro-endoscopic fenestration. In this technique, the neurosurgeon, by some preoperative MR images, makes a small incision near the cyst and he inserts, along a precise and perpendicular to the skull surface trajectory, a rigid or flexible endoscope with a small camera on its tip. The surgeon uses the endoscope to analyze and to gently open the cyst, allowing the fluid inside to drain into CSF system, where it will be redistributed through the body and thus minimizing the risk of injuring surrounding neuro-vascular structures.

The neuro-endoscopic fenestration is a high success rate, safe, effective and less invasive therapeutic technique; it avoids the shunt implant in patients and it involves a shorter postoperative period. However, some studies suggest that neuro-endoscopy remains a superior approach, with a lower risk of surgical complications associated with craniotomy and shunting, because of the high risk of shunt failure.

The last conventional method is the shunting procedure; it is a simple, cost effective, reliable surgical technique for the treatment of the arachnoid cyst. The surgeon places a derivation device in the patient brain that, through a pressure difference, allows the fluid inside the arachnoid cyst or the brain ventricles, to drain in a one direction, to another part of the patient body, such as the peritoneum where the fluid is absorbed as part of the circulatory process. Shunt placement has several disadvantages and limitations; it also carries the additional risk of lifelong shunt dependence and over-drainage.

The shunting system, in particular, the cysto-peritoneal shunt will be in detail investigated in the next chapters.

Surgical treatment of arachnoid cysts may occasionally result in complications, including subdural hygroma, subdural hematoma, CSF leak, wound complications, subdural empyema, meningitis, cranial nerve palsy, spasticity, hemiparesis, hydrocephalus, seizure, and the need for more than surgical treatment after failure of an initial surgical attempt. Seizures and headaches, however, often persist despite adequate surgical treatment of the cyst [6, p. 227].

Chapter 2

Shunting system for the arachnoid cyst treatment

In this chapter, after a brief explanation of the shunting device features, we will describe and experimentally test two shunting systems kindly offered by Regina Margherita Hospital, in Turin, Italy.

2.1 General description of the device

The introduction of modern shunting systems, for the hydrocephalus treatment or, in particular, for the arachnoid cyst treatment, occurred due to the silicone discovery in the 1950s; it is a synthetic, biocompatible, fatigue-free material and it is used for the valvular components and shunt catheters construction, because silicone is able to withstand severe and long-term mechanical stress.

A shunt is a derivation device that works through a pressure difference ΔP , between the proximal catheter and the distal catheter.

Since its introduction, shunting system design remained almost unchanged and it consists of (Figure 2.1):

- *an inflow, proximal or closer to the inflow site, catheter* which drains CSF from the ventricles or the subarachnoid space; this tube leaves the brain through a small hole in the skull and then runs for a short distance under the skin;

- *a valve mechanism* that maintains unidirectional flow, works through a specific pressure difference ΔP between the pressure at the proximal catheter tip and the pressure at the drainage site and it controls flow through the shunt tubing. This device is connected to the proximal catheter and lies between the skin and the skull, usually on top of the head or just behind the ear. The pressure difference depends on the patient age, ventricle size, ICP level and other factors;
- *an outflow, distal or farther away from the inflow site, catheter* which runs under the skin and directs CSF from the valve to the abdominal or peritoneal cavity, heart or other suitable drainage site.

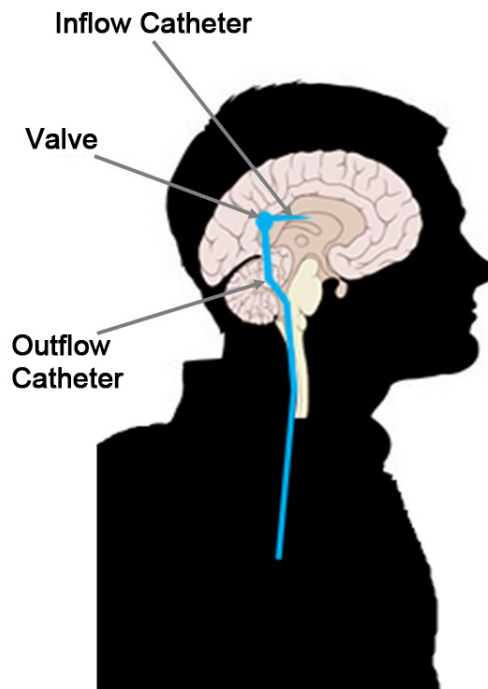


Figure 2.1: Configuration of an implanted shunt system[8]

The catheters are made of silicone and they are frequently impregnated with radiopaque material to aid in their radiographic visualization. Some tubes, which can be present in the system and which connects the catheters and the valve, are instead made of plastic. Others catheters can be impregnated with antibiotic to reduce the infection rate in the post-operative period.

The components of a shunt system are named according to where they are implanted in the body; in fact, the Table 2.1 illustrates some shunt system configurations:

Shunt Pathway	Shunt Type	Proximal catheter position	Distal catheter position
Ventriculo-peritoneal	VP	Ventricle	Peritoneal cavity
Cyst-peritoneal	CP	Cyst cavity	Peritoneal cavity
Ventriculo-atrial	VA	Ventricle of the heart	Right atrium
Ventriculo-pleural	VPL	Ventricle	Pleural cavity
Lumbo-peritoneal	LP	Lumbar spine	Peritoneal cavity

Table 2.1: Example of shunt devices depending on the positioning and pathway of their catheters

In addition to the above mentioned components, a shunting system can also include other components like:

- *chambers* or *reservoirs* to take CSF samples through a syringe, to release some specific drugs or to measure the ICP level. They can be inserted within the shunt or added as secondary components; they can also reveal the presence of an obstruction inside of the distal or proximal catheter, if the reservoir, as a result of a mechanical pressure doesn't come back to original configuration or if it is stiff, respectively;
- *anti-siphon* or *gravitational devices*, to prevent the siphon effect (the gravity "sucks" fluid out the shunt) and its main complication, named over-drainage, that is an excessive CSF drainage compared to the CSF quantity produced by the body, that occurs when patient stands up in upright position. The anti-siphon device includes a silicone membrane, whereas the gravitational device can include a spring-ball mechanism or two metallic spheres. The membrane, during position change, progressively increases the required valve opening pressure, providing big resistance to the CSF flow and avoiding

CSF drainage because of the weight of the hanging hydrostatic column in the distal catheter. Instead, the spring-ball mechanism, when patient is lying down, provides little resistance to the CSF flow because the ball is far from the fluid path; but when patient moves to a vertical position, the metal ball falls within a cone-shaped opening and close the valve, providing a greater resistance to the CSF flow.

The Figure 2.2 shows the difference between two mechanisms.

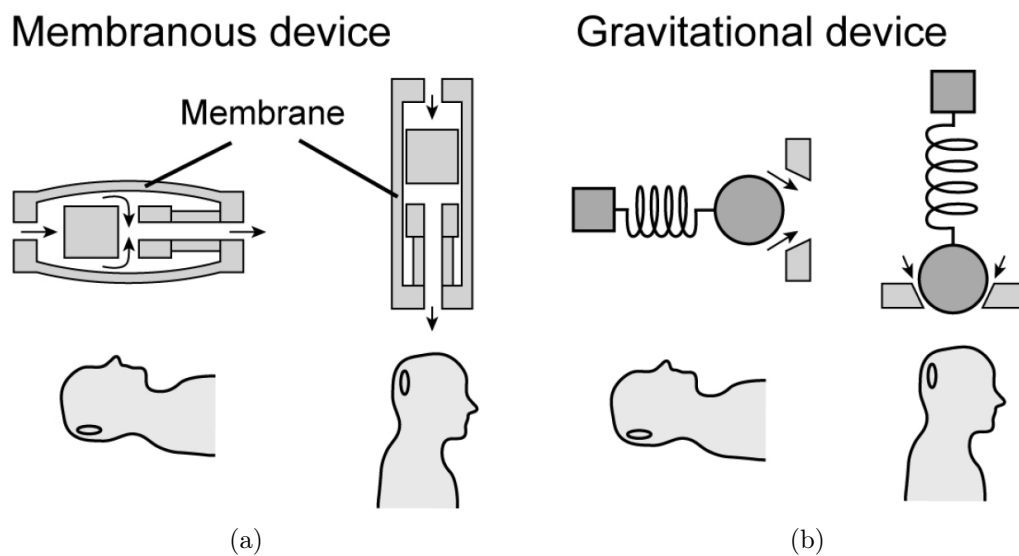


Figure 2.2: Siphon resistive devices to prevent the overdrainage event due to the postural change. (a) Membranous devices include a pressure sensitive membranous compartment. (b) Gravitational mechanisms include a mass-spring system that reacts to gravity and regulates the opening of a valve.[9]

- *flow-regulating device*, to maintain a constant CSF flow through the valve at different pressures, despite changes in the CSF pressure and patient position; the resistance of the device rises up when the differential pressure across the valve increases and vice versa.

The shunt valve intrinsically functions as a kind of resistance mechanism within the shunt system, which operates to control ICP in patient with hydrocephalus or other neurological diseases [10].

The shunt valve can be classified as first, second, third and fourth generation valve. At present a large variety of valves is commercially available, and the main manufacturers on the market scene are Medtronic, Codman, Aesculap-Miethke and Integra LifeSciences.

The first generation is constituted by the *fixed Differential Pressure (DP) valve*; it usually has three differential pressure range (low, medium and high) based on the opening pressure of the valve and it drains fluid at one setting pressure. After shunt system implantation, the valve opening pressure can be only modified through a further surgical procedure; for this reason the fixed DP valve can be inappropriate for the patient clinical requirement.

The second generation includes both the *fixed DP valve with an anti-siphon mechanism* and the *programmable DP valve*; this generation was designed to overcome the problem of the CSF overdrainage in the vertical position.

In a programmable DP valve, the opening pressure can be non-invasively adjusted, from outside the body, through a magnetic field. It guarantees a specific ICP level for each patient, in particular for the children, whose values of the opening pressure of the valve change during their growth.

The programmable DP valve will be described in detail in the next sections.

The valve types of the second generation later have been united into the *programmable DP valve with an anti-siphon mechanism* which can be classified as the third generation valve.

Recently, the anti-siphon mechanism has become controllable and it should rightly be classified as the fourth generation valve [10].

Several types of design valve are commercially available:

- *slit valve*, which consists of a cut (slit) in the wall of the distal catheter extremity. When the CSF pressure is sufficient, the slit opens and permits CSF to flow out of the catheter. The pressure that allows slit to open up is determined by the thickness of the catheter wall. The slit valves in a shunting system can be located in the proximal or distal catheter; in some configuration a pumping chamber can support the slit valves to prevent inverting pumping slit and the CSF reflux;
- *spring-loaded, ball-in cone valves*, which consist of a metallic coiled or a flat spring that applies a force to a synthetic ruby ball located in a cone-shaped

hole. When the CSF force, that is its pressure, increases and exceeds the spring force, it pushes the ball against the spring and opens the valve to allow the CSF flow. When the fluid pressure is reduced the ball returns to its original position and closes the valve (Figure 2.3a);

- *diaphragm valve* which consists of a flexible membrane that moves in response to pressure differences; the diaphragm movement permits CSF to flow around it (Figure 2.3b). When the pressure is reduced, the membrane returns to its original position and seals the mechanism [11].

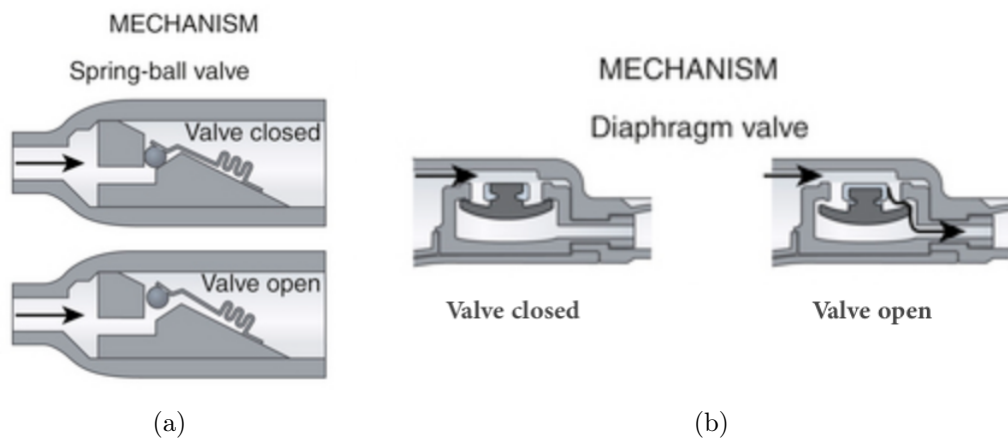


Figure 2.3: Two examples of shunt valve design: the spring ball (a) and the diaphragm (b) mechanisms in open and closed configuration[12]

The shunt system type is chosen by the neurosurgeon and depending on the clinical history and condition of the patient, on the age of the patient, on the cyst dimensions and localization etc.; despite these premises, neurosurgeons prefer the programmable differential pressure valve compared to the fixed differential pressure valve as a first choice for the hydrocephalus treatment.

However, it is still unclear what type of shunt valve is suitable for each individual case.

Fixed-pressure valves	Hakim	Codman (Johnson and Johnson) Built-in siphon guard Zero–five centimeters H ₂ O outflow resistance
	PS Medical	Medtronic Four different fixed-pressure increments Injectable proximal reservoir
	Chhabra	Very low cost Gravitational three-ball mechanically regulated system for incremental drainage
Flow-regulated valves	Delta	Medtronic Elastomer diaphragm regulate Five different flow levels
	Orbit-Sigma	Integra Three-stage variable resistance mechanism MRI compatible

MRI Magnetic resonance imaging

Figure 2.4: List of the main fixed-pressure and flow-regulated valves commercially available and their features [13, p. 268]

Programmable pressure valves	Strata	Medtronic Magnetic programmable ball and spring delta valve Can be manipulated by MRI
	Codman-Hakim	Codman (Johnson and Johnson) Magnetic programmable ball and spring valve One centimeter H ₂ O incremental settings Can be manipulated by MRI
	Sophy	Sophysa Silicone-coated chamber Ball cone with variable pressure set to spring One centimeter H ₂ O incremental settings Can be manipulated by MRI
	Polaris	Sophysa Silicone-coated chamber Magnetic field self-locking safety feature One centimeter H ₂ O incremental settings MRI compatible
	ProGav	Aesculap Magnetic field self-locking safety feature One centimeter H ₂ O incremental settings MRI compatible

MRI Magnetic resonance imaging

Figure 2.5: List of the main programmable-pressure valves commercially available and their features [13, p. 268]

2.2 The *Codman Hakim Shunt*, a programmable differential pressure valve

The Codman Hakim Shunt, produced by the Johnson&Johnson company (Raynham, Massachusetts, USA), is one of the most used shunting systems in the clinical practice for the treatment of hydrocephalus, arachnoid cysts and to overcome the over-drainage and under-drainage phenomena.

It is a programmable differential pressure valve, that consists of a proximal catheter, a valve and a distal catheter, similarly to the others commercially available programmable shunting systems.

The device allows the neurosurgeons to non-invasively change the valve opening pressure between 30 mmH₂O and 200 mmH₂O in steps of 10 mmH₂O, before and after its implantation through a codified magnetic field applied from the outside of the body. In this way patient, after the shunt insertion, avoids further revision surgeries to change the valve pressure according to the clinical symptoms and conditions. [4, 14, 15].

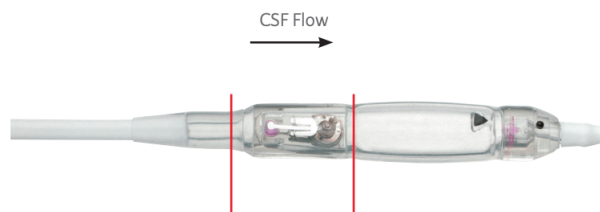


Figure 2.6: Design of the Codman Hakim valve [16]

The valve design characterizing the shunt system is the *spring-load, ball-in cone valve*, which consists of a stainless steel flat spring and a synthetic ruby ball, indicated by black arrows and upper white arrows respectively in Figure 2.7.

The flat spring, with its proximal extremity, presses the synthetic ruby ball whereas, with its distal extremity, it leans against the coiled cam.

The ball, due to the tension exerted by the spring, gets in position in the valve seat where the CSF flow passes, providing more or less flow resistance; the spring intensity on the ball depends on the spiral staircase cam, a pressure control cam, which includes a stepper motor and which turns thanks to a servomotor activated by an external codified magnetic signal [14]: a greater spring tension, due to the

slight cam rotation, increases the valve opening pressure and vice versa, providing more or less resistance to CSF flow respectively.

The cam is supported by a titanium plate.

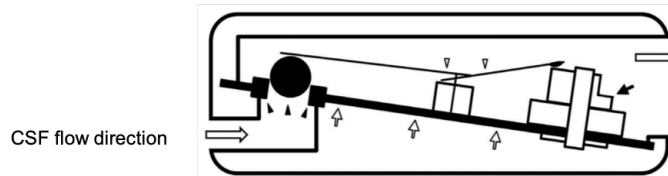


Figure 2.7: The inner mechanism of the Codman Hakim Shunt valve from the side view: it is a spring-loaded, ball-in cone mechanism [14]

2.2.1 The Codman Hakim Shunt programming

The Codman Hakim Shunt, as previously mentioned, is a programmable differential pressure valve and it requires, as necessary, to be re-adjusted in the post operative period, according to the symptoms, the clinical history and the radiological findings of the patient or his growth, if a children. To adjust the device, the neurosurgeons need a *Programmer Unit*, supplied with the Codman Hakim Shunt (Figure 2.8a); it includes a *Programmer Panel* and a *Transmitter Head* (Figure 2.8b): the first is used by the clinician to choose the correct and appropriate value of the valve opening pressure, between the available 18 pressure levels; the second instead generates a codified magnetic field, used to modify the valve opening pressure.

After a meticulous head palpation, the surgeon positions the transmitter head on the patient scalp in correspondence with the implanted valve: the programming tool shall be aligned with the CSF flow direction to instantly change the opening pressure threshold for drainage.

It is recommended, after the valve implantation, to subject the patient to X-ray or MR imaging, to have a clinical proof of the complete system of the valve and of the position of its components, and to verify the valve opening pressure value. This operation is also advisable after every pressure valve re-programming.



Figure 2.8: The Codman Hakim Shunt equipment. On the left, the programmer unit which includes the programmer panel and the transmitter head; this unit permits the neurosurgeon to change the valve opening pressure after the shunt insertion in the patient’s brain. On the right, the transmitter head which is positioned in correspondence with the valve, on the patient scalp; it produce a codified magnetic field that allows to externally and non-invasively adjust the programmable Codman Hakim shunt [16].

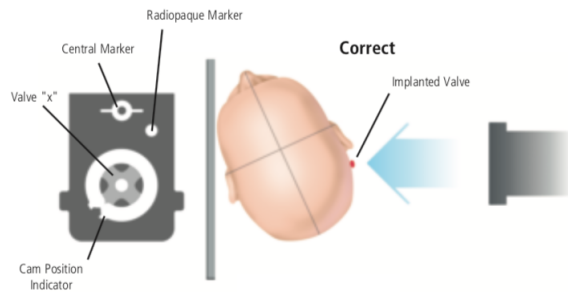


Figure 2.9: The radiographic elements positioned on the Codman Hakim Shunt that permit clinician to qualitatively determine the valve opening pressure. The radiographic film is shot perpendicular to the plane of the valve with the non-implanted side of the patient’s head resting on the plate.[16]

The valve setting is interpreted through X-ray by comparing the radiopaque indicator positioned on the cam, which turns through the application of an external codified magnetic field, with the fixed indicator located on the right side of the titanium support plate.

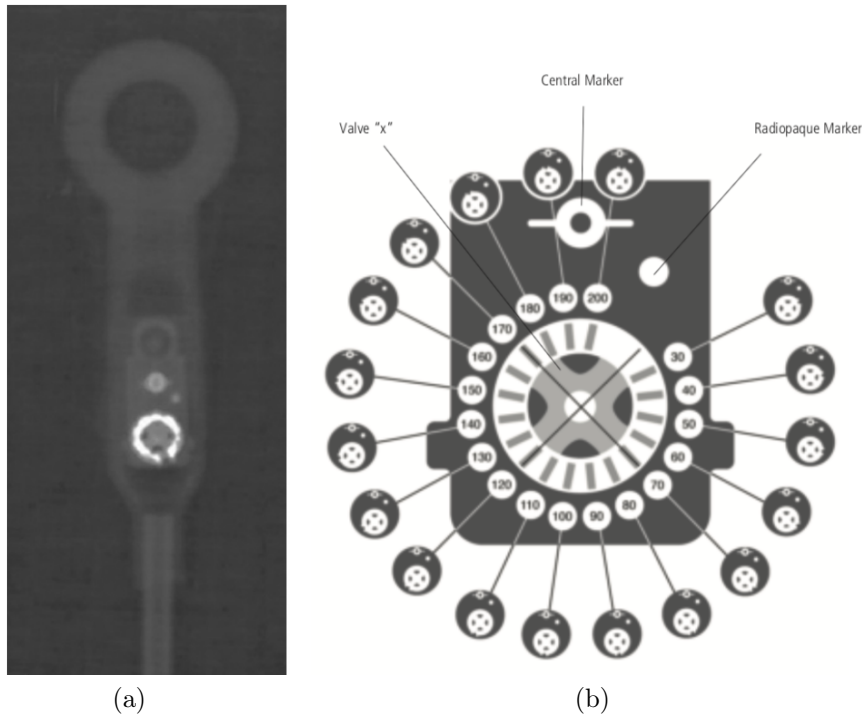


Figure 2.10: The X-ray image of the Codman Hakim Shunt. On the left, a radiographic image of the Codman Hakim Shunt. On the right, the radiographic interpretation of the valve opening pressure value, through a comparison between the fixed radiopaque marker in the upper side of the valve and the cam position indicator on the titanium plate. [16]

The current informations about this device declare that patients with an implanted Codman Hakim Shunt can safely undergo MR imaging under the following conditions:

- static magnetic field of 3 Tesla,
- spatial gradient of $720 \frac{G}{cm}$,
- limited radio-frequency energy to a whole body-averaged specific absorption rate of 3 watts per kilogram for 15 minutes [16, p. 1344].

2.2.2 The Codman Hakim Shunt configurations

The device is available in eight different configurations, as shown in Figure 2.11:

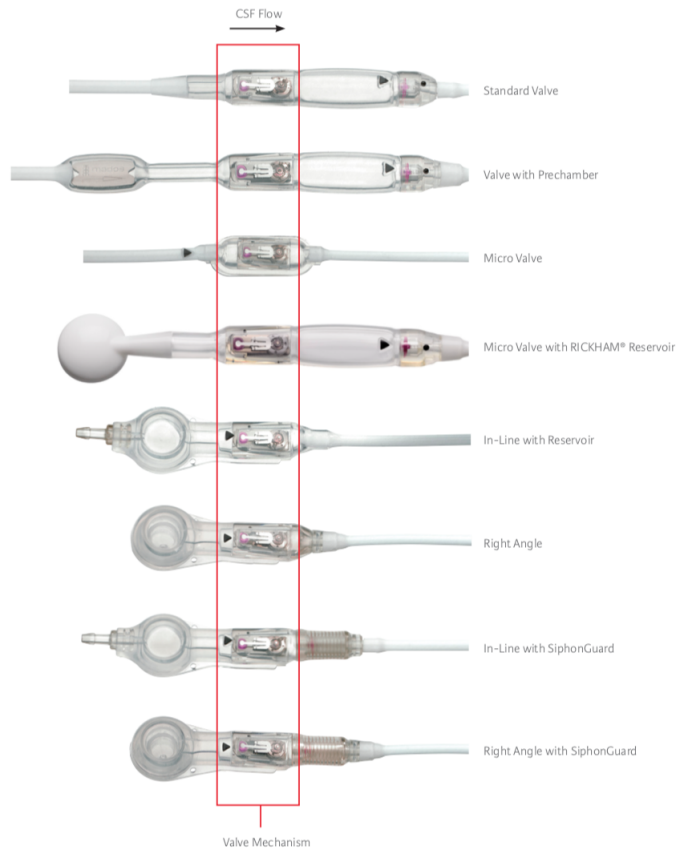


Figure 2.11: The eight configurations of the Codman Hakim Shunt. From the top: Standard Valve, Valve with prechamber, Micro valve, Micro valve with Richkam Reservoir, In-Line with Reservoir, Right Angle, In-Line with SiphonGuard, Right angle with SiphonGuard. [16]

The several valve settings are chosen by the neurosurgeon, according to his practical experience and the patient clinical symptoms and history.

Some shunt components, like pre-chamber and reservoir, have been discussed in the previous paragraph; whereas in this section the *Siphon-guard mechanism*, that belongs to the flow-control devices, will be briefly debated.

This mechanism is produced by the Johnson&Johnson company; it can be used as a stand-alone unit, connected to an existing shunting device (Figure 2.12a) or it can be connected to the output section of a traditional programmable DP valve

(Figure 2.12b), as the Codman Hakim shunt in line or right angle configuration [17].

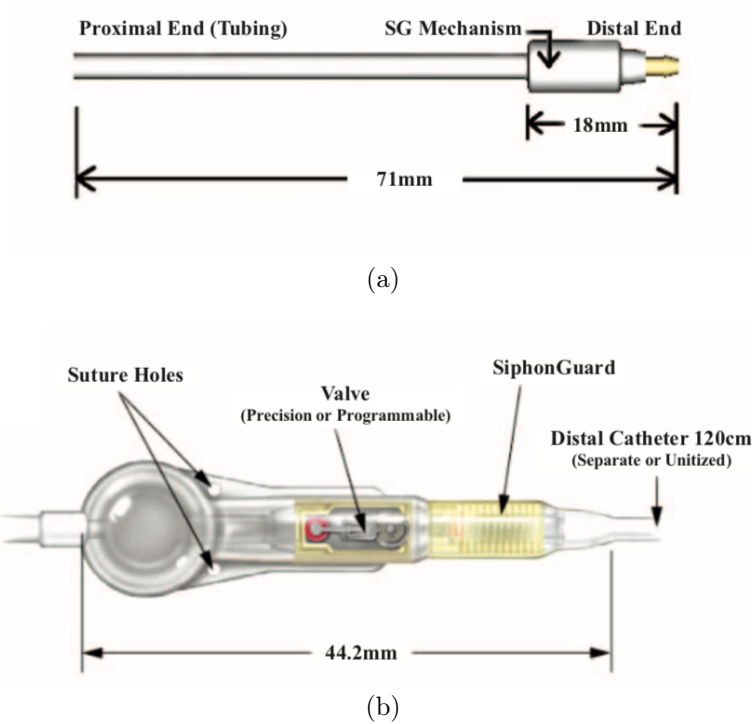


Figure 2.12: The Siphon-guard mechanism as a stand-alone unit attached to an existing shunting system (a) or in line with the programmable DP valve, in this case attached to the outlet of the Codman Hakim Shunt [17].

Siphon-guard mechanism is a flow-control device and, in fact, it differs from the traditional anti-siphon mechanism; it prevents the overdrainage phenomenon during the upright position, the excessive CSF excretion, thus improving the quality life of the patient. Siphon-Guard mechanism is a classical flow regulator that provides a big resistance if flow increases above certain threshold. As shown in Figure 2.13, Siphon-Guard internally consists of two flow pathways and the central channel includes a ball on spring valve mechanism that responds to changes of CSF: when the patient is lying down, CSF flow passes through both pathways; when the patient is standing in upright position, since the CSF flow quickly increases, the primary

pathway closes and the CSF flow is forced to pass through the secondary pathway, which introduces a greater flow resistance [17].

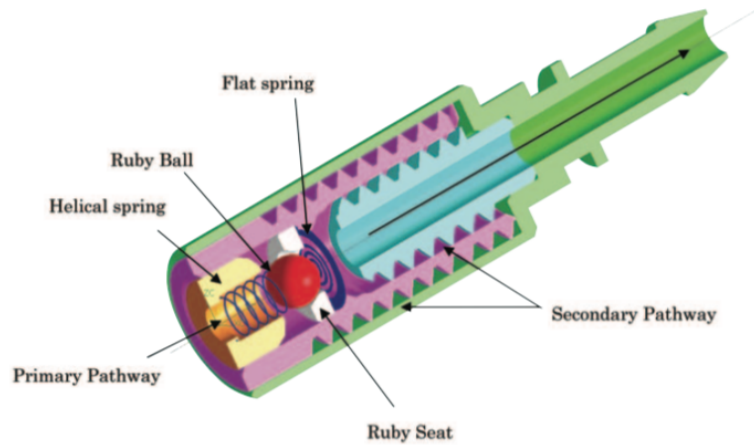


Figure 2.13: An inner view of the Codman Hakim Shunt with the Siphonguard mechanism

This device has a potential problem: after switching to the high-resistance state, it may never switch back to low resistance (this happens when differential pressure goes back to zero or negative values), which may contribute to intracranial hypertension. [18, p. 1387].

2.3 The *Miethke proGAV 2.0 Adjustable Shunt System*

ProGAV 2.0 shunt system, produced by Christoph Miethke GMBH & Co.(Postdam, Germany) is one of the most innovative shunting systems, designed to ensure the optimal ventricular pressure, for the treatment of hydrocephalus, arachnoid cysts and to overcome the over-drainage and under-drainage phenomena.



Figure 2.14: The Miethke ProGAV 2.0 Adjustable Shunt System design [19].

It is an adjustable valve, commercially available as a shunt system or as individual valve units, constituted by :

- an inlet section for the proximal catheter (internal diameter 1.2 mm and external diameter 2.5 mm),
- an adjustable differential pressure (DP) unit,
- a connecting catheter,
- a fixed gravitational unit,
- an outlet section for the distal catheter (internal diameter 1.2 mm and external diameter 2.5 mm).

The adjustable DP unit is composed by a solid body, made of titanium, with a ball-in cone mechanism valve, which is included in its proximal part, and by a bow spring that determines the ball-cone valve opening pressure.

As the Codman Hakim Shunt previously described, the valve opening pressure can be adjusted from 0 to 20 cmH₂O, even when the shunt is implanted in the patient's brain, through the application of an external magnetic field that causes the rotor turn.

The gravitational unit consists of a tantalum ball that determines the opening pressure of this unit and of a sapphire ball that guarantees the precise closure of the valve. It exists with different opening pressure setting like 10, 15, 20, 25, 30 and 35 cmH₂O.

The DP unit and the gravitational unit are connected each others by a connector.

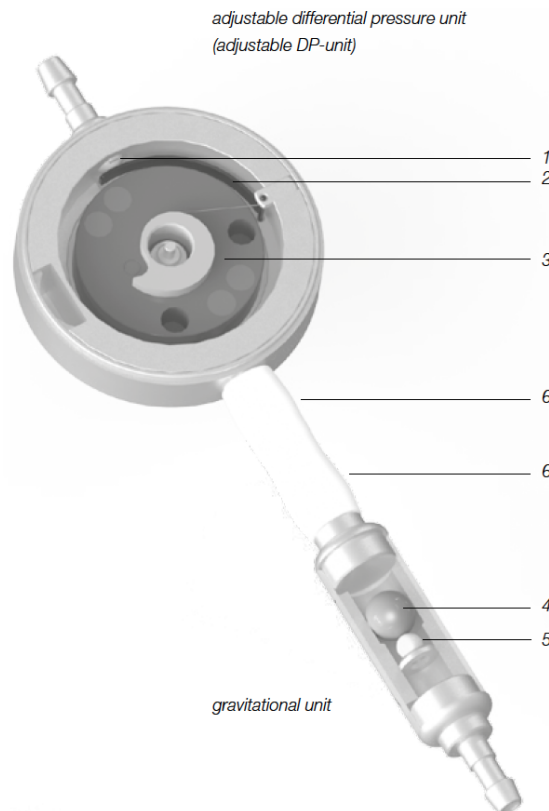


Figure 2.15: The Miethke ProGav 2.0 Shunt System configuration: it consists of two unit, the adjustable DP unit and the fixed gravitational unit. In the adjustable DP unit: 1 sapphire ball, 2 bow spring, 3 rotor; in the fixed gravitational unit: 4 tantalum ball, 5 sapphire ball. Both units are connected by a connector (6)[19].

The ProGAV 2.0 shunt system is a posture dependent valve as its opening pressure is defined by the opening pressure of the DP unit and by the opening pressure of the gravitational unit if patient is in upright position, otherwise it depends by the opening pressure of the adjustable DP unit, if patient is lying down.

Particularly, when patient is lying down, the fixed gravitational unit remains open without resisting the CSF flow (Figure 2.16a); so the ProGav 2.0 opening pressure is only defined by the opening pressure of the adjustable DP unit. In this position the operational principle of the DP unit is depicted in Figure 2.16b: when the patient’s intraventricular pressure (IVP) is lower than the DP unit opening pressure, the ball-cone valve is closed, impeding CSF flow; but when IVP increases and the spring force is exceeded, the closing ball moves out the cone and opens, allowing CSF drainage.

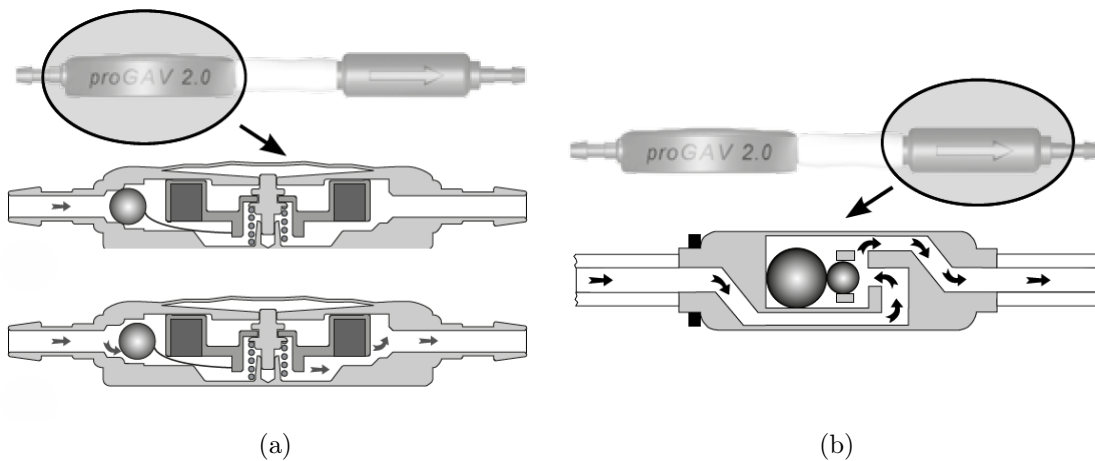


Figure 2.16: Functioning of the ProGAV 2.0 Shunt System when patient is lying down. (a) The fixed gravitational unit remains open since the sapphire ball do not close the path of the CSF flow; thus CSF can flow until its drainage site. (b) The adjustable DP unit: when IVP is lower than the value of the valve opening pressure, the ball-in cone valve remains closed; when IVP exceeds the valve opening pressure, CSF flow presses the ball and overcomes the spring force and it begins to flow until its drainage site [19].

Instead, when patient moves into a standing position the gravitational unit closes in order to prevent the CSF over-drainage caused by the upright position(Figure 2.16); in this case the ProGav 2.0 opening pressure is defined by both the opening pressure of the adjustable DP unit and by the opening pressure of the gravitational unit: now, the weight of the tantalum ball in the gravitational unit has to be exceed; for this reason, in the vertical position, the opening pressure of

the shunting system significantly rises up.

Also in this body position, the functioning of the adjustable DP unit may be described by the 2.16b.

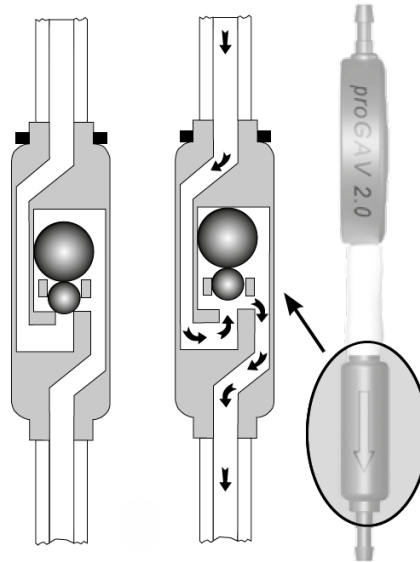


Figure 2.17: Functioning of the fixed gravitational unit when patient moves in upright position: when the pressure exerted by the CSF flow overcomes the weight of the tantalum ball, the gravitational valve opens allowing the CSF drainage; otherwise it remains closed, in order to avoid the CSF suck caused by the negative pressures that generate when patient moves from an horizontal position to a vertical position [19].

2.3.1 The ProGAV 2.0 Adjustment

ProGAV 2.0 is a programmable differential pressure valve and it can be adjusted, in the post-operative period, according to the clinical situation and condition of the patient.

The programming tools, named the *ProGAV Tool set*, are supplied with the shunting system and they allow to determine, change and control the selected opening pressure of the ProGAV 2.0. The set consists of two elements:

- the *ProGAV 2.0 Compass* that includes a dial that allows to locate and verify the opening pressure of the adjustable DP unit;
- the *ProGAV 2.0 Adjustment Tool* that permits to adjust the opening pressure of the DP unit into a pressure range from 0 cmH₂O to 20 cmH₂O in increments of 1 cmH₂O.



Figure 2.18: The ProGAV Tool set for the adjustment of the valve opening pressure. On the top: the ProGAV 2.0 Compass is positioned on the patient’s scalp in correspondence of the valve, so it is useful to locate the valve and the direction of the CSF flow, and later it allows to verify the value of the valve opening pressure directly on the tool. On the bottom: the ProGAV 2.0 Adjustment Tool is characterized by a graduated scale, from 0 cm₂ to 20 cmH₂O so it is useful to reprogram the valve opening pressure, because it includes two magnets that generate a magnetic field which allows rotor to turn. [19].

A new valve is always preset to 5 cmH₂O but the neurosurgeon, according to the specific clinical case, can change the value of the valve opening pressure through some precise operations.

The clinician, with the forefinger, has to position the ProGAV 2.0 Compass (open) on the patient's head in correspondence of the valve, identifying through two arrows on the instrument, the CSF flow direction. When the compass is closed, the pressure setting is automatically indicated on the tool.

Subsequently, the neurosurgeon has to position the ProGAV 2.0 Adjustment Tool on the patient's head, centrally on the valve: the new selected opening pressure of the valve must point on the scale in direction of the connector and the ventricular catheter. Through a light pressure, applied on the skin with the forefinger, the rotor-brake will be released and the opening pressure can be modified; the application of a light pressure on the skin and consequently on the valve housing provokes an acoustic signal (a clicking sound) that indicates rotor-brake can turn freely. When the valve is released another clicking sound is produced and the rotor-brake is again safety locked: this tactile feedback mechanism avoid spontaneous re-adjustment of the valve.

After every valve reprogramming, the set opening pressure has to be verified through the compass and confirmed by X-ray.

In a radiograph, the information about the correct pressure setting is provided by the rotor position. The rotor consists of four magnets, arranged in pairs and face to face on the top of the rotor and identifiable in the X-ray like four white small dots, and by two drill holes identifiable in X-ray as two black small dots.

The rotor side with two magnets and two drill holes can be identified as the back side of the rotor while the other two magnets opposite to them create a triangle tip; the sharp corner of the triangle, formed by visually connecting the magnets and the drill holes, indicates the position of the triangle tip while the direction of the triangle tip indicates the pressure setting of the valve.

The setting of the fixed gravitational unit in a radiograph is instead recognizable through the number and the dimensions of a coding ring that characterizes the gravitational valve (Figure 2.20).

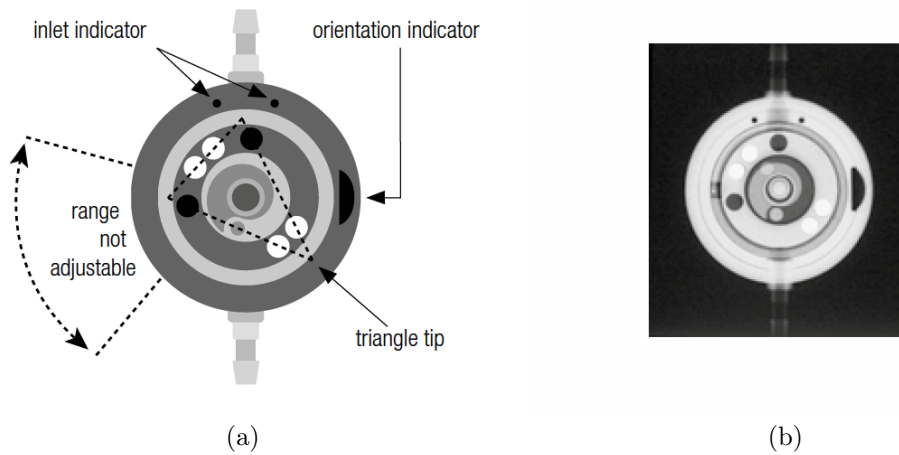


Figure 2.19: The radiographic visualization of the adjustable DP unit. (a) The schematic top view of the adjustable DP unit by X-ray; in order to avoid wrongly recognize the opening pressure of the DP unit in the X-ray image, the valve is marked with an orientation indicator identifiable as a black cut-out, visible on the right hand side of the housing of the valve. The four white small dots represent the magnets, while the two black small dots the drill holes. These elements, if visually connected, form a triangle: the sharp corner of the triangle indicates the position of the triangle tip while the direction of the tip indicates the valve opening pressure. (b) Pressure setting 13 cmH₂O [19]

A patient with the ProGAV 2.0 shunt system implanted in his brain can safely undergo MR imaging only if the magnetic field of the MRI scanner is lower than 3 Tesla. Neurosurgeon has to use ProGAV 2.0 far from pacemakers, MRI scanner or others metallic objects because of the magnets inside the ProGAV 2.0 Tools.

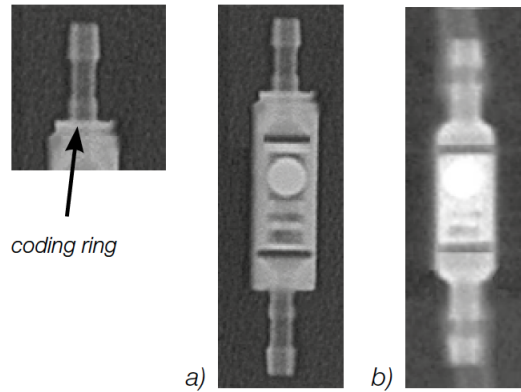


Figure 2.20: The radiographic visualization of the fixed gravitational unit. Coding ring permits to recognize the opening pressure of the gravitational unit: a large coding ring means an opening pressure of 20 cmH₂O, no coding ring an opening pressure of 10 cmH₂O[19]

Opening pressure values for the upright position	Coding of the fixed gravitational unit
10 cmH ₂ O	small, no ring
15 cmH ₂ O	large, no ring
20 cmH ₂ O	large with 1 ring
25 cmH ₂ O	large with 2 rings
30 cmH ₂ O	large with 3 rings
35 cmH ₂ O	large with 4 rings

Table 2.2: Different types of the ProGAV 2.0 gravitational unit and their features to identify the valve opening pressure through a X-ray image

2.4 Problems and constraints of the shunting systems

Regardless the type of the shunt system model, every shunt has its own vantages and disadvantages.

In particular, the fixed DP valve does not permit non-invasively and external adjustments of the valve opening pressure and it does not allow to choose a specific value of the opening pressure, especially in children, because of its pressure range, limited to only three values (low, medium and high): in fact, during the growth of a child, the ICP level increases and the valve opening pressure has to periodically adjusted in order to adequately drain CSF. This operation is possible only with additional surgical procedures.

Whereas the programmable DP valve, despite it allows reprogramming of its opening pressure from outside of the body and in a non invasive way, according to the patient symptoms or the patient growth, and despite it is capable to overcome the over-drainage event, it has a complication rate about 2%.

Furthermore, based on some scientific studies, (Ozturk et al.[20], Utsuki et al. [21]) the programmable DP valve can be subjected to involuntary changes of its setting, because of weak magnetic fields produced by instruments or things of everyday usage, like TV, mobile phones, tablet, headphones, electrical appliances with which patients are in close contact for a long period.

The shunting systems are life-saving devices and they are very used for the arachnoid cysts treatment; but they are negatively characterized by a high failure rate and by a high morbidity rate. In addition, it is difficult to identify and to diagnose their malfunctioning, since they are not equipped with feedback systems which allows to control the system from the outside in a non invasive way. It is scientifically demonstrated that 40% of shunts fails within the first 2 years and 98% of shunts within 10 years after their implantation.

Shunt malfunctions are generally not detected before they manifest clinically; in fact, in some patients they are a real medical emergency and they become life threatening if not discovered in time and treated promptly to avoid serious complications.

Regardless of the shunt valve type, fixed or programmable DP valve, the principal failure causes of shunting systems are:

- infections,
- proximal and distal catheters obstruction: about 60% of obstructions occur at the proximal catheter, 30% at the valve itself,
- tubes or catheters disconnection from the valve,
- tube or catheters migration in the brain area,
- block valve,
- fractures, wear and corrosion of the system components,
- over-drainage and under-drainage as a functional failure,
- hemorrhagia,
- slit ventricle syndrome,
- CSF accumulation.

Despite the introduction, over the years, of anti-gravitational devices, anti-siphon mechanisms, antibiotic impregnated catheters, flow-regulator valves, and despite the surgical techniques are improved, the shunt failure rate and the infection onset have not decreased; on the contrary they remain too high within the first years after the shunt implantation. Nowadays there is no scientific evidence that proves that some shunt system types can prevent or limit their malfunction or other failure causes. However, it is proven that the use of programmable DP valve can both reduce the insurgence of the over-drainage and under-drainage phenomena and the number of the surgical procedures of the shunt revision the patients have to undergo. The last aspect, consequently, decrease the infection, morbidity and mortality rates associated to a further operation.

Currently, the shunt systems commercially available, don't allow some feedback with regard to the patient ICP level, the CSF flow rate or to the correct functioning of the shunt system and do not permit a self-diagnostic: timely detection of an elevated ICP level is strictly necessary to decrease the risk of permanent brain damage and to mitigate the hydrocephalus symptoms during the patient entire life. Indeed a complication in the derivation system or a failure are identified by realizing

a clinical investigation of the patient symptoms and by examining or interpreting the clinical images (X-ray or MRI) of patient skull.

Through radiography or MRI the neurosurgeons can verify the valve opening pressure setting and the position of the valve system in the brain and the possible disconnection or migration of the catheters; instead through CT and MRI clinicians can verify the ventricle size and the hydrocephalus appearance and sizes

For the patient health a technologic shunt system would be necessary, that is able to manage all of limitations and complications of the current shunt system.

2.5 The *Smart Shunt* concept

The smart shunt concept arises to overcome the previously described constraints and drawbacks of the current shunting devices.

The researchers interpret the smart shunt as a device more technological and more interactive (with sensors, control systems and telemetric systems) than the current shunt system that is characterized by a passive and mechanical valve. Its aim would be to automatically manage the CSF flow, to permit a better diagnosis and a better control about the shunt functioning and about ICP variations using some ICP readings in real-time and feedbacks from patients; in addition its aim would be to reduce the risk of catheters obstruction, to monitor the performance of its components so to decrease the shunt revisions, to personalize the treatment and to make it patient-specific, to reduce the shunt dependency, the pain and hospitalization of the patient [5, 10].

The smart shunt is a system ideally constituted by two sub-systems: an implantable part under the patient scalp and an external component. The *implantable subsystem* would consist of :

- one or more sensors to continuously detect interesting data: a pressure sensor to detect the ICP level, a flow sensor to measure the CSF variations, an orientation sensor to detect the patient position;
- a control mechanism of the CSF flow, like a valve or a pump;
- an actuator to move the valve or the pump;
- an housing to electrically isolate the internal components from the patient body;
- an energy source;
- a low frequency transmitter useful both to monitor in real time the several parameters, to detect and to collect the data from patient and the informations about the shunt functioning, and to permit the clinician to change from the outside the device settings;
- hardware and algorithms.

On the other hand, the *external subsystem* should include a personal computer or a hand-held smartphone, with a screen and an user-friendly interface, a data storage to collect and save data detected by the sensors and a bidirectional communication system that works through radio frequency. This unit should be able to interface and to communicate wireless with the outside and to download data from the implantable subsystem; in addition the external subsystem could be managed by the clinician or by the patient at home, during his daily routine (in a limited way): the clinician, through the external subsystem, could change the valve setting or the valve opening pressure; he also could verify the patient clinical parameters (ICP value or CSF flow) and the correct shunt functioning. While the patient could use the smartphone at home to provide feedbacks about his symptoms, his physical conditions and his daily activities and he could save these informations in a digital medical chart.

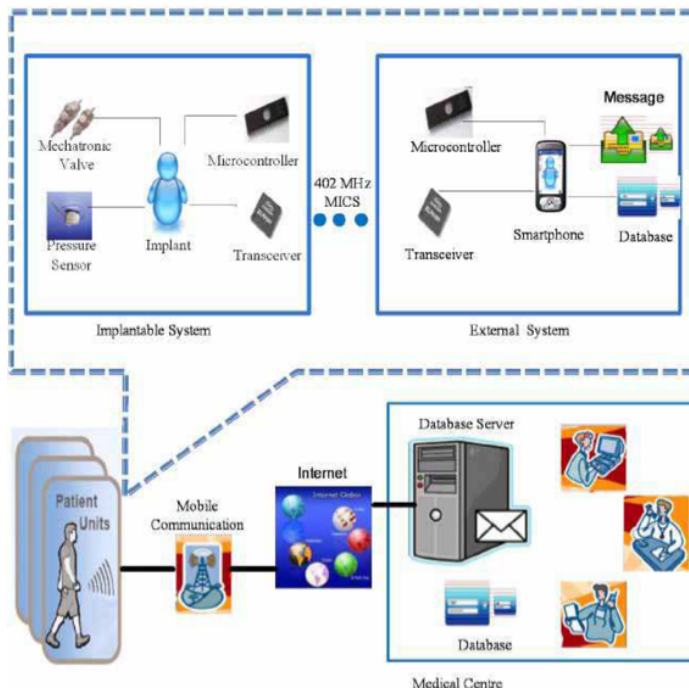


Figure 2.21: The Smart Shunt concept: the implantable system and the external system communicate and interact each other and the medical centre to improve the life quality of a shunted patient[22].

Additionally, the presence of intelligent and technologically advanced components and of specific algorithms in the smart shunt concept would allow the device

to self-regulate through different inputs, like the patient feedbacks and the operations realized by the clinician. In this way it would be possible to reduce the hospitalization of the patient and the shunt revisions.

The smart shunt, as it has been previously described in this subsection, still remains a planning idea as the researchers have to confront several challenges (technological, financial and about legislation) about the device itself and its components.

Analysis of the different smart shunt parts reveals some considerations about both the limitations to overcome and the necessary requirements for these components: the pressure sensors, the CSF flow sensors and the sensors of the patient orientation should supply accurate, reliable, real-time and continuous measurements about the physical quantities of interest; they would require a periodic calibration after the smart shunt implantation, without subjecting the patient to further surgeries and they should avoid producing a significant drift during their employment. The sensors also should be electrically isolated from both the body fluids and the moisture, they have to be hermetic and they can absorb power.

In addition, the sensors dimensions should be small as they condition the device positioning in the body and, in this specific case, in the brain; the materials used for the sensors construction should be biocompatible, compatible with the current and modern imaging techniques like magnetic resonance, computed tomography, ultrasound investigation and they should comply with the FDA guidelines.

The last three requirements should be in general respected by the smart shunt itself, but they are in particular required by the flow control mechanism, the device housing and the actuator.

The power source and the communication system prove to be the biggest challenges for the researchers.

A smart shunt should be powered through a battery to operate: a battery usually requires a periodic recharge or it is replaced when it exhausts; after the device implantation in the patient body, to avoid further surgeries, a solution to recharge the smart shunt could be the inductive coupling. This charging method has the advantage to reduce the battery size, but it could introduce different problems such as a lower compatibility of the shunt system with the magnetic resonance.

Instead the battery replacement would involve larger dimensions, that could influence the device positioning in the brain; so the device could be implanted in a different area compared to the brain or to the head.

Thus in addition the battery size that condition the general device dimensions and its positioning, an other important aspects concern the battery energy consumption that could generate heat damaging the tissues around the implant.

Regarding the communication system, it should be a bidirectional system as it should permit both the transmission of data detected by the sensors to the external subsystem, and the device handling from the outside by the clinician to change the smart shunt settings.

Radio frequency is the most used wireless communication method: the principal challenge concerns the choice of the frequency range that depends on the device location, the necessary power for the smart shunt functioning, the quantity of downloading data. There are different frequency ranges to use in a wireless device, but for a device that has to implant in the human body, RF with a frequency in the low range is the best solution: in this way the researchers reaches a compromise between the bandwidth, the heat absorption and the tissue energy.

The most important smart shunt limitations can be summarized as follows:

- inaccuracy or breakage of the pressure (ICP), CSF flow, patient orientation sensors;
- technical issues;
- power limitation (battery's charge and dimensions) ;
- product size limitation;
- potential faults;
- patient and clinicians mentality;

Currently there are no public evidences that a smart shunt has been completely developed and realized; on the other hand the single components, that could compose the smart shunt, are commercially available and they have different applications, also in medicine.

This technological device is still a concept, an idea of project, despite from 1980 until today several studies, scientific researches and patents, regarding the smart shunt development, have been published. These references discuss the adjustments and the improvements of the different components of a commercially available shunting device.

Recently, some monitoring systems have been developed as optional components of the shunting devices to detect ICP; for example *Telesensor* (Radionics), *SensorReservoir* (Miethke), *flow probes and sensors* (Transonic).

Chapter 3

Intracranial Pressure Sensors

3.1 The Intracranial Pressure

Intracranial Pressure (ICP) is the pressure inside the skull exerted by the cranium components, which are the brain parenchyma, the cerebrospinal fluid (CSF) and the cerebral blood flow (CBF); they constitute the *total intracranial volume*.

The conventional ICP unit of measurement is mmHg; but ICP can be also expressed by mmH₂O (1 mmHg is equivalent to around 13.595 mmH₂O).

According to the Monro-Kellie doctrine¹, ICP is the result of the volume and compliance of each intracranial component within the intracranial compartment. When patient is in good health, the total intracranial volume remains unvaried, because of some compensatory mechanisms which are able to maintain a constant and appropriate cerebral blood flow (CBF) and an appropriate ICP level (The compensatory mechanisms or the auto-regulation are only effective with a Mean Artery Pressure (MAP) between 50 and 150mmHg; the MAP is the result of the

¹Alexander Monro secundus was a Scottish anatomist, physician and medical educator while George Kellie was a Scottish surgeon; both described the intracranial pressure-volume relationship. After several experiments, studies and researches they introduced in 1800 an hypothesis, named “Monro-Kellie doctrine”, according to which the sum of the volume of the brain, the CSF, and the intracranial blood must remain constant. Any change in one of the intracranial components must be compensated by a reciprocal change in the volume of another component: a volume increase of one intracranial component should cause a decrease of the volume of one component or both of the remaining two components. This hypothesis has substantial theoretical implications about the increase of the intracranial pressure and about the decrease of the CSF volume.[23, p. 1746] [24, p. 1300].

sum between one-third pulse pressure (PP) and diastolic blood pressure (DBP)). Instead, when an intracranial mass like an hematoma, or hydrocephalus or an abscesses appears within the cranium, these compensatory mechanisms maintain steady levels of CBF and ICP by displacing CSF into the dural sac and by compressing the cerebral venous compartments via vena-constriction and extracranial drainage [25].

The relation between the ICP and the intracranial volume is not linear but it is described by a mono-exponential curve as shown in Figure 3.1.

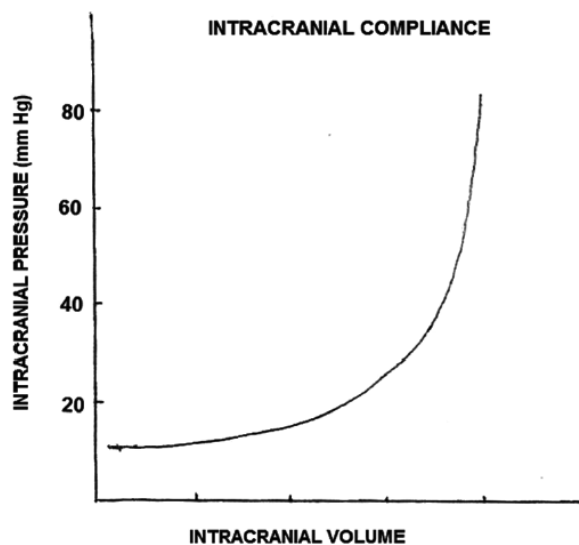


Figure 3.1: The Intracranial Pressure-Volume relationship. The graph depicts the exponential relation of the intracranial compliance: initially, when the volume rises, ICP barely increases until approximately 25-30 mmHg because of the compensatory mechanisms that provoke the displacement of CSF from the cranial to the spinal compartment. Whereas, when the compensatory mechanisms are exhausted/ or when auto-regulation is damaged, further small variations of the intracranial volume cause significant and dramatic increases in ICP [26].

ICP varies because of the age, the body position, the clinical and physiological conditions, the brain activity, the cardiovascular function and the respiratory function of the patient: in a good health adult person the ICP values range from 5 mmHg to 15 mmHg; in a healthy children and in a supine position the values range from 3 mmHg to 7 mmHg and in an infant, from 1.5 mmHg to 6 mmHg. In

a vertical position, the ICP of a healthy person assumes a negative value, approximately -10 mmHg without exceeding -15 mmHg.

ICP values above 20 mmHg are pathological (intracranial hypertension, ICH) and they demand an immediate control measure; whereas ICP values about 40 mmHg are intolerable and life-threatening: in general, high ICP levels can cause physical disabilities, irreversible brain damages and in the worst case, also the patient death.

The main purpose of controlling ICP is to monitor the cerebral perfusion pressure (CPP), which is the pressure differential across the MAP and the ICP; CPP is responsible for a correct blood perfusion and oxygenation of the total intracranial components: a sufficient CPP level is required to maintain a stable CBF; an ICP increase causes a reduction of blood flow to the brain.

An accurate and continuous monitoring of the ICP value is important to clinically diagnose a neuropathology and to control the patient cerebral condition after an accident or a trauma; in addition it is necessary to define the correct treatment for the patient with different neurological, neurosurgical and medical conditions.

ICP monitoring permits instantaneous measurements of ICP and the clinician can obtain more informations about intracranial pressure dynamics and brain compliance from the waveform assessment.

3.2 The standard ICP measurement techniques

Different methods exist to detect and to measure ICP and they can be classified into two categories: *invasive and direct measurement techniques* and *non-invasive measurement techniques*.

The clinician chooses the correct type of the monitoring technique according to the clinical patient conditions, to the risks associated with the chosen approach and to the possible need of CSF's drainage.

3.2.1 Invasive ICP measurement techniques

The invasive measurement techniques provide direct signals from a CSF occupying space, brain tissue or dura mater and they include : *External Ventricular Drainage (EVD)*, *subarachnoid bolt* and *microtransducer ICP monitoring devices*.

ICP can be invasively detected in different intracranial anatomical areas, like the intra-ventricular, intra-parenchymal, epidural, subdural, subarachnoid areas (Figure 3.2.); the neurosurgeon evaluates which area is the optimal point to measure ICP.

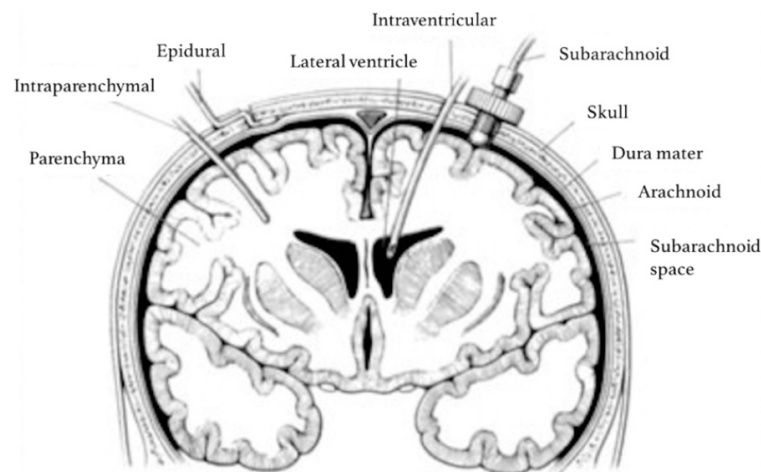


Figure 3.2: Access points in the intracranial cavity for invasive ICP measurement techniques [27]

External Ventricular Drainage, EVD

It is considered the "gold standard" in the ICP measurement field since it is a reliable and accurate method that also permits the CSF therapeutic drainage, in case of elevated ICP, and the antibiotic drugs administration when infection occurs due to the investigation method itself.

A catheter is positioned within one of the lateral ventricles, through a burr hole; it is externally connected to a saline solution filled tube by a three-way valve: the pressure inside the catheter balances the intra-ventricular pressure, and it is detected by an external pressure transducer held at the same level of the patient head and connected to a monitor or a collection bag.

In addition to the advantages described above, EDV can be recalibrated at any time after the ICP measurement, by resetting the transducer at the atmospheric pressure level (zero reference point).

On the other hand, this measurement technique presents also some limitations and disadvantages. EDV is characterized by patient restricted mobility and hospitalization, an hemorrhage risk with a rate of 5-7% during the catheter insertion and by an infection rate of more than 5%; the infection is due to: the burr-hole, the prolonged use for more than five days of the catheter, the intra-ventricular or subarachnoid hemorrhage, the catheter misplacement and the use of a faulty or a non-sterile catheter. Moreover, this technique does not allow to long-term monitor ICP because of the infection risk; lastly, the catheter placement depends on the ventricle size: if the ventricle is thinner, like in a young patient, the catheter insertion proves to be more complicated.

Subarachnoid Bolt

A hollow screw is positioned, through a hole executed in the patient skull, in the sub-arachnoid space; then it is connected to an external fluid filled tube and a pressure transducer. This ICP measurement system is currently disused and it does not permit CSF's drainage; as it is quickly and easily placed, without accessing the brain ventricles, subarachnoid bolt is characterized by a low rate of infection and a low rate of brain trauma. On the other hand this detection method underestimates the measured ICP value and it is inclined to some errors like screw misplacement and its occlusion by debris [26].

Micro-transducer ICP monitoring Devices

This class of invasive ICP measurement devices has been developed in the last 20 years and it includes *fiberoptic devices*, *strain-gauge devices* and *pneumatic sensors*. They prove to be an efficient alternative compared to the "gold standard" method, because these monitoring devices provide ICP measurements comparable to the assessments with the intra-ventricular catheters. Furthermore they are minimally invasive, they are able to record ICP regardless of the patient positioning and they have minimal baseline drift if placed for a few days; anyway they do not allow the therapeutic CSF's drainage and they do not ensure the ICP reduction.

The miniaturized transducers are positioned on the tip of a catheter, which can be inserted in different intracranial areas, such as the epidural area, the subdural area and the intra-parenchymal area, depending on the specific device.

Consequently, the pressure transducers are directly placed in the intracranial space and they are in direct contact with CSF, unlike the previous methods where the pressure transducer is external (micro-transducer ICP monitoring devices do not need a fluid-filled tube system to communicate ICP value to an external pressure transducer; thus the erroneous readings concerning to the obstructions, air bubbles or movement of the patient fluid lines are no longer a concern).

Fiberoptic devices

The fiberoptic devices use the reflection light to detect ICP: the light is transmitted through a fiberoptic wire in the direction of a mirror, which is moved by a flexible membrane or diaphragm situated on the tip of a tight fiberoptic catheter. ICP variations displace the mirror and changes in reflected light intensity to a return fiberoptic 2are converted into ICP values [28, p. 151].

An example of a fiberoptic monitoring device is the "Camino ICP Monitor" (Natus Neuro, Middleton, WI, USA): it is a compact and portable device, constituted by a touch-screen monitor with an user-friendly and intuitive interface, where an intra-parenchymal fiberoptic catheter is connected.

This tool permits to real-time capture instantaneous ICP values when catheter is inserted in the brain, but also to detect ICP trend data on a period prolonged for more than 5 days. Regardless it is incompatible with MRI.

The system permits an *in vivo* recalibration only in cases with suspected wrong measurements and it allows the positioning of the device through the same burr-hole, without increasing the infection risk.

In general, fiberoptic devices have several advantages: they can be easily and quickly placed, they allow direct, minimally invasive and reliable ICP readings also in patient with particular pathologies (for example compressed ventricles), where the intra-ventricular catheter insertion (EVD) can be difficult. In addition, they provide ICP waveform with a good resolution; and they have a low risk of infection and hemorrhage. They also have some disadvantages: the device cost is high; fiberoptic catheters are fragile and disposable; the devices cannot be re-calibrated *in vivo* after their insertion and they may be subjected to drift² when they are used for more than five days [29].

Strain-gauge devices

Strain-gauge ICP monitoring devices exploit the change in electrical resistance in response to ICP, which is translated into a pressure dependent electronic signal; the pressure variations cause the sensor diaphragm bend, provoking a change in the electrical resistance of the piezoresistive strain gauge, yielding the ICP value.

An example of these devices is the “Codman MicroSensor” (Codman&Shurtleff, Inc., Raynham, MA, USA): a miniaturized piezoelectrical strain-gauge is installed on the end of a thin flexible cable in nylon; the wire is positioned within the intracranial space (via a parenchymal, or subdural or intra-ventricular access area) through a twist drill hole, to directly monitor ICP.

The ICP collected data are electronically transferred to an external monitor, without using a hydraulic or fiberoptic system.

This device is accurate, reliable, stable and with a low daily drift; it is used both for the instantaneous ICP measurements and for the continuous ICP collecting data for a maximum of two weeks in order to avoid infection and other complications, due to the external wiring through the skin.

²The drift of the ICP sensors is calculated as the difference between the initial pressure value, when the sensor is calibrated (0 mmHg) and the final pressure value after a known time period; it is an important parameter as it can indicate the potential deviations from the real ICP of patient. Drift can be provoked by some probes mechanical defects or by the material used for the probes construction [29, p. 439].

The micro-sensor is also compatible with MRI and it does not require constant alignment of the transducer to the patient’s head and a periodic re-zeroing.

Pneumatic Sensor

The ICP monitoring devices with a pneumatic sensor use a small air-filled balloon, installed on the catheter’s tip, which is inserted into the intracranial space to detect both ICP variations and intracranial compliance.

The air-pouch probe can be inserted into the patient’s ventricle, parenchyma or dura for intra-ventricular, intra-parenchymal or epidural ICP measurements respectively. The pressure exerted on the balloon surface, which causes its compression, will equal the surrounding pressure, that is the ICP.

An example of these devices is the “Spiegelberg Brain Pressure Monitor (Spiegelberg GmbH & Co.KG, Hamburg, Germany): it is a fluid-filled catheter system constituted by an air-pouch probe connected to a monitor with a simple and digital interface, that permits to display both the ICP’s mean value and its waveform. The intracranial pressure is transmitted through the thin pouch wall to the air volume in the balloon and it is transformed into an electric signal by the pressure transducer.

In contrast to the others micro-transducer ICP monitoring devices previously described, which cannot be recalibrated after their *in vivo* insertion, the “Spiegelberg Brain Pressure Monitor” is capable to automatically re-calibrated every hour, avoiding drift problems and ensuring accurate results. Despite of this important advantage, the device is characterized by a limited bandwidth which makes impossible the analysis of ICP waveform.

In general, the different implantable micro-transducers previously described in this section, share the same features: these systems ensure infection rates and risks of hemorrhage lower than EVDs; they can be easily and quickly placed but they are expensive and, except pneumatic sensors, they usually cannot be recalibrated after their in situ insertion, so they could provoke imprecise ICP’s measurements. Micro-transducers are used in cases where EVD’s placement is not successful or when, according to the clinicians, CSF’s drainage is not necessary [27].

3.2.2 Non-invasive ICP measurement techniques

The invasive ICP measurements techniques are accurate and reliable, but because of the infection and hemorrhage risks, the elevated costs related to the sensor insertion and the request of a specialized neurosurgeon to execute the measurements, the invasive techniques cannot always be realized. For these reasons, it has been necessary to find some alternative and efficient methods to detect ICP: the non-invasive ICP monitoring techniques. They are characterized by null risks of infection and hemorrhage and they allow long-term monitoring without inserting a new catheter or a sensor in the patient brain, at every measurement. Moreover, they are considered as supporting tools, since they provide an approximate ICP's evaluation and they help in deciding which patient needs an invasive ICP's monitoring. Through the non invasive methods, the physician can monitor the ICP's level when the invasive techniques cannot be applied because of some particular patient clinical conditions or in absence of the specialized neurosurgeon.

These techniques are screening and prevention tools; they provide an ICP's assessment as they measure physiological variables that are indirectly correlate with ICP.

The non-invasive methods are numerous but, in this section, the techniques principally performed in the neurological field will be briefly described.

Trans-cranial Doppler Ultrasonography (TCD)

TCD uses the ultrasound (US) and through US, the clinician detects the cerebral blood flow (CBF) velocity in the middle cerebral artery: when ICP rises up, CBF is impeded and, consequently, the CBF velocity, in the investigated artery, decreases.

Successively, a parameter named *Pulsatility Index (PI)* is calculated as the difference between the blood flow systolic velocity and the blood flow diastolic velocity, divided by the mean flow velocity. This equation can only be calculated when ICP values are lower than approximately 30 mmHg; PI's value equal to 1 can affect a wide ICP range between few mmHg and about 40 mmHg [28, p. 158].

A correlation between ICP, PI and the slopes of the TCD waveforms has been found in several scientific studies, through some comparisons between ICP's values acquired by the accurate and dependable invasive techniques and ICP's value obtained via TCD.

As TCD provides an ICP's estimate, this technique slightly supplies imprecise ICP's measurements, with a margin of error of $\pm 10 - 15$ mmHg; in addition, TCD cannot be applied to older patients because ultrasound cannot penetrate the skull.

TCD is a cheap and portable technique, it provides real-time informations with high temporal resolution but it requires inter and intra-observer variation³ and a trained and competent physician that is able to find the correct blood vessel and to accurately interpret the results. However, the last aspect has improved over recent years and TCD is routinely performed in many hospital centers.

TCD is a screening technique that provides a single measurement at any time, so it is not practical to continuously monitor ICP.

Optic Nerve Sheath Diameter (ONSD)

The optic nerve is physiologically surrounded by the dural sheath; the space between the nerve and its sheath is a continuation of the CSF-filled subarachnoid space, whose pressure corresponds to ICP. When ICP increases, the optic nerve sheath tends to expand and the sheath diameter variations can be detected by the trans-ocular ultrasonography. Several studies demonstrated a relation between ICP invasively measured and the sheath diameter changes of the optic nerve.

ONSD detected by ultrasound is a simple, quick and cheap method but it cannot be applied to patients with facial injuries, tumors, serious diseases and inflammations; in addition, it requires training and intra and inter-observer variability, although it is lower than variability of the previously technique. The technique specificity decreases when ICP's fluctuations are very high.

Currently, ONSD is not an accurate and reliable method to completely substitute the invasive ICP measurement techniques but it has a good discriminatory property: it is able to differentiate high ICP's values (ICP > 20 mmHg if sheath diameter exceeds 5 mm) from low ICP's values.

ONSD is a potential screening and prevention tool to apply when direct ICP monitoring methods are non promptly available and to use with the aim to individuate elevated ICP.

³The intra-observer variation is the variation attributed to the quantitative measurements of a physical quantity realized by the same observer. The inter-observer variation is the variability concerning the quantitative measurement realized by different observers.

Tympanic Membrane Displacement (TMD)

The tympanic membrane displacement occurs when stapedius reflex⁴ is externally stimulated through an acoustic signal; TMD indirectly measures the cochlear fluid pressure related to ICP: CSF and perilymph, an extracellular fluid that characterizes the inner section of the ear, communicate throughout the cochlear channel; an elevated ICP's value is directly transmitted to the stapes covered by a flexible membrane: ICP's variations cause changes in the stapes and in the initial position of the membrane, and they influence the direction and the amplitude of the tympanic displacement, in response to an acoustic stimuli.

On the audiogram, that is the TMD layout, a negative pressure peak, concerning the inward tympanic membrane displacements, indicates a high ICP's value; whereas the outward displacements, so a positive pressure peak on the audiogram, state a normal or a low ICP's value.

This method also provides an inaccurate ICP's evaluation with a margin of error of ± 15 mmHg; so it is an imprecise technique that can be used as a screening and prevention tool with the purpose to individuate high ICP's levels.

Imaging based methods

Magnetic Resonance Imaging (MRI) and Computed Tomography (CT) belong to this category; this imaging techniques permit to detect big anatomical variations of the patient brain volume in response to an elevated ICP.

The motion-sensitive MRI detects CSF and trans-cranial blood volumetric rates during the cardiac cycle within the brain and it allows to measure ICP by the *Elastance Index (EI)*; it is calculated as the ratio between pressure and volume variations, in fact it is the opposite of the compliance. EI seems to be correlated with invasively measured ICP with a correlation coefficient equal to 0,96 [30].

MRI provides qualitative informations about ICP through a measurement at a time; so it is considered as a screening technique that it could be used to assess if patient needs to an invasive monitoring of the ICP's level, after a traumatic head injury. In addition, the MRI also could be used to diagnose and to evaluate several chronic cerebral disorders, related to elevated ICP's values, like hydrocephalus.

⁴It is an involuntary contraction evoked by an acoustic stimulus of the stapedius muscle, the smallest skeletal muscle of the human body placed in the ear, whose aim is to stabilize the stapes.

On the other hand, CT is more available than MRI and less operator dependent as compared to US, used in the TCD's technique.

Some pilot studies proved that both MRI and CT have good discriminatory properties: MRI, by assessing the trans-cranial blood and the CSF flow, is able to differentiate patients with normal or elevated ICP's values; whereas, CT, by determining a ratio between the CSF's volume and the total intracranial volume, is able to differentiate normal and elevated ICP's values.

3.2.3 Telemetric Sensors

In recent years, different methods to detect ICP and to transmit outwards its data via telemetry have been developed because of the previously described limitations of the invasive ICP-measurement techniques and the inaccuracy of the non-invasive ICP measurement techniques.

Currently, the application of the telemetric ICP monitoring in the hospitals is still limited due to the several technical problems despite the great support it can provide to shunted-patients or for hydrocephalus, arachnoid cysts and others cerebral diseases treatments.

The advantages of a telemetric ICP sensor are numerous: it is a wireless and minimally invasive system that reduces the infection risk; it permits to detect overdrainage, under-drainage or shunt malfunctioning in case of a patient with a shunt device and it is also able to detect elevated ICP's levels in the absence of specific patient symptoms or when MRI or other imaging techniques results do not reveal nothing. Furthermore, through the telemetric devices, the ICP's measurements can also be executed at home during the daily patient activities, reducing the hospitalization period.

Nowadays two telemetric sensors are commercially available and both enjoy the advantages previously described: "Raumedic Neurovent P-tel" (Raumedic company, Helmbrechts, Germany) and "Sensor Reservoir/Sensor Prechamber" (Aesculap-Miethke, Tuttlingen and Potsdam, Germany).

Raumedic Neurovent P-tel

The *Raumedic Neurovent P-tel*, shown in Figure 3.3, is a device constituted by: an implantable probe named "Neurovent P-tel" to detect ICP; an external

reader unit, named “Raumedic TDT 1 readP”, constituted by a radio-frequency transmission antenna and by a recording device powered by a rechargeable battery; a monitor to display ICP’s values or its waveform and a portable recording device that includes a USB port and a data management and analysis software.

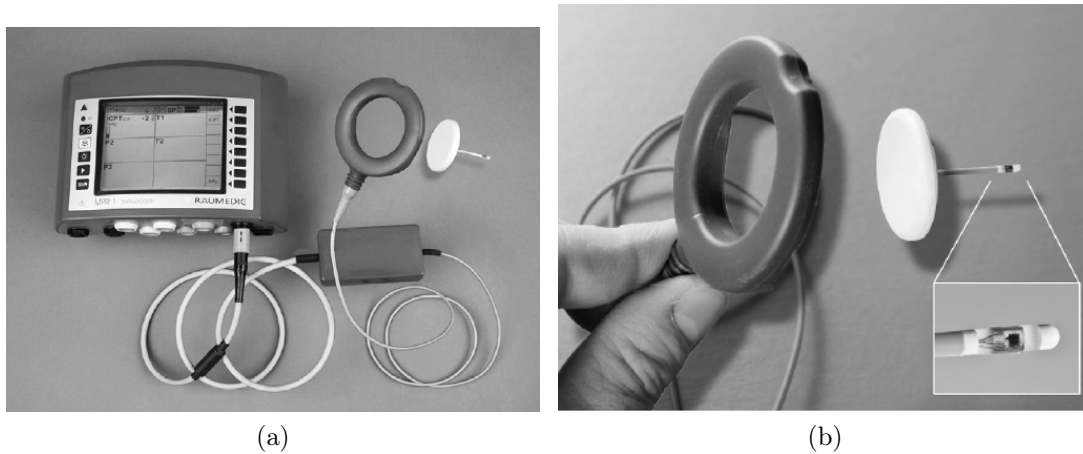


Figure 3.3: The Raumedic Neurovent p-tel telemetric sensor for ICP monitoring. (a) Monitor and storage unit are connected to the antenna, the external reader unit named Raumedic TDT 1 readP; by placing the reader unit on the patient scalp close to the implant (white probe in figure) it is possible to establish a wireless connection for measurement of the ICP’s value. (b) The Neurovent P-tel implantable probe for the intraparenchymal ICP’s measurements: the polyurethane catheter tip comprises a piezoresistive pressure transducer constituted by numerous electric resistors. These resistors are doped on a flexible membrane which stretches depending on the current ICP. On the left, the reader unit that simultaneously allows, through radio-frequency identification technique, energy supply (from the antenna to the implantable probe) and data transmission (from the implantable probe to the reader unit) about the current ICP [30].

The telemetric probe comprises a piezoresistive pressure sensor, installed on the distal end of the polyurethane catheter and placed within the brain intraparenchymal area, and a round ceramic housing transducer with an internal microchip placed under the galea aponeurotica, a tough layer of fibrous tissue which covers the higher part of the human cranium (Figure 3.4).

The pressure sensor is constituted by several electric resistors doped on a flexible membrane, which straightens according to ICP since it is in direct contact with the brain parenchyma. When the membrane stretches, the resistors length and

electrical resistance change; these variations are revealed by a microchip in the probe housing that converts the electric variations into ICP's values. The microchip activation occurs only when the antenna is placed close the housing.

In fact, during the measurements, the clinician arranges the external reader unit (Raumedic TDT 1 readP) on the patient scalp, directly on his skin or on the bandage: the ICP's recording is accomplished only when the external reader unit is placed close to the housing. The implantable probe communicates with the external reader unit through radio-frequency identification technique; it is a bidirectional communication because the antenna simultaneously allows energy supply (from the antenna to the implantable probe) and data transmission (from the implantable probe to the reader unit) about the current ICP.



Figure 3.4: X-ray image that shows the implantable probe P-tel on the left hemisphere of a shunted patient (on the right side it is possible to notice two different valves in series). The catheter with the pressure transducer on its tip is placed in the frontal subcortical brain parenchyma, whereas the probe housing is externally located on the skull surface.[30]

The implantable device does not require calibration after every ICP measurement and it permits a continuous ICP monitoring until 29 days; it is compatible with MRI, if its static magnetic field is lower than 3 Tesla. It allows two different types of ICP's measurements: a short term measurement with a sampling rate of 5 ICP values every second or a long term measurement with a sampling rate of 1 ICP

value every second. These different samples concerning the data storing capacity, so it is not necessary to eliminate every time data previously detected.

Raumedic Neurovent P-tel is also equipped with an acoustic alarm system which rings when ICP exceeds an imposed threshold.

The Miethke Sensor Reservoir/Sensor Prechamber

The Miethke Sensor Reservoir/Sensor Prechamber is the second telemetric system commercially available from 2015.

It can be integrated in an existing shunt device and it consists of two elements, an implantable unit named “Sensor Reservoir” and an external reader unit named “Sensor Reservoir Reader”: if the internal unit is in line with the shunt valve system, the device takes the name of *Sensor Prechamber* otherwise, if it is placed in burr-hole position, *Sensor Reservoir (SR)*.

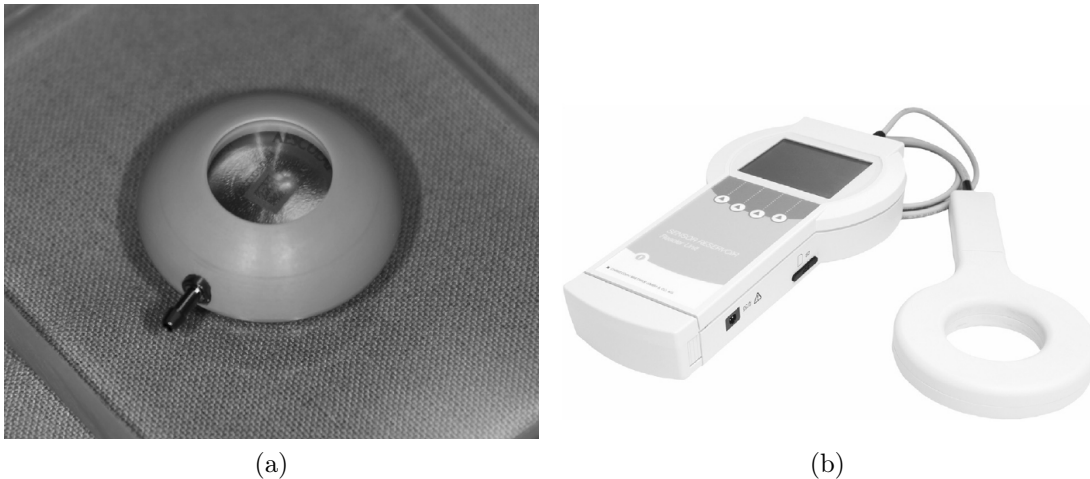


Figure 3.5: The Sensor Reservoir telemetric sensor for ICP monitoring[31].

Antes et al. [31] report the second configuration. The implantable unit of the Miethke Sensor Reservoir (Figure 3.5.a) is constituted by a roundly configuration housing, in polyether ether ketone, whit a silicone dome and two outlet sections, one in the lower part of the unit directly connected with the ventricular catheter and the other connected with the proximal catheter. Silicone dome permits the drugs administering, the CSF’s removal and the valve inspections.

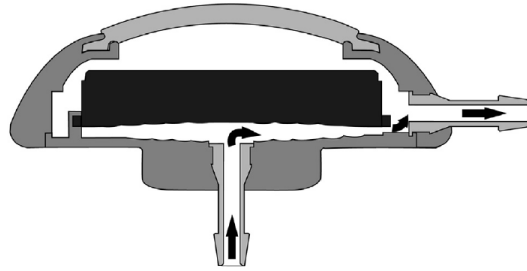


Figure 3.6: Cross section of the Sensor Reservoir implantable unit.[31].

The implantable unit is a kind of CSF reservoir and it comprises a measuring cell covered by titanium that protects it from possible CSF's penetration; the measuring cell consists of an application-specific integrated circuit (ASIC) with 64 capacitive pressure sensors: when CSF goes in the reservoir, through the outlet section connected to the ventricular catheter, it perfuses the measuring cell and the exerted pressure by CSF is directly transmitted to the ASIC (Figure 3.6).

The Sensor Reservoir reader consists of an antenna connected by a cable with a monitor; like the previously telemetric sensor, the reader simultaneously allows to supply energy to the Sensor Reservoir and to transmit ICP detected data to a monitor that displays ICP value and curves, by a radio-frequency identification technique. Its sampling rate is up to 44 Hz and the ICP readings are automatically stored on an SD card.

The Miethke Sensor Reservoir is a passive device: the ICP measurements occur only when the external reader with its radio-frequency transmission antenna is placed on the patient scalp, close to the inner reservoir. The implant could last for an unlimited period except some complications.

This telemetric ICP sensor allows to non-invasively verify the over-drainage and the under-drainage phenomena and to also evaluate the correct functioning of the shunt system. Moreover it permits the neurosurgeon to optimally set the shunt valve opening pressure according to the ICP level detected by Sensor Reservoir itself and to choose the correct surgical procedure. It allows three different types of ICP measurement that can be directly selected in the external reader: quick, continuous and individual measurement.

The infection rate is 5-6% lower than the invasive ICP measurement techniques infection rate (whose range is between 5% and 15%).

Despite of its advantages, Sensor Reservoir does not permit to accomplish continuous ICP measurements for at least 24-48 hours, useful to detect some important ICP parameters like ICP peaks or pathological slow waves. This limitation is principally caused by the heaviness and the big dimensions of the external reader transmission antenna, that prevents the permanent fastening of the reader unit on the patient scalp. It could also cause the disorder wound healing appearance in patient with thinner skin, due to the inner unit height (approximately 8 mm). In addition, the ICP measurement accuracy could decrease if the implanted unit of the Sensor Reservoir rests within the patient brain for over 5 years, causing so some drift problems.

Lastly this device is expensive, so it cannot be used routinely; its use and insertion, to identify and solve complex shunt problems, is recommend as final approach to obtain measurements about the correct functioning of the shunt system.

3.3 Some examples of alternative proposals of ICP measurement systems in literature

At the beginning, the purpose of this thesis work was to design a mechanical pressure sensor to monitor the intracranial pressure and to identify if catheters were clogged. The initial idea was both to insert the sensor inside an existing shunting device using the pre-chamber or the reservoir and to investigate the sensor, in a minimally invasive way, through ultrasounds or other imaging techniques, like MR or X-Ray, to which a shunted patient normally undergoes.

From the beginning of this work, we preferred to shelve the idea to create a sensor with electronic components, for different reasons: the area treated by a shunt system is fragile and, to design an electronic pressure sensor, it is also necessary to simultaneously meet the needs of specific dimensions, biocompatibility, type of power supply, type of data transmission mode to an external receiver, type of frequency band to sample data etc. .

However different studies in scientific literature show that the idea of a mechanical pressure sensor had already been proposed by several researchers, so in this section we will describe some of these projects.

3.3.1 Intracranial Pressure Sensor

Matthew Murray and Jared Shimada [32] propose, in their bioengineering senior thesis work, an ICP sensor: the developed prototype could be integrated in an existing shunt system and it could be investigated through US, with the purpose of helping neurosurgeons in the intracranial hypertension diagnose and treatment, of draining CSF, of suppling immediate ICP readings and of assessing the potential presence of some occlusions inside the catheters.

It is a minimally invasive, not expensive and easy to use sensor, with a highly sensitivity and accuracy.

The intracranial pressure is made of epoxy resin and it consists of a capillary tube with a diameter of $50\mu m - 100\mu m$ and permeable to gas that communicates with an air-filled reservoir: when the CSF enters the tube, an air-liquid interface will be create at a specific height; the fluid-air line position will determine the ICP level inside the cranial cavity and it could be a first indication of occlusion within

the catheters.



Figure 3.7: Prototype of the intracranial pressure sensor [32]

The prototype of the ICP sensor has been fabricated by applying some thin layers of epoxy resin, successively polymerized by UV light, on two Polydimethylsiloxane (PDMS) molds, with the purpose of obtaining the top and bottom surfaces of the ICP sensor.

The PDMS molds have been created by spin coating a thin layer of a cross-linker and PDMS based mixture, on a photomask; the photomask, containing a negative of the structure required to create the PDMS mold, instead has been designed on the AutoCad 3D software and fabricated through the soft- lithography technique.

A single drop of PDMS has been applied to the negative structures to increase gas-reservoir size and so to avoid its collapsing.

The authors modified the design of the ICP sensor over the period of their thesis work; compared to the initial prototype design, the researchers changed the dimensions of the air reservoir to increase sensor specificity and sensitivity and also the reservoir's geometry to create a tapered end useful to attach the reservoir to the capillary tube. In particular they designed three different sensor templates, each with different channel diameters ($100\mu m$, $200\mu m$, $300\mu m$) for the purpose of creating a template for a mask.

Furthermore the top and bottom surfaces have been plasma treated to prepare them to their union: after plasma treatment, the sensor's channel has been aligned and clamped with the tapered end and cured under UV light.

Lastly the capillary tube has been fitted to the completed sensor, by inserting it into the sensor channel and sealing it with PDMS.

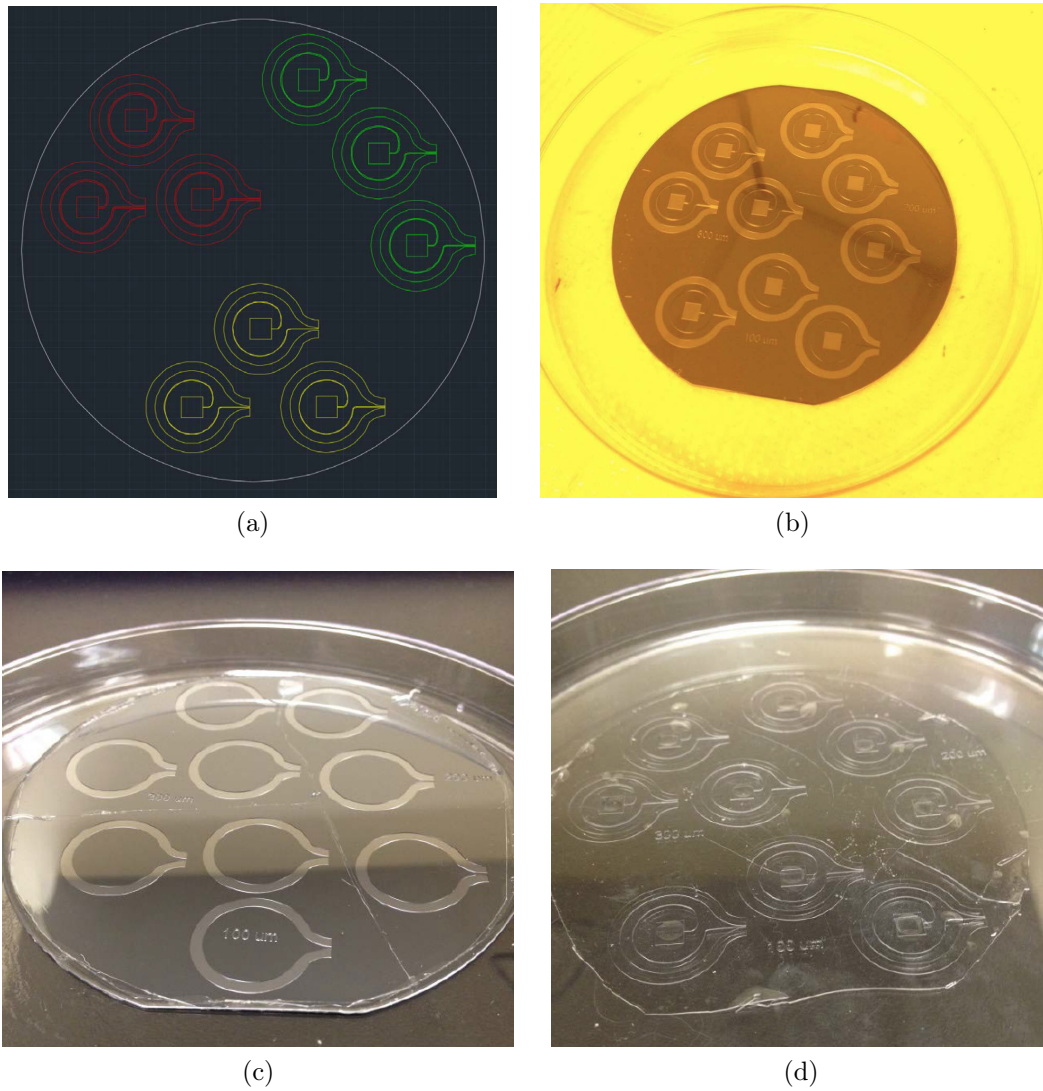


Figure 3.8: Some fabrication steps of the ICP sensor prototype. (a) The 3D model of the ICP sensor prototype created through the AutoCad software. Three different sensor templates with different channel diameters: $100\mu\text{m}$ in yellow, $200\mu\text{m}$ in green, $300\mu\text{m}$ in red. (b) The photomask created from the AutoCAD model, by soft-litography; it contains a positive of the structure of the ICP sensor but a negative of the structure required to create the PDMS mold for ICP sensor prototype. (c) and (d) The bottom surfaces and the top surfaces respectively obtained by applying some thin layers of epoxy resin to PDMS molds, created by spin coating a cross linker and PDMS based mixture on the photomask, to create the sensor. The epoxy resin has been succesively polymerized by UV light.

The prototype of the ICP sensor is able to accurately measure pressure range between 0 mmHg and 60 mmHg ($0\text{ cmH}_2\text{O} - 81,5\text{ cmH}_2\text{O}$); it is also efficient to both detect ICP in normal conditions (0-15 mmHg) or when ICP exceeds 20 mmHg in pathological conditions.

The developed sensor has been only in vitro tested in a test rig constituted by: the sensor with a channel diameter of $200\ \mu\text{m}$, a water-filled chamber connected to a pressure simulating device, called *Elveflow* and by a light microscope, connected to a software called *Infinity Analyze* that permits to capture microscopic images.

The researchers tested both the sensor without capillary tube and the sensor with capillary tube with a diameter of $50\ \mu\text{m}$ attached to the sensor channel; they proved that in both modalities the sensor is able to register changes in pressure through variations in the position of the fluid-air interface.

Some pressure variations between 0 mmHg and 22,5 mmHg have been simulated through the “Elveflow” device, also reaching ICP values roughly 45 mmHg to verify if the sensor could accurately measure ICP over the physiological ICP range.

A linear relation between pressure changes and fluid-air interface distance has been found and it is shown in Figure 3.9: the air-fluid interface moves about 0,152 mm every 3,75 mmHg.

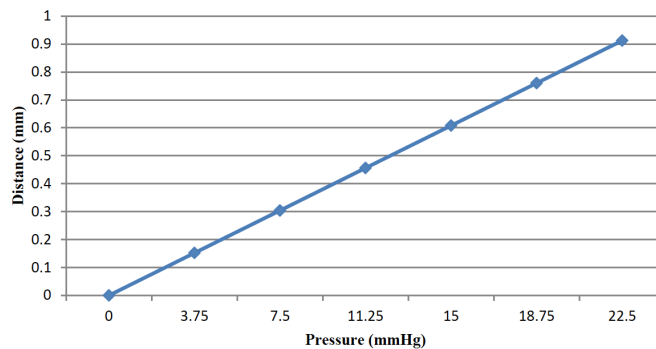


Figure 3.9: The linear relation between the pressure variations in mmHg and the distance of the fluid-air interface: the air-fluid interface moves about 0,152 mm every 3,75 mmHg up to 22.5 mmHg [32].

The Figure 3.10 shows instead the different positions of the fluid-air interface when pressure is 0 mmHg and when it is 22,5 mmHg; the interface moves about 0,912 mm.



Figure 3.10: The position of the fluid-air interface when pressure assumes the smallest value, 0 mmHg, and the greater value 22,5 mmHg regarding the pressure range tested. The interface totally moves about 0,912 mm [32].

The ICP sensor in this work has been tested only in water to verify its functioning. Additional in-vitro experiments to determine the safety and the efficiency of the sensor in a physiological environment are necessary.

The device should be undergo some specific test like toxicity test, biocompatibility test and it should be mechanical characterized to know its stress-strain curve and its loading characteristics.

The authors only designed and developed a prototype, so this device is not commercially available. In this work, they did not read the fluid-air interface by ultrasounds, so in future the device could be tested through an ultrasound machine to verify its visibility and to test the specificity of the pressure readings. To obtain a greater accuracy in ICP readings, the authors suggested, in future works, to increase the air reservoir sizes and to minimize the sensor channel size, so that the interface can move also for small ICP variations.

3.3.2 The Baric Probe

David Limbrick et al. [33] in their work propose a long-term implantable ICP monitoring device, termed *baric probe*, that can be interrogated through an ultrasound probe, to verify the correct functioning of a shunting system. It is a simple device, MRI compatible, inexpensive and it can be easily implanted in the patient brain through the standard surgical techniques. The baric probe can be included inside the shunting system or it can be implanted as an additional part in line with a shunt.

The baric probe design is very simple and it is based on the mechanical compression of a gas; it consists of three components: a subdural fluid bladder as a pressure sensor, a subgaleal indicator and a connecting catheter. The Figure 3.11 depicts the baric probe prototype developed in this work.

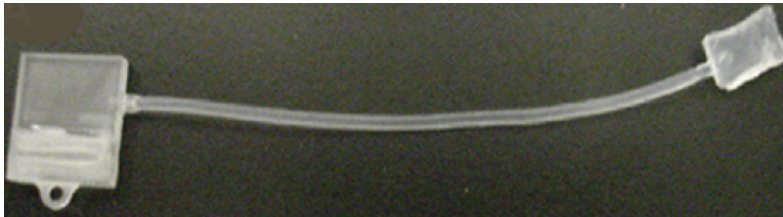
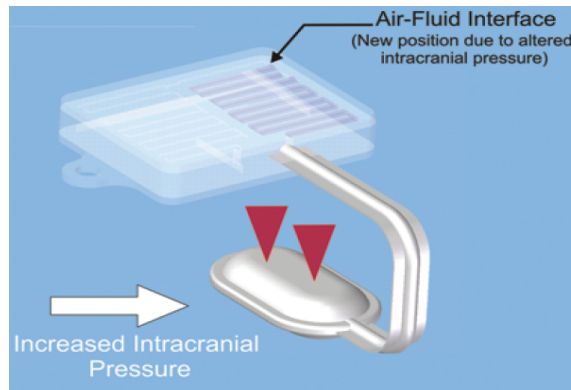


Figure 3.11: Prototype of the “baric probe”, a long-term implantable ICP monitoring device [33].

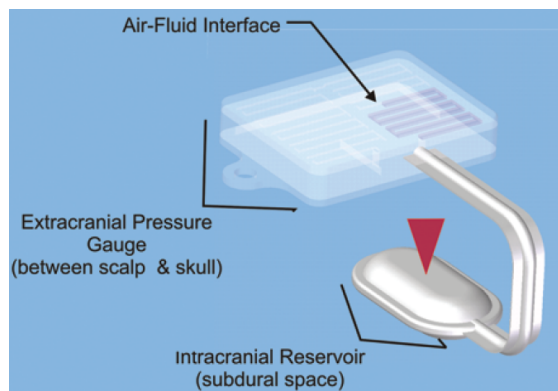
The subdural fluid bladder and the connecting catheters are saline solution filled; the subgaleal indicator is constituted by several air-filled channels.

The indicator allows fluid to flow inside its channels according to the ICP variations; it is rigid to impede the atmospheric pressure from influencing ICP readings.

The baric probe functioning is simple and immediate: when the pressure exerted by CSF on the subdural bladder increases, the gas within the bladder is compressed, thus forcing the saline solution inside the connecting catheter to flow into the indicator channels (Figure 3.12(a)).



(a)



(b)

Figure 3.12: Drawings of the basic probe design and functioning. The ICP monitoring device consists of three components, an intracranial reservoir in the subdural space as a pressure transducer, a connecting catheter and an extracranial pressure gauge between scalp and skull. The exerted pressure by the CSF on the the subdural fluid bladder causes the movement of the saline solution in the connecting catheter up to the air-filled channels in the subgaleal indicator, thus creating a fluid-air interface. (b) Because of increasing ICP level, the subdural fluid bladder is compressed, provoking a shift in the position of the air-fluid interface, in comparison with a normal or decreasing ICP level as shown in (a) [33].

Contrarily, when the CSF pressure on the subdural bladder decreases, the saline solution begins to move away from the channels (Figure 3.12(b)).

In both cases, an air-fluid interface inside the indicator channels will form: a handheld pen-sized ultrasound probe, that could be interfaced with any PCs or smartphones, is used to scan the patient scalp and to visualize the channels inside the indicator. The ICP reading is obtained with the ultrasound probe, by detecting

the air-fluid interface through the different reflectivity of air and saline solution.

In this research, the baric probe has been both in vitro and in vivo tested. The in vitro evaluation has been accomplished by sealing the subdural bladder inside a H₂O column (in this way the physiological environment has been simulated) and by leaving the subgaleal indicator exposed to the atmospheric conditions. The pressure exerted on the fluid bladder depends on H₂O column height; in fact, the position variation of the air-fluid interface in the channel, is achieved by adjusting the H₂O column height and thus provoking increases or decreases of the pressure exerted on the bladder.

When the indicator of the baric probe is monitored through ultrasound probe, two different lines could be distinguished: the top line is the reflection of the surface

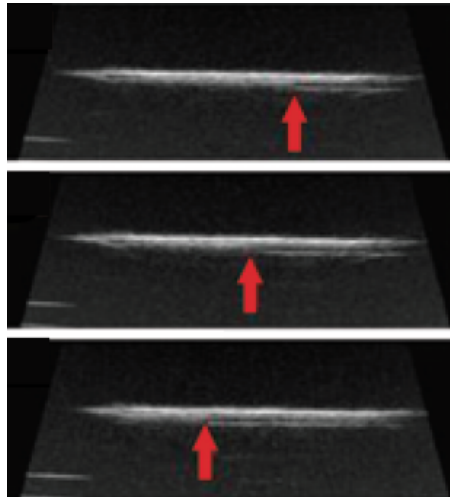


Figure 3.13: The ultrasonographic image of the baric probe under different pressure levels obtained by modifying the height of the H₂O column: from the top under 2, 12, and 22 cmH₂O respectively. Red arrows indicate the location of the air-fluid interface at each setting [33].

of the indicator, while the bottom line is the reflection of the channel within the indicator. When the air-fluid interface is examined, a noticeable step creates in the bottom line, caused by the difference in impedance between the portion of the channel containing air and the portion containing fluid [33, p. 520].

The in vivo test has been accomplished by implanting the baric probe in some porcine models: ICP has been evaluated simultaneously using a fiberoptic ICP

transducer, inserted opposite the baric probe. The ICP variations has been provoked by injecting saline solution through a lumbar drain.

In both tests, a consistent linear relation between increasing pressure and the change in position of the air-fluid interface has been obtained; it is shown in Figure 3.14a for the ex vivo evaluation and in Figure 3.14b for the in vivo test.

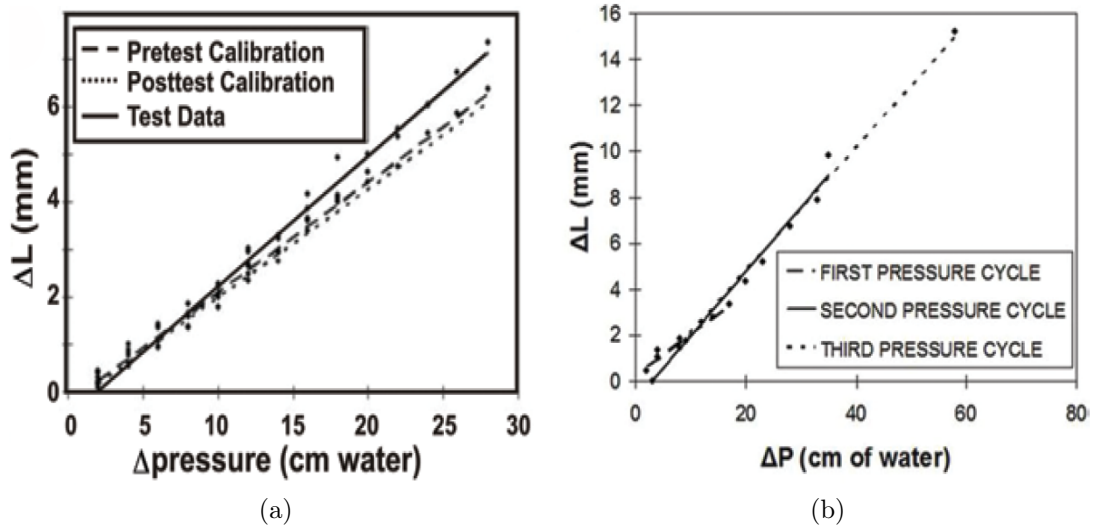


Figure 3.14: The graphic relation between change in pressure (in cmH_2O) and the change in position of the air-fluid interface (in mm). (a) The graph depicts the linear relationship between change in pressure ΔP (in $\text{cm H}_2\text{O}$) and the change in position of the air-fluid interface (ΔL in mm) in a single baric probe prototype, obtained in in vitro test. (b) The graph illustrates the linear relationship between ICP's variations (ΔP in cmH_2O) and displacement of the air-fluid interface (ΔL in mm) in vivo, through 3 separate pressure cycles [33].

Furthermore, the device performance has been also evaluated in a chronic implant in a pig: after 14 days since implantation, the baric probe continued to demonstrate a robust and reproducible linear response to ICP rises.

The baric probe, in this configuration, allows ICP readings within $5 \text{ cmH}_2\text{O}$. It promises to have a low malfunctioning rate, thanks to its simple design; the ultrasound investigation permits to reduce the use of dangerous diagnostic ionizing radiation, in the evaluation of shunt malfunction. Moreover, the pen-sized ultrasound probe, that can interface with a smartphone, could be create the challenge for home use of the baric probe.

By the time of this research, the baric probe was not yet in standard production.

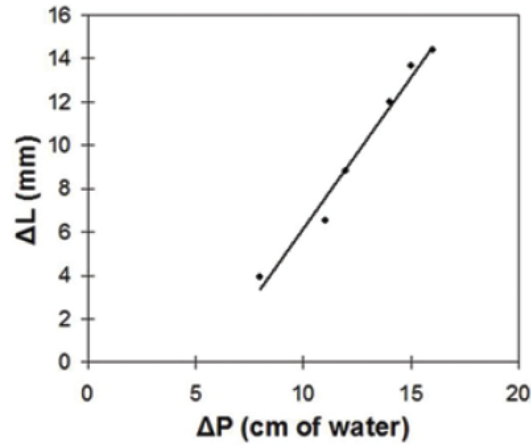


Figure 3.15: The graphic relation between ICP (ΔP in cmH_2O) and the position of the air-fluid interface (ΔL in mm) after two weeks in situ: the graph shows a consistent linear relation after two weeks since the baric probe implantation in the brain of the porcine model. The slope of the ICP and the air-fluid interface is approximately greater than the slope in the other tests; this difference depends on the leakage of gas (air) from the device over time. A problem than could be resolved by coating the baric probe with a gas-impermeable polymer [33].

3.3.3 The snap valve cerebral shunt design

Mitchel et al. [34] in their research work propose a device able to detect the shunt blockage prior to the appearance of the neurological diseases related symptoms by using a snap-through buckling shell (STB). The STB shell can be transformed into a pressure-relief valve, placed in series with the CSF's flow, able to work in the physiological ICP's range (6-25 cmH₂O). The functioning mechanism of the STB is visible through ultrasound and the valve has a form factor similar to the currently available shunt systems. So the device could be successfully used in the clinical application; in fact, despite the STB devices are not currently used in the cerebral shunt systems, they are used in other medical implants, like for example the ventricular assist device (VAD).

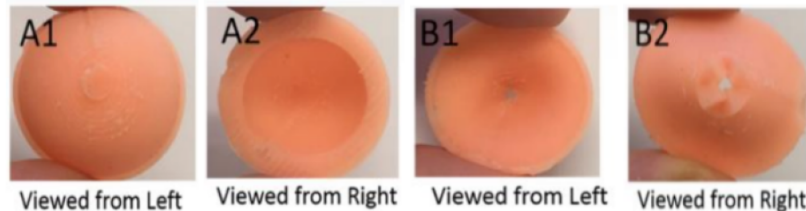


Figure 3.16: The valve snap design and its different configurations in response to the ICP levels or to the testing pressure levels. A1 and A2 depicts the STB shell in a relaxed configuration. B1 and B2 depicts STB shell in an open state, allowing the CSF's drainage [34].

The device is made of silicone and it consists of two elements: a rim to securely place the shell and a hemispheric dome with a hole, exposed to the testing pressure or the ICP's level.

The device has been fabricated with three different thickness (0,5 mm, 0,75 mm and 1 mm) by pouring silicone in the molds created by SolidWorks.

The STB mechanism is explained in Figure 3.17: when ICP assumes values lower than the rebound pressure, the shell is in relaxed or closed configuration (Figure 3.17a). The rebound pressure is that pressure value that allows the shell to get back to its initial conformation.

When ICP instead begin to increase up to a critical pressure threshold, the shell moves into an open configuration (Figure 3.17b); the hole placed in the top of the shell's dome allows CSF to flow from the ventricle to the drainage site, provoking

the ICP decrease. In fact, when ICP assumes again a normal level, in particular when it assumes the value of the rebound pressure, the shell rebounds to its original closed state (Figure 3.17c).

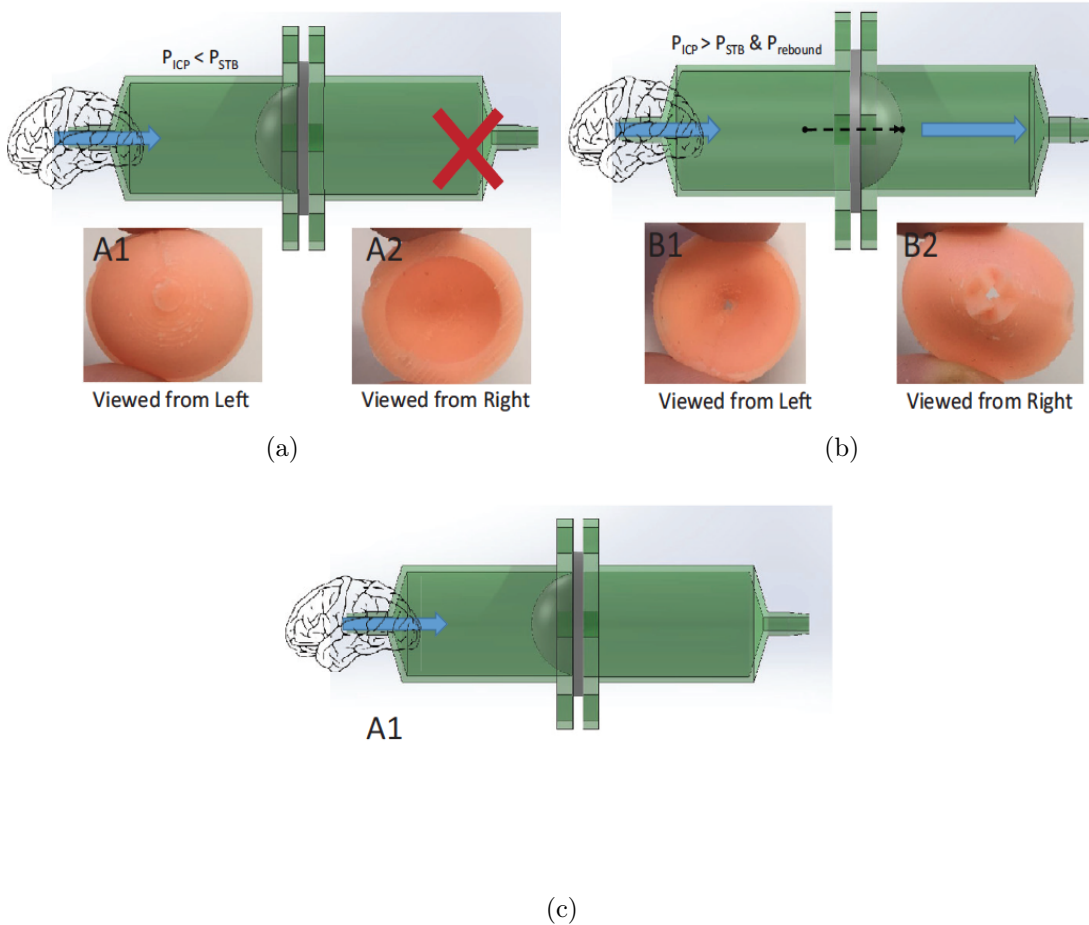


Figure 3.17: Schematic demonstration of the functioning and of the dynamic permeability of the STB device. (a) When the pressure exerted by the CSF (the blue arrow indicate the CSF direction from the brain ventricle to the peritoneal cavity) is lower than pressure that causes the STB event, the shell is in a closed state and it is also impermeable to CSF flow. (b) When ICP is greater than pressure that causes STB event, the shell changes its configuration, moves into an open state and it becomes permeable to CSF flow. (c) As ICP begin to decrease, because of the CSF's drainage, the shell rebounds in its initial configuration (the dashed arrow indicates the rebound phase of the cycle and may cause back-flow or pressure in the catheter) [34, p. 3].

The shell works as a valve by opening a hole in the top side of the dome at a specific pressure and closing the hole at the rebound pressure. Dynamic permeability is the term used to describe the ability for the shell to block flow (impermeable) in one conformation and to allow flow (permeable) in its inverted conformation [34, p. 2].

The STB device in this work has been in vitro tested in a test rig constituted by a small water filled chamber placed above the convex part of the shell, thus leaving the concave part exposed to room air. A water column, sourced by a beaker, has been applied on the convex side of the shell in a relaxed state through a flexible tubing, with the purpose of evaluating the STB event pressures. To simulate increasing ICP, the height of the water column has been steadily raised to increase the pressure exerted by the water column. When the testing pressure assumes a critical value, the shell deformed and begins to drain water through the outlet of the test apparatus. To simulate decreasing in ICP because of the drainage of CSF, once the shell opened, the height of the water column has been instead reduced until the shell rebounded to the closed position and no fluid drained; the pressure relating to the shell rebound event has been recorded as the “rebound pressure”.

A linear relation between flow rate through the open valve and the column water pressure has been recorded.

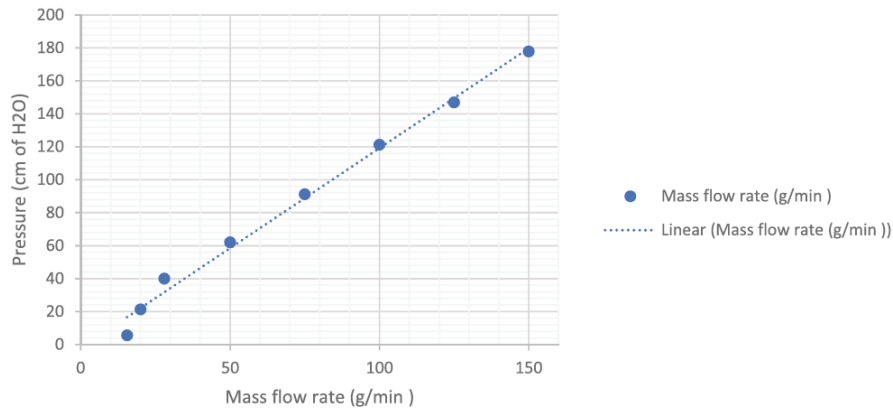


Figure 3.18: The linear relationship between mass flow rate (in $\frac{g}{min}$) through a dome, characterized by 0.5 mm of thickness and 10 mm of radius, and pressure (in cmH_2O) [34].

The snap valve could be monitored through ultrasound allowing the clinician to verify if there is flow or no flow in the shunt system during some clinical operations that raise ICP, like coughing.

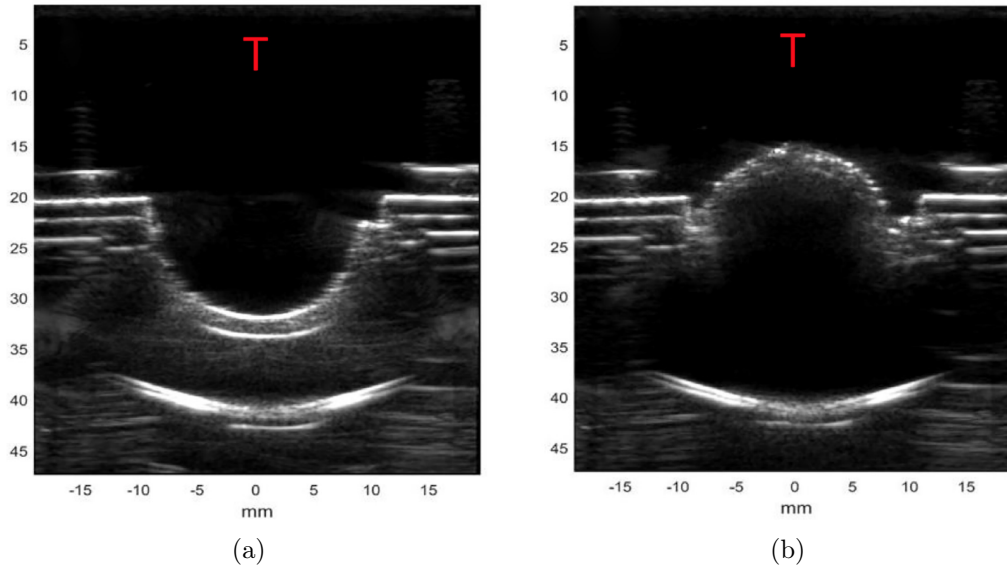


Figure 3.19: Ultrasound imaging of the STB valve achieved with a transducer marked with “T”. (a) The closed shell configuration after rebound event and before a further STB event. (b) The open shell configuration after STB event [34]

In this work, the authors tested several shell parameters like its thickness, its stiffness and its radius with the purpose of identifying the better parameters to create the smallest, efficient and reliable STB valve working in the physiological ICP’s range.

The STB device could reduce the shunt system malfunctioning; it could be used as screening tool, thus reducing the costs related to the diagnostic procedures for the evaluation of the shunt functioning. Moreover it is able to evaluate the presence of CSF flow through the shunt, thus to identify a shunt blockage prior to the onset of patient neurological symptoms.

During the bibliographic research, several studies that propose some alternatives to the current ICP measurement systems have been found, like for example implantable and miniaturized ICP sensors that communicate with the environment via wireless, or inductive passive ICP sensors or piezoresistive ICP sensors fabricated by MEMs process, with a high sensitivity, allowing ICP's measurement through minimally invasive techniques etc. .

These technological proposals were not considered because the aim of this thesis work is to characterize a shunt system and to evaluate its hydrodynamic properties, like the specific pressure range that ensures its functioning.

Chapter 4

Evaluation of the hydrodynamic properties of the shunt system

The scope of this thesis work was to verify the functionality of a shunting device, supplied by the Regina Margherita Hospital, in Turin, in order to highlight some problems or possible engineering criticalities. Thus a hydrodynamic characterization of the device has been performed and the functioning range of the device, in terms of flow-pressure curve, has been obtained.

The pressure-flow characteristics of the shunt systems, supplied by the manufacturer, have been compared with the pressure-flow characteristics obtained through our test rig in laboratory. The pressure/flow curves are a graphic representation of the performance characteristics of a population of flow impedance devices.

Additionally, it was verified if the device works properly, since the above mentioned shunt systems have been removed from two different patients.

In the next sections the experimental tests accomplished at the mechanical and fluid dynamic laboratory inside the Polytechnic of Turin will be described and the tests results will be analyzed.

Two devices to test, the Miethke ProGAV 2.0 Adjustable Shunt System and the Codman Hakim Shunt could be characterized; only the first device has been tested because, through it, it would be possible to examine the functioning range of the adjustable DP valve and the functioning range of the fixed gravitational unit, that work when the valve is in a horizontal and in a vertical position respectively.

The second valve type, unlike the Miethke ProGAV 2.0 Shunt System, does not include an anti-siphon mechanism or a gravitational device, so the resulting obtained informations would be more restricted.

4.1 The test method for determining pressure and flow characteristics

For the test method realization, some of the guidelines reported by the “Standard practice for evaluating and specifying implantable shunt assemblies for neurosurgical application” (ASTM F647-94 (Reapproved 2014)) and by the British Standard “Neurosurgical implants-sterile, single use hydrocephalus shunts and components” (BS ISO 7197:2006) have been complied.

4.1.1 Test Rig

Test rig includes a source reservoir filled by distilled water at room temperature, a peristaltic pump, silicone tubes, three-way valves, a further graduated reservoir as damping system, two pressure sensors calibrated in mmHg, a data acquisition system, the shunt element to be tested and some holders. Figure 4.1 shows the test rig for testing the device in horizontal position. The same test rig has been used for testing the device in vertical position, but some elements have been removed like the peristaltic pump, the damping system whereas an electronic balance and a further reservoir, like drainage site, have been inserted.

The source reservoir

The source reservoir, made of glass, have a capacity of 500 ml and it has two inlet sections and two outlet sections. The peristaltic pump is connected to the source reservoir, by the silicone tubes, through the smallest sections. Instead, the largest sections of the source reservoir allows the free surface of the distilled water to be at the atmospheric pressure, like the shunt system.

The reservoir has been filled with around 400 ml of distilled water.

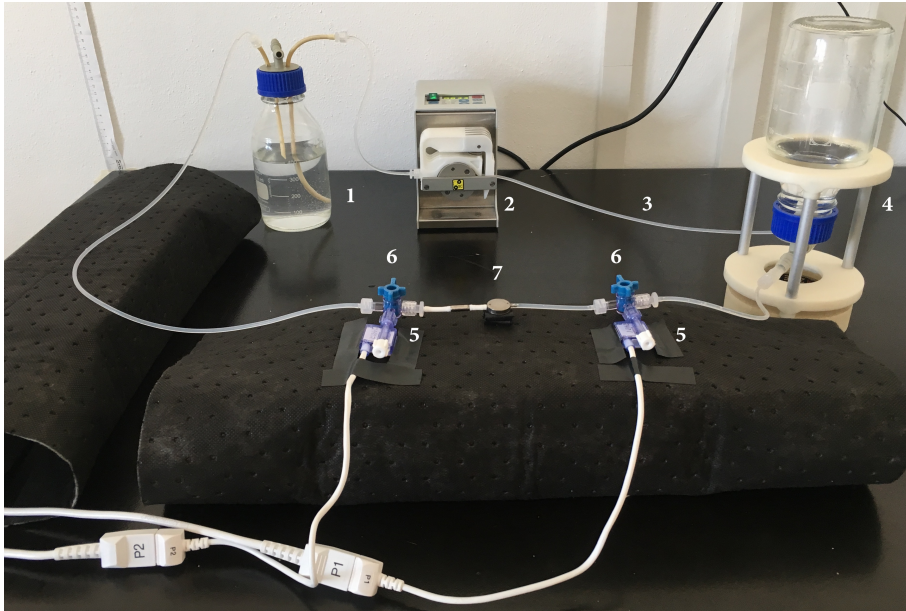


Figure 4.1: Test rig for testing the shunting device in a horizontal position:
1. Reservoir used both as source reservoir and as drainage reservoir 2. Peristaltic Pump 3. Damping System 4. System Tubing ($\Phi = 1.65 \text{ mm}$) 5. Pressure sensors 6. Three-way valves 7. Miethke ProGAV 2.0 Adjustable Shunt System

The peristaltic pump

The peristaltic pump is a type of positive displacement pump used to pump a large variety of fluid. It allows to set flow-rate regardless of the pressure value. It usually consists of a circular casing, a flexible tubing system and a rotor as pump head. The rotor includes two or more rollers attached to the external circumference; in fact the peristaltic pump is also known as rollers pump. These rollers turn and compress the fluid-filled flexible tubing against the pump's casing; in this way a pressure is generated within the tube and the fluid is sucked, so it can move (forward) toward the opposite extremity of the tube.

The rollers force the fluid transport and they prevent any back-flow. Their functioning is based on the peristalsis concept (used by our intestine to provoke the food motion in a specific direction).

Specifically, at the beginning of the pumping cycle sequence, if the rotor of the peristaltic pump includes two rollers then the first roller closes the fluid-filled tubing inlet, it moves forward by turning and it sucks the fluid. Hence, it pushes the fluid inside the tube forward and generates a pressure wave. Before reaching

the outlet section of the tube, the second roller closes the tube inlet, avoiding the back-flow. After the first roller leaves the tubing outlet, the other will generate the next pressure wave.

The flow-rate supplied by the peristaltic pump is increased by accelerating the rotation of the rotor's rollers, so by increasing the frequency of the rhythmically occlusion of the tube.

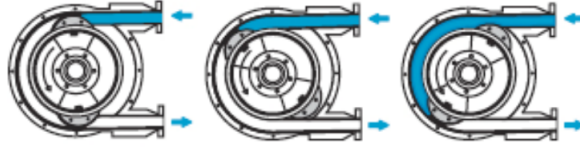


Figure 4.2: Schematic functioning of a peristaltic pump with a pump head characterized by two rollers: the upper blue arrow specifies the fluid direction. When the rotor turns, the first roller compresses the tube and pushes it against the pump casing, sucking the fluid and forcing it to move forward through the tube. In this way a pressure wave generates. Before reaching the tubing outlet section, during the rotor rotation, the second roller closes the tubing inlet section in order to avoid any back-flow; in the meantime, the first roller releases the tube. Subsequently the first roller generates again the next pressure wave and so on [35].

The flow rate in a peristaltic pump is determined by the: tube internal diameter (ID), pump head outside diameter (OD) and pump head revolution per minute (RPM).

The peristaltic pump used in the test rig is the ISMATEC REGLO Digital MS-4/6 ISM 833 model; it consists of 4 channels and 6 pump rollers. It guarantees flow rates between $0.002 \frac{ml}{min}$ and $100 \frac{ml}{min}$ and it can work only with tubes characterized by an inner diameter value between 0.13 mm and 3.17 mm.

It allows by several modes of operation, like pumping by flow rate (in $\frac{ml}{min}$), dispensing by volume (in ml), dispensing by time, dispensing at time intervals etc.; the pumping by flow rate in $\frac{ml}{min}$ has been chosen.

The pump, before every test, has to be accurately calibrated according to the guidelines supplied by its manual, to reach an acceptable accuracy in the measurements. The calibration has to be accomplished in two different ways: the flow-rate calibration and the dispensed volume calibration.

After selecting the number of channels (4), the number of rollers (6) and the inner diameter of the silicone tubes ($\Phi = 1.65$ mm) and before starting the pump calibration, the pump has been primed in order to eliminate air within the tubing system; this operation has been accomplished by using the same circuit for the experimental tests, but bypassing the shunt device by closing the three way valves upstream and downstream the device.

After priming the tubing system, a silicone tube has been connected, through a three-way valve, to the test apparatus and its outlet section has been connected to a graduated cylinder in order to measure the effective volume of dispensed distilled water, after 60 s.

The required flow rate ($10 \frac{ml}{min}$) has been defined through the operating panel; mode has been changed to DISP-time and a time equal of 60 s has been inserted. When the calibration process finished, the measured volume of the dispensed liquid has been inserted in the pump setting.

For the volume calibration, the same circuit as before has been used, but the pump operation mode has been changed into DISP-volume; the required dispensing volume has been set and, when the calibration process finished, the dispensed liquid has been measured through a graduated cylinder and the measured volume has been inserted in the pump's setting.

A stopper has been used in order to avoid the slip of the tube during the pump's head rotation.

The peristaltic pump is a pulsing pump, since its flow rate is unsteady on a single revolution. To reduce the pulsating events and to obtain an almost steady flow rate, an upside down reservoir as damping system has been used. The damper was studied and designed by two interns of the Biomedical Engineering Bachelor's Degree, for their degree thesis work [36]. Only the conclusions of their study about the dampener have been reported.

The damping system

The homemade damping system consists of a simple upside down reservoir with an inlet section and an outlet section. It is a closed chamber filled with gas (air) and liquid (distilled water) and it works as a compliance chamber: the gas component provides compliance through its compression capability, while the liquid component provides compliance through variations in its height. The chamber permits to trap

a volume of air and to regulate the ratio between air and distilled water (in the our specific case). The device works also as a damper because it absorbs and discharges pressure energy; so it is able to convert an intermittent water injection, due to the peristaltic pump that generates a peristaltic jump (because of its rollers) at every rotation, into a continuous flow. It shifts the evident pulsation of flow to a lower magnitude, reducing the maximum flow but maintaining the same mean flow variation.

By modifying the ratio between air and water in the chamber, the magnitude of the pulsation generated by the pump can be changed: if the percentage of the air in the chamber increases, the ratio between air and water rises and consequently the amplitude of the pulsatile flow decreases; while, if the percentage of air decreases, the amplitude of the pulsations increases.

The interns accomplished thermodynamical studies and experimental tests in order to evaluate the right amount of water and air, by taking inspiration by some studies of homemade dampeners in literature.

The calculations and the specific studies present in their work will not be deepened, only the results obtained by their work will consider.

They suggest a ratio $\frac{V_{\text{water}}}{V_{\text{total}}} = 0.4$ and a ratio $\frac{V_{\text{air}}}{V_{\text{water}}} = 1.5$ in order to achieve flow-rates approximately constant; the ratio between gas volume and liquid volume within the damping system is the fundamental parameter to determine if a dampener can or not attenuate a pulsing flow.

After these considerations, the reservoir ($V_{\text{total}}=500$ ml) used as dampener was filled with a volume of distilled water equal to 200 ml ($V_{\text{water}} = V_{\text{total}} * 0.4 = 200$ ml).

By accomplishing some tests with our peristaltic pump and by setting the flow-rates required by the shunt system to work, a better damping effect on the flow (through the pressure signals detected upstream and downstream the shunt valve) has been noted, by decreasing the volume of distilled water from a value of 200 ml to a value of approximately 100 ml: a larger compliance, given by the air volume, is needed to fully dampen the unsteady nature of the flow moved by the peristaltic pump.

The pressure sensors

the piezoresistive pressure transducers, are specifically the fluid-filled pressure sensors, that are clinically applied for example to monitor the blood pressure.

The *piezoresistive pressure transducers* use the electrical resistance strain gage as sensing element; they could be formed, in the lower pressure range, by a diaphragm strain gage (in fact these transducers are also known as “diaphragm strain gage pressure transducers”).

The piezoresistive effect is the ability of some materials to change their electrical resistance when they undergo the action of an external force. These variations of the electrical resistance occur both with a static external force and with a dynamic external force, unlike the piezoelectrical devices that can measure only dynamic variations.

Strain gage is an element that measures strain in structures; strain consists of tensile and compressive strain, distinguished by a positive or negative sign respectively. It is defined, if it is the axial strain, as the amount of deformation per unit length of an object, when a load is applied ($\varepsilon_a = \frac{\Delta L}{L}$). Thus, strain gage can be used to detect expansion and contraction.

When they are deformed by an external mechanical solicitation, their electrical resistance (R) changes:

$$R = \frac{\rho L}{A} \quad (4.1)$$

where ρ is the resistivity of the material of the strain gage, L is the the length of the strain gage element and A is the cross-sectional area of the strain gage.

The pressure exerted by the test fluid is applied to one side of the diaphragm, as shown in Figure 4.3; instead a reference pressure is applied to the other side of the diaphragm.

If the reference pressure is the atmospheric pressure (in the most common design) the transducers measures gage pressure; otherwise, if transducer is vacuum-sealed, it measures absolute pressure. Both transducer sides could be connected to different test pressures, so a differential pressure is obtained as measurement.

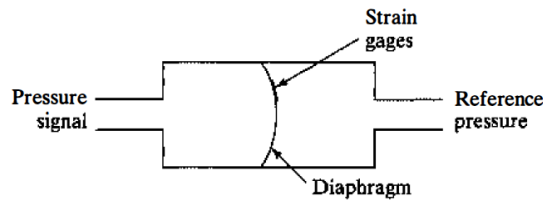


Figure 4.3: The strain gage pressure transducer: it includes a diaphragm, made in a semiconductor material like silicon, as sensing element with semiconductor strain gages formed into the diaphragm. They are characterized by a good sensitivity. [37].

When pressure loading is applied to diaphragm, usually made of a semiconductor material (like silicon), a deformation is generated. The piezoresistors, that are the semiconductor strain gages, are usually placed on top of the diaphragm or they are placed in the highest stressed points in order to maximize the sensitivity of the sensor [37].

The strain gages are characterized by a parameter, named *strain gage factor* S , that explains the relation between the change in resistance of the strain gage compared to its undeformed resistance ($\delta R/R$) and the corresponding strain (ε_a):

$$S = \frac{\delta R/R}{\varepsilon_a} \quad (4.2)$$

This parameter conditions the sensor sensitivity: if it assumes a high value, the sensor sensitivity improves.

Furthermore, the piezoresistive pressure transducers but in general all piezoresistive transducers require an electrical connection in order to allow for a good amplification of the signal and precise and constant measuring results. It is often necessary to reliably measure much lower values of strain, also on the order of the resolution of the measuring device. The circuit, that executes these functions, conditions the electrical signal and converts the resistance change into a voltage change is called *Wheatstone Bridge* .

If the Wheatstone-bridge is built within the transducer, all branches of the bridge are in an active state and they are connected each other in order to provide a further important benefit, that is the temperature compensation.

The resistivity of the most materials is influenced by the temperature; consequently, the resistivity influences the strain gage factor and thus the sensitivity of the sensor. In fact a variation in temperature of a strain gage as sensing element in a transducer, provokes an apparent strain also without a real mechanical solicitation [37].

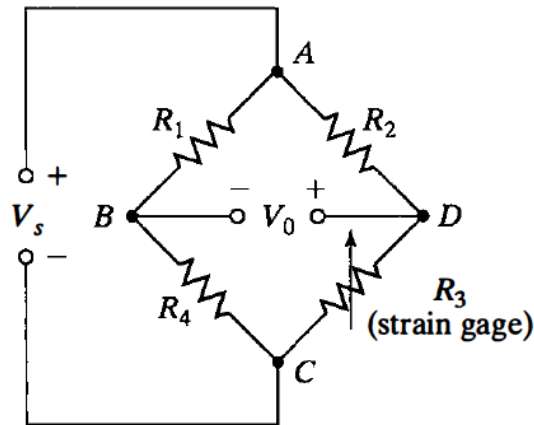


Figure 4.4: Example of the Wheastone-bridge whit one strain gage activated[37]

The strain gage pressure transducers generates an electrical dc output in mV but, if they include internal amplifiers, they supply outputs in the range between 0 to 5 V or between 0 to 10V.

The pressure sensors are provided with the PD-110 pulsatile pump. The IS-MATEC peristaltic pump has been chosen for the testing rig: the first mentioned pump guarantees flow-rates much greater and incompatible with the flow-rates provided by the shunt device.

They were calibrated by a technician after their installation, according to some guidelines provided by their manual; sensors have these features after the calibration outline:

Pressure Sensors	Offset Value	Slope
P1	5.422 V	$198929.59 \frac{mV/V}{mmHg}$
P2	0.095 V	$199298.96 \frac{V}{mmHg}$

Table 4.1: Features of the pressure sensors used in the test apparatus

Table 4.2 reports the pressure sensors specifications supplied by the manufacturer (BDC Laboratories).

Detail	Specification
Accuracy	- Better than $\pm 2\%$ of reading in the range of 0 to 310 mmHg - Better than $\pm 3\%$ of reading in the range of 310 to 1551 mmHg - In range of 1551 to 3102 mmHg typically better than $\pm 5\%$ of reading
Pressure Range	-362 to 3878 mmHg
Frequency Response	1200 Hz
Biocompatibility	All materials in contact with product fluid path meet USP Class VI requirements
Manufacturing Environment	FDA Registered, ISO 13485 certified facility; class 100,000 clean room
Operating Temperature	15° C to 40° C (other ranges with process qualification)
Storage Temperature	-25° C to 65° C
Input/Output Impedance	270 to 400 Ω
Excitation Voltage	2.5 to 10 VDC
Connector	Custom molded water-tight 4 pin connector; signal \pm and excitation \mp

Table 4.2: Pressure Transducers specifications supplied by the manufacturer

The offset value and the slope, also known as sensitivity, are two of the several characteristics that describe any type of sensor.

Measurement systems have a point in their functioning range, called *zero point*, that corresponds to the output value supplied by the system, when it has no measurand in input. In some cases the zero point does not coincide with zero; so it is a value to which the measurement systems should to be correctly regulated. If the device does not provide the correct output at the zero point, it is characterized by a *zero offset*. Additionally, if the zero offset is not considered when using the device, it results in a systematic error that invalidates all readings; it is called *zero error* [37].

The sensitivity instead is defined as the ratio between the variation in magnitude

of the sensor output and the variation in magnitude of the sensor input, that is the measurand. It is not directly correlated with the sensor inaccuracy, since a sensor more sensitive could be less accurate and vice-versa.

$$Sensitivity = \frac{\delta output}{\delta input} \approx \frac{\Delta output}{\Delta input} \quad (4.3)$$

The Data Acquisition System

The Daq System used for the pressure signals acquisition belongs to PD-110 Pulsatile Pump, which includes also a pulsatile pump and a control module. The PD-100 System includes the Statys PD software that allows a full control of test set up and monitoring, through a simple and user-friendly interface.

The PD-100 System employs proven National Instrument (NI) hardware for reliable data acquisition and system control. The system is configured to read pressures, flow and temperature; but only the pressure signals provided by the sensors are required for this work.

The main component of the Daq system is the “Data Acquisition Chassis”, NI cDAQ-9178 that provides module installation slots.

The shunt system

The Miethke ProGAV 2.0 Adjustable Shunt System has been previously described in the chapter 2.

It is clarified that the device consists of an adjustable DP unit characterized by an opening pressure value of 0 cmH₂O and of a fixed gravitational unit, by an opening pressure of 25 cmH₂O. In this phase of work, the instrumentation was not equipped the adjustment tools useful to re-adjust the DP unit at different opening pressure values between 0 and 20 cmH₂O. So tests are relative only to the valve with the minimum adjustment value.

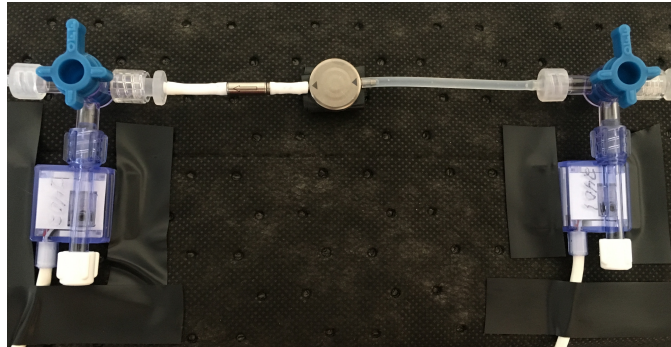


Figure 4.5: The testing device, the Miethke ProGAV 2.0 Adjustable shunt system: it is possible to observe the roundly adjustable unit and the fixed gravitational unit, linked each other though a white connector. The black arrows on the surface of the adjustable unit indicate the CSF flow direction. Upstream and downstream the valve a pressure sensor has been connected in order to measure the pressure drop of the shunt valve.

The Electronic Balance

The electronic balance, model ORMA EB100S (Eurotek), has been used during the qualitative tests of the shunting device in vertical position. Table reports its technical specifications.

Detail	Specification
Weighing Range	110 g
Reading Accuracy	0.1 mg
Time for Settlement	< 6s
Calibration Range	0-110 g
Linear Error	$\pm 0.0005gr$
Pan Diameter	$\Phi 80$ mm



Figure 4.6: Electronic Balance specifications supplied by the manufacturer

The balance performs an automatic calibration in 30 minutes.

4.2 Experimental tests of the shunting system in a horizontal position

The first experimental tests have been performed by positioning the Miethke Pro-GAV 2.0 Adjustable Shunt System in a horizontal position, on a rigid support.

The source reservoir has been filled with around 400 ml of distilled water at room temperature; one of the two smallest inlet section of the reservoir has been connected, by a long silicone tube, to the peristaltic pump.

The pump allows to move fluid and to simulate the physiological functioning of the shunt system, that exploits a pressure gradient between the collection point of the accumulated CSF in the brain and the drainage cavity, such as the peritoneum, in order to drain CSF and to reduce the increased ICP.

The peristaltic pump has been joined with the damping system through a silicone tube. Initially the damping system was not included in the test bench; the first pressure signals acquired by the sensors showed a waveform influenced by the pulsatile effect generated by the peristaltic pump.

It is a pulsing pump, so the flow-rate is not constant on a single rotation; in fact every time a nominal flow-rate is set¹. Usually a greater number of rollers in the pump's rotor is used to reduce the flow-rate and consequently to damp the pulsatile events.

Figure 4.7 shows three different signals, acquired for the greatest flow-rate tested through the shunt system $Q=50 \frac{ml}{h}$, characterized by a pulsatile waveform: the shunt system upstream pressure signal (P_1), the shunt system downstream pressure signal (P_2) and the differential pressure ($\Delta P = P_2 - P_1$) with the sign reversed.

All the differential pressure signals, ΔP , detected in this thesis work are depicted with the sign reversed; the sensor P_1 has been connected upstream the shunt and the sensor P_2 downstream the shunt.

¹The nominal flow-rate is the flow-rate for which the pump has been designed by the manufacturers; it is defined by measuring several flow-rates at different values of water pressure and calculating the mean flow-rate

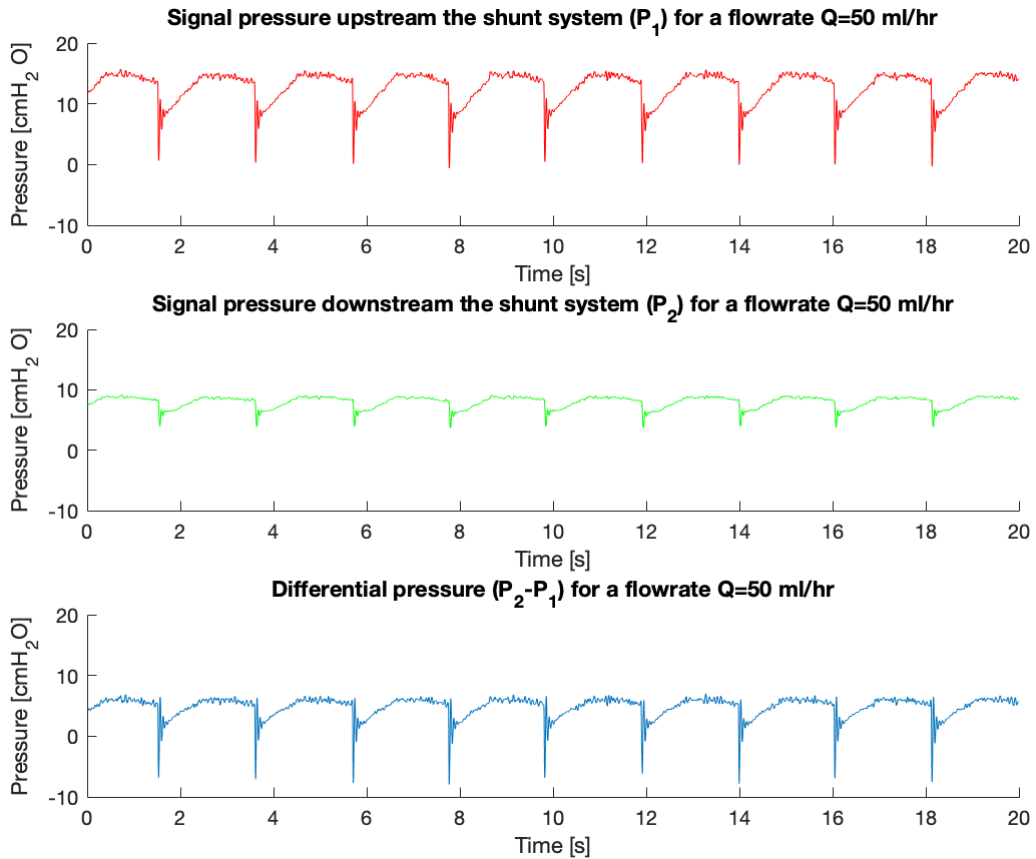


Figure 4.7: Graphs show the pressure signal detected at the upstream of the valve, the pressure signal detected at downstream the valve and the differential pressure signal, respectively. These waveforms are characterized by a clear pulsatility caused by the peristaltic pump that generate a flow-rate with periodic variations.

For the previously mentioned reasons, the damping system has been inserted into the test rig in order to reduce the pulsatile events and it has been placed downstream the pump; this new element allowed to absorb the peaks of the pulsating flow, generated by the pump and lastly to obtain a flow-rate approximately smoother and constant. The new pressure signals have width values oscillating between 0.1 and 0.2 mmHg (0.13595 and 0.40785 cmH₂O). Figure 4.8 shows the pressure signals, acquired for a flow-rate $Q=50 \frac{ml}{h}$ characterized by a dampened pulsatile waveform.

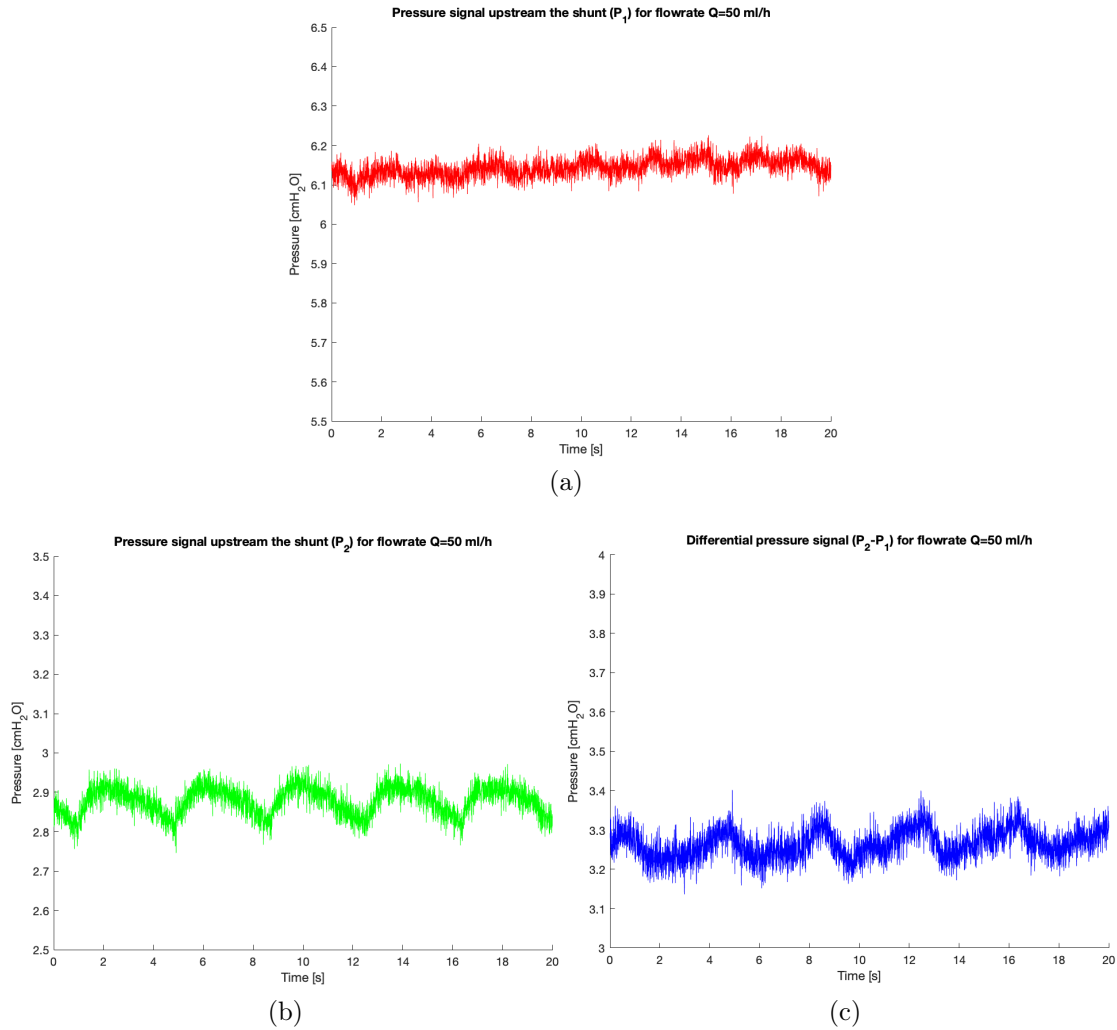


Figure 4.8: Graphs of pressure signals detected with the damping system in the test rig, for a flow-rate $Q=50 \frac{ml}{h}$. Plots show the pressure signal detected the upstream of the valve (a), the pressure signal detected downstream of the valve (b) and the differential pressure signal (c), respectively. These signals are characterized by a smoother waveforms even if they are corrupted by noise (probably environmental noise and mains interference at 50Hz), with an amplitude (that is the difference, at any given time, between the maximum pressure value and the minimum pressure value) oscillating between 0.13595 and 0.40785 cmH₂O. A significant reduction has been observed compared to the amplitude of the signals obtained without the damping system, whose amplitudes assumed values between 5-10 cmH₂O or more.

Two three-way valves have been used to connect, through the flexible tubes, the damping system with the shunting system and the device with the reservoir, that

worked both as source reservoir where pump sucks distilled water and as drainage reservoir, where the distal catheter of the shunt device bleeds.

These elements allowed to bypass, in a primary step, the shunting device in order to purge the system from the air bubbles and to calibrate the pump. Subsequently, they permitted to connect the pressure sensors upstream and downstream of the device.

The height of the support, where the testing device has been placed, has been adjusted in order to arrange the shunt system on the same level of the free surface of the distilled water within the source reservoir. This operation has been necessary in order that the free surface of the distilled water, the shunting system and the end of distal catheter were at the same height (with an error margin of ± 2 mm), thus at the same pressure, that is the atmospheric pressure.

For testing the device, the regulations suggest to use only a pressure sensor (that could be a manometer) upstream the shunting system because the fluid drainage, permitted by the shunt, occurs in the same water-filled reservoir where the device was placed.

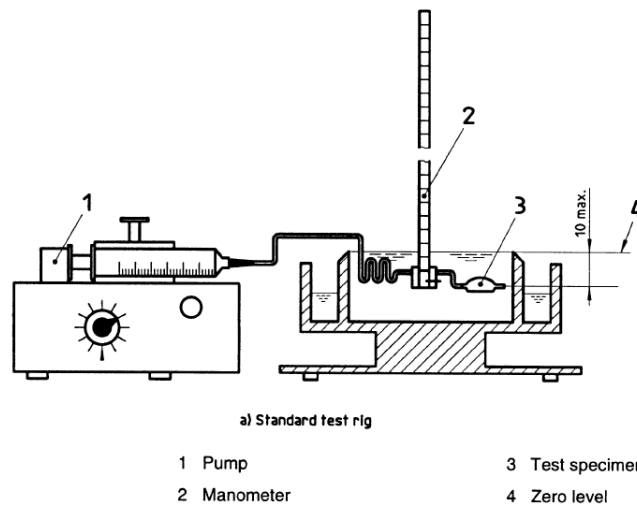


Figure 4.9: Example of a test rig, proposed by the Standard ISO 7197:1997, for determining the functioning range of a shunting device[38].

The outlet of the distal catheter should be at the same level with the surface of the water bath and the meniscus position of the manometer is adjusted at the level

of the zero mark on the graduated scale of the manometer itself. In these testing conditions, the shunting system and the distal catheter, in the water bath, would be at the same pressure, assumed as reference pressure for the differential pressure calculating. So ΔP should be the pressure read upstream the shunt.

Instead two pressure sensors have been employed, because a closed system has been implemented where the pump sucks out the distilled water from the source reservoir and permits the fluid flow through the shunt system, which drains the water into the same reservoir. The pressure sensor P_2 has been used as additional pressure measurement, because we did not know for sure that the shunt system and the end of the distal catheter in the reservoir were at the same pressure, despite the biggest inlet sections of the reservoir permitted the free surface of the water to be at the atmospheric pressure

In fact, in a horizontal position where all the elements are approximately at the same height, pressure downstream the shunt tended to stabilize with the pressure of the free surface of the distilled water in the source reservoir (that is the atmospheric pressure), assuming values lower than the pressure values detected by the sensor upstream the valve.

Pump has been started by setting a flow-rate value $Q=55 \frac{ml}{h}$, for a sufficient period of time in order to eliminate further air bubbles into the tubing system and the valve; this operation has been also necessary to allow the shunting device to reach an equilibrium state and to work at operating speed.

Before connecting the pressure sensors, the three-way valve has been opened in order that the distilled water could flow out; in this way sensors were in direct contact with the liquid instead of the air. Sometimes small air bubbles formed during the sensors insertion; to obtain reliable pressure readings instead of erroneous data, bubble air have been removed through a syringe.

It was difficult, during test, to remove all the air bubbles formed because of the small flow-rates that characterize the shunt valve functioning.

We interested to evaluate some hydrodynamics properties of the shunt system, like the pressure drop and consequently the functioning range of the shunting valve; thus the device has been tested by adjusting the pump speed in order that provided different flow-rates between $10.44 \frac{ml}{h}$ and $50 \frac{ml}{h}$.

According to the regulations of these devices, a shunting system should be tested at different flow-rate values from $5 \frac{ml}{h}$ to $50 \frac{ml}{h}$. In this case, the device has been

tested from flow-rate value equal to $10.44 \frac{ml}{h}$, because it is the smallest value assured by the peristaltic pump used for our test rig, with a silicone tube characterized by a diameter $\Phi = 1.65$ mm.

Test started by adjusting the peristaltic pump to a flow-rate of $50 \frac{ml}{h}$ and waiting for the valve to stabilize.

The experimental test continued by adjusting the pump with reducing flow-rate values: 40, 30, 20, $10.44 \frac{ml}{h}$.

For each flow rate value set, the corresponding pressure signals have been recorded.

Subsequently, we started from the smallest flow-rate and we continued with increasing flow-rate values, until reaching $50 \frac{ml}{h}$. This testing cycle has been repeated two times, recording in total four pressure signals for each flow-rates.

The experimental test has been performed for a few days.

4.2.1 Analysis of the pressure signals

Pressure signals have been detected through the two pressure sensors for a time interval of 3 minutes, with a sample rate of 250 Hz. The pressure sensors acquire data with a default value of sample rate of 5000 Hz; with this value, only a period time of 15 s could be detected, too short to analyze the signals and assess the hydrodynamic features of the shunt device.

The software interface allows to monitor simultaneously three different signals: the pressure signal against time, detected by the first sensor placed at the valve upstream, named P_1 ; the pressure signal against time, detected by the second sensor placed at valve downstream, named P_2 and lastly, their difference ($\delta P = P_2 - P_1$). The software calculates instantaneously and shows on the screen the mean value, the maximum value and the minimum value of each pressure signal.

The pressure signals detected at different flow-rates were corrupted both by mains interference at 50 Hz and by noise at high frequency, probably environmental noise. These informations have been acquired by executing the spectral analysis of some pressure signals taken at random between all the signals detected at different flow-rates.

The spectral analysis allows to represent the frequency components of a signal in a plot by depicting width components against frequency. It provides more

informations compared to the time analysis.

The *Fast Fourier Transform (FFT)* function in Matlab has been used; FFT is an optimized and computationally efficient algorithm that permits to calculate the *Discrete Fourier Transform (DFT)* of a signal or its inverse transform. DFT is a type of the Fourier analysis, which describes the transformations between the signal representation of the time domain and the signal representation of the frequency domain. DFT is applied to signals that periodic both in time and in frequency; so, it transforms a discrete, periodic sequence in time in a discrete and periodic representation in frequency.

FFT function requires as input parameters, the signal and the number of points that define the transform length (NFFT); the length is usually specified as a positive integer scalar in order to increase the algorithm performance and as a power of 2. A NFFT=65563 has been chosen, that is the power of 2 closer than the length of the pressure signals.

FFT returns a symmetric frequency representation, thus only its first positive half corresponding to the transform points between 1 and $\frac{NFFT}{2}$ has been considered. FFT is also characterized by a real part and by an imaginary part; so the absolute value of the Fast Fourier Transform of the pressure signals has been calculated, obtaining a complex magnitude because FFT is a complex entity.

Figure 4.10a and 4.10b show the spectrum of the signals pressure, P_1 and P_2 detected for a flow-rate $Q=50 \frac{ml}{h}$.

After the frequency analysis, the pressure signals have been filtered with a low-pass filter in order to attenuate the noise; the low-pass filter is characterized by an order equal to 6 and by a cut-off frequency equal to 45 Hz.

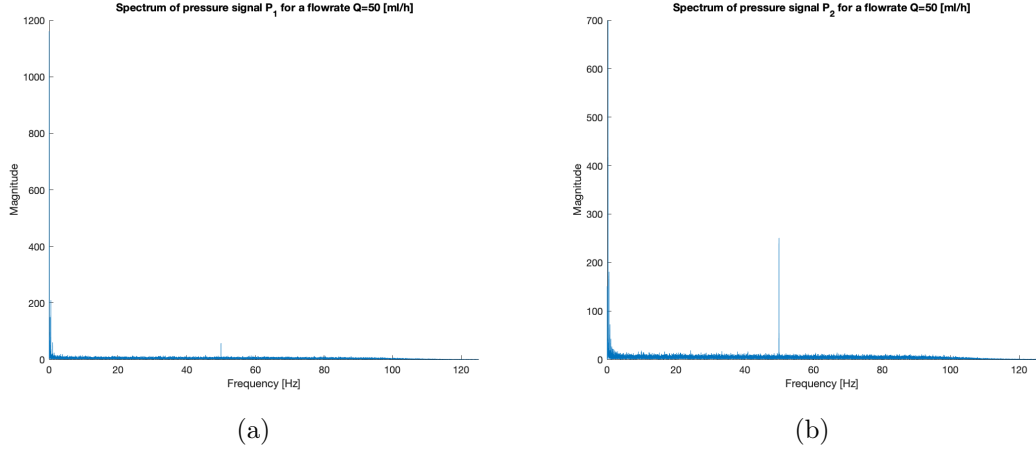


Figure 4.10: Spectral analysis of the pressure signals detected upstream (P_1) and downstream (P_2) the shunt system at a flow-rate $Q= 50 \frac{ml}{h}$. Both graph show a frequency peaks at 0 Hz and at 50 Hz. The frequency component at 50Hz should be caused by the mains interference; despite the removal of the mean value from the signals, the frequency components at 0 Hz still remained. A signal with a component not null at 0 Hz, is a signal with null mean value, since its mean value coincides with the frequency component width at 0 Hz. Pressure signal is corrupted by the mains interference at 50 Hz and by noise at high frequency

Figure 4.11, 4.12 and 4.13 depict a comparison between the P_1 original signal and the P_1 filtered signal, a comparison between the P_2 original signal and the P_2 filtered signal and a comparison between the ΔP original signal and the ΔP filtered signal, respectively.

From each differential pressure signals recorded at reducing flow-rate values ($50 \frac{ml}{h}$, $40 \frac{ml}{h}$, $30 \frac{ml}{h}$, $20 \frac{ml}{h}$, $10.44 \frac{ml}{h}$), the mean value, the standard deviation, the maximum value and the minimum value have been calculated. The same values have been calculated from the differential pressure signals detected at increasing flow-rate values ($10.44 \frac{ml}{h}$, $20 \frac{ml}{h}$, $30 \frac{ml}{h}$, $40 \frac{ml}{h}$, $50 \frac{ml}{h}$).

For each testing day four mean values, four standard deviation, four maximum values and four minimum values of pressure have been detected

For depicting the functional range of the shunt system tested, a plot representing the pressure drop across the valve expressed in [cmH₂O] (Y-axis) against the flow-rates expressed in [$\frac{ml}{h}$] (X-axis) has been constructed. Sensors acquire the pressure data in [mmHg]; therefore, before starting data analysis, they have been converted

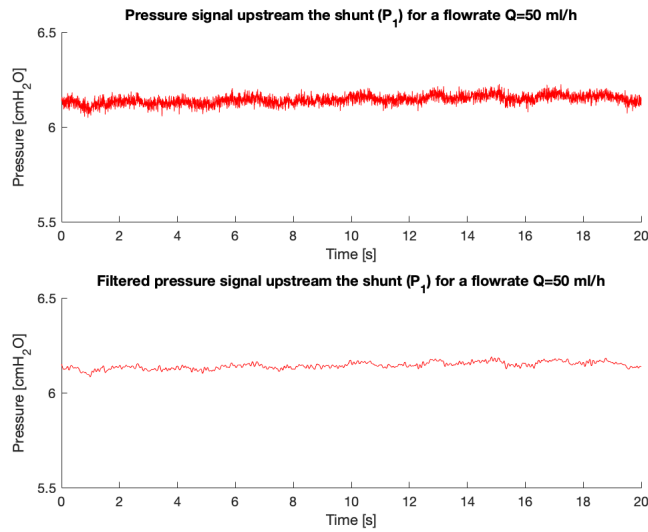


Figure 4.11: Comparison between the original pressure signal (P_1) detected upstream the valve and the filtered pressure signal through a low-pass filter ($f_{\text{cut-off}}=45$ Hz, order =6)

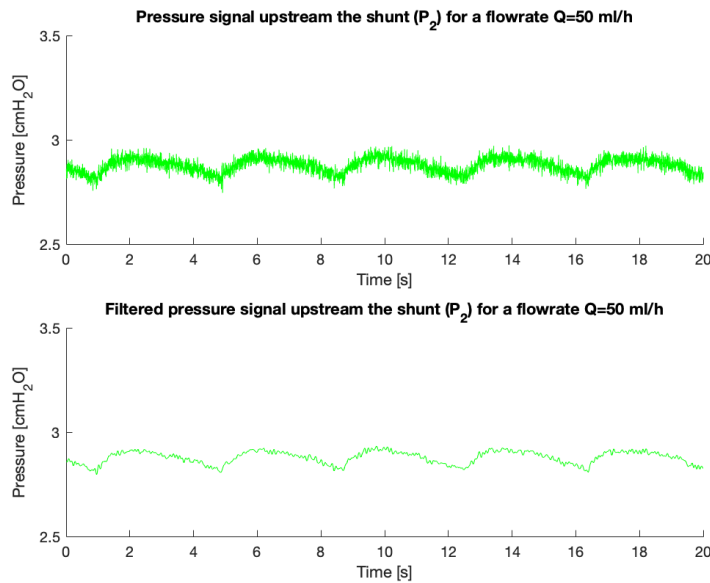


Figure 4.12: Comparison between the original pressure (P_2) signal detected downstream the valve and the filtered pressure signal through a low-pass filter ($f_{\text{cut-off}}=45$ Hz, order =6)

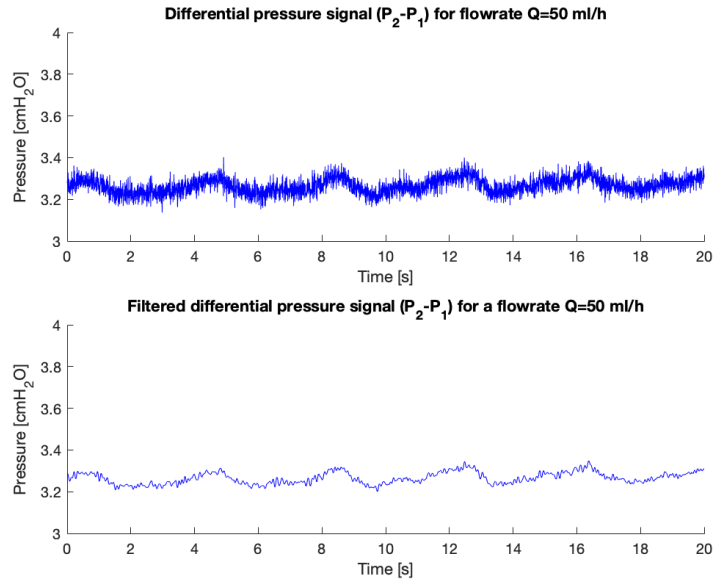


Figure 4.13: Comparison between the original differential pressure signal $\Delta P = P_2 - P_1$ and the filtered differential pressure signal through a low-pass filter (cut-off frequency, $f_{\text{cut-off}}=45$ Hz, order =6)

in [cmH₂O] by multiplying each value by 1.3595 (1 mmHg corresponds to 1.3595 [cmH₂O]).

This graph will show, for each flow-rate, the corresponding mean pressure value calculated as the arithmetic average of the all mean values of the differential pressure signals obtained for each flow-rate in the different testing days.

It also will show, for each flow-rate, the corresponding standard deviation calculated as the arithmetic average of the all standard deviation of the differential pressure signals obtained for each flow-rate in the different testing days.

Lastly, it will show, for each flow-rate, the corresponding minimum and maximum pressure values calculated as the arithmetic average of the all minimum and maximum values of the differential pressure signals obtained for each flow-rate in the different testing days.

An error bar was created and it represents the mean value and the standard deviation of the differential pressure at different flow-rates; these value have been calculated as the arithmetic average of the mean values and as the arithmetic average of the standard deviations of the all differential pressure signals obtained

for each flow-rate in the different testing days.

The experimental tests have been repeated for several days in order to establish the flow through the device, to regulate its functioning and to obtain flow-rate/pressure characteristics comparable with pressure data provided by the shunt manufacturer.

Table 4.3 reports the averaged pressure values obtained by testing the shunting device in a horizontal position, during different days.

Functioning range of the ProGAV 2.0 Shunt system in a horizontal position				
Q $\left[\frac{\text{ml}}{\text{h}}\right]$	ΔP_{mean} [cmH₂O]	Standard Deviation [cmH₂O]	ΔP_{max} [cmH₂O]	ΔP_{min} [cmH₂O]
10.44	2.6083	0.5052	2.7626	2.4966
20	2.9788	0.6201	3.1101	2.8697
30	3.4094	0.6417	3.5548	3.2921
40	3.8425	0.7319	3.9855	3.7255
50	4.1965	0.7706	4.3440	4.0646

Table 4.3: Differential Pressure data ($P_2 - P_1$) for the final flow-rate/pressure curve, determining the functioning range of the shunting device

Figure 4.14 shows the functional range of the Miethke ProGav 2.0 Adjustable Shunt System.

Figure 4.15 shows the final average values ($\Delta P = P_2 - P_1$) and the corresponding standard deviations, calculated from the mean values of the differential pressure signals ($\Delta P = P_2 - P_1$) detected for each flow-rate, during different.

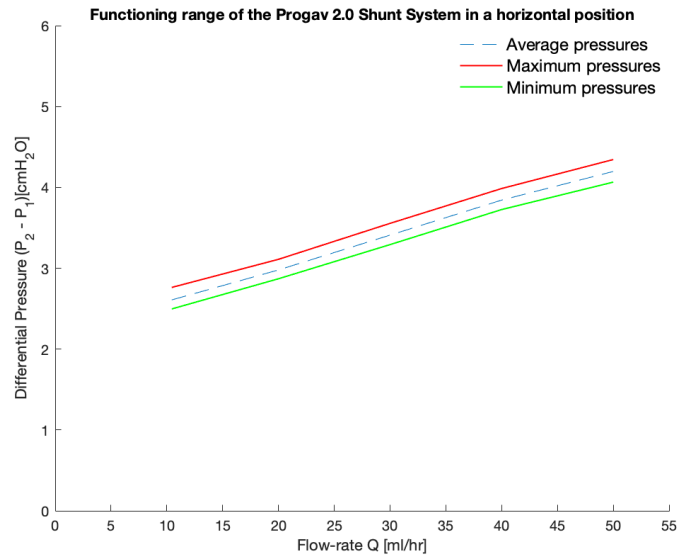


Figure 4.14: Functioning range of the Miethke ProGAV 2.0 Adjustable Shunt System. Graph shows the final mean values (blue dotted line), the final maximum values (red line) and the final minimum values (green line) of the differential pressure signals ΔP detected at different flow-rates.

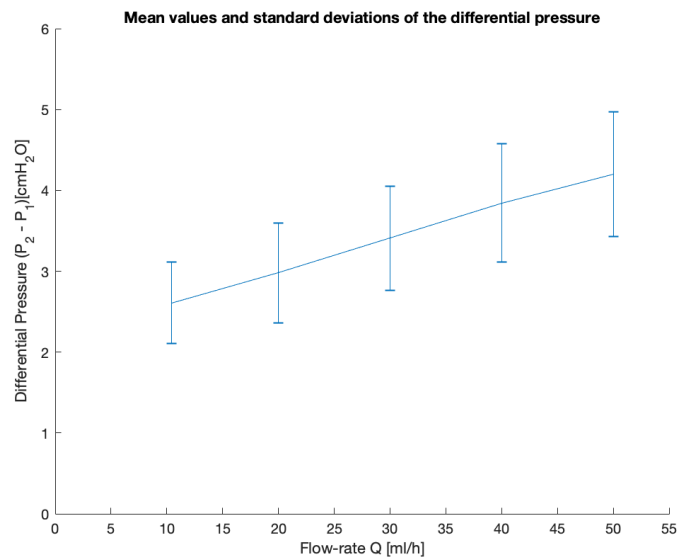


Figure 4.15: Error bar representing the final mean pressure values and the standard deviation calculated for each flow-rate

4.3 Qualitative tests of the shunting system in vertical position

The qualitative tests about the Miethke ProGAV 2.0 Adjustable Shunt System in a vertical position began modifying the test rig used for testing the device in a horizontal position. The peristaltic pump and the damping system have been removed, an electronic balance and a further reservoir, below the valve, as collection point of the distilled water have been inserted and the valve orientation has been changed moving it from a the horizontal position (0°) to a vertical position (90°).

Some changes to the test apparatus have been performed because, in this orientation, the hydrostatic pressure, that is the water column inside the system tubing, is sufficient to move fluid from an upper region (source reservoir) toward a lower region (drainage reservoir), exploiting the force of gravity.

A qualitative test has been executed in order to understand the functioning of the shunting system, especially of the gravitational unit that works only in vertical position. It was not possible to replicate the same testing conditions and the same set up in several days, thus the shunting device has not been characterized vertically and consequently the flow-pressure curve has not been obtained.

To evaluate the mode of operation of the device in a vertical position, reference was made to a research in literature conducted by the Freimann et al [39], who performed an in vitro study about the performance and principles of some anti-siphoning devices. They studied only the hydrostatic valves like the gravity-assisted anti-siphon devices (ASDs), the membrane controlled ASDs and the flow regulated ASD, without considering the combination between a fixed or programmable differential pressure valve and a gravitational unit.

The shunting system has been vertically tilted; a shorter tube (around 50 cm long) connects the reservoir above the device with the shunting valve and a longer tube (around 90 cm long) connects the device with the drainage reservoir below the valve.

The upstream reservoir was filled with distilled water, whose free surface is at atmospheric pressure through a tube which creates a direct communication between the air volume within the reservoir and the outside.

Figure 4.16 depicts the schematic drawing of the test rig.

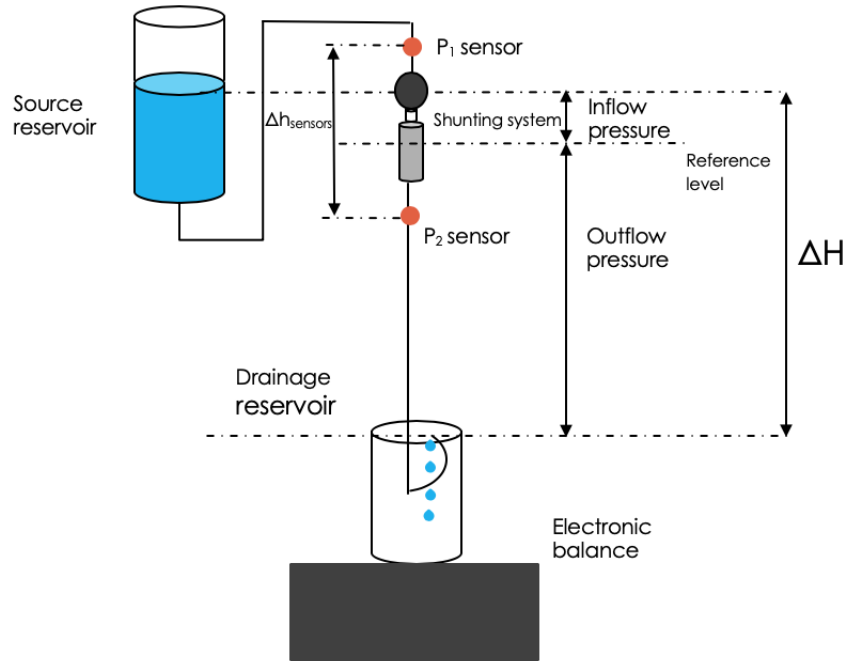


Figure 4.16: Schematic drawing of the experimental set-up for testing the shunting device in a vertical position. ICP is represented by the inflow pressure, obtained by adjusting the height of the source reservoir to the reference level on the device; IAP is represented by the outflow pressure obtained by adjusting the height of the drainage reservoir to the reference level on the device. P_1 and P_2 are the pressure sensors in front of and behind the test device. ΔH represents the overall height difference between the free surface of the distilled water within the reservoir upstream the device and the end of the distal catheter connected to the reservoir downstream the valve; it generates the corresponding hydrostatic pressure. For each ΔH defined, the collected fluid is measured through an electronic balance in order to calculate the corresponding flow-rate across the shunting valve.

Fluid will start to move when the hydrostatic pressure, between the free surface of the distilled water upstream the valve and the end of the distal tube connected to the drainage reservoir, is greater than the opening pressure of the valve.

A point in correspondence with the center of the device along its longitudinal axis has been chosen as reference level.

This test involves modifying both the geodetic height of the free surface of the fluid within the source reservoir relative to the device, in order to provide an inflow pressure range between 40 cmH₂O and 0 cmH₂O and the geodetic height of the end of the distal catheter connected to the drainage reservoir relative to the device, in order to provide an outflow pressure between 0 cmH₂O and 40cmH₂O. Thus, an overall hydrostatic pressure between the reservoir upstream the device and the reservoir downstream the valve, adjustable from 0 cmH₂O to 80 cmH₂O has been tested.

Two pressure sensors have been connected through the three way valves; a transducer has been placed above the valve and the other below the valve, in order to detect the differential pressure signal across the device.

For every height defined, thus for every hydrostatic pressure, the amount of fluid across the shunting device has been measured, after 3 minutes, using an electronic balance in order to obtain the flow-rate expressed in $\frac{g}{min}$, thus in $\frac{ml}{min}$ because the testing fluid is the distilled water.

Before starting the qualitative test, the system tubing was filled with distilled water in order to eliminate air inside and trigger the siphoning: only when tube is full of water, the fluid located in the longest tube section, downstream the valve, tends to go down because of its weight and consequently, it sucks the fluid in the shortest tube section located upstream the valve, characterized by a lower weight.

The siphoning effect has been tested by adjusting the height of the drainage reservoir relative to the device, to height values of 0, -10, -20 and -40 cm in order to determine the outflow pressure, simulating the IAP, equal to 0, -10 -20 and -40 cmH₂O.

The increased ICP has been also evaluated by adjusting the height of the source reservoir relative to the device to height values of approximately 0, 10, 20, 30 and 40 cm in order to determine an inflow pressure of 0, 10, 20, 30 and 40 cmH₂O respectively.

Few seconds before closing the upper three way valve and stopping the fluid flow, the instantaneous pressure data P_1 , P_2 and ΔP have been recorded; after closing the tap. the collected fluid in the draiange reservoir has been measured though the balance.

The qualitative test began by placing the source reservoir, the device and the drainage reservoir at the same height without generating inflow pressure and outflow

pressure respectively. After 3 minutes, pressure data has been detected and the possible amount of fluid collected in the drainage reservoir was weighed. These operation have been repeated three time, replicating every time the same testing conditions.

Subsequently, the reservoir upstream the shunting device was maintained at the same height and from time to time, the height of the drainage reservoir has been modified in order to provide an inflow pressure of 0 cmH₂O, an outflow pressure of -10, -20 and -40 cmH₂O respectively and an overall hydrostatic pressure of 10, 20, 30 and 40 cmH₂O. After 3 minutes pressure data have been monitored and the flow-rate across the valve has been calculated.

Test continued by adjusting the position of the source reservoir relative to the device at a height value of 10 cm. Then, from time to time, the position of the drainage reservoir has been changed at height values of 0, -10, -20 and -40 cmH₂O in order to provide an inflow pressure of 10 cmH₂O, an outflow pressure of 0, -10, -20 and -40 cmH₂O and an overall hydrostatic pressure of 10, 20, 30, 40 and 50 cmH₂O.

The reservoir upstream the valve has been placed to a height of 20, 30 and 40 cm in order to ensure an inflow pressure of 20, 30 and 40 cmH₂O and an outflow pressure of 0, -10, -20 ad -40 cmH₂O for each inflow pressure tested. So the overall hydrostatic pressure assumed values equal to 20, 30, 40 and 60 cmH₂O for an inflow pressure equal to 20 cmH₂O; it assumed values equal to 30, 40, 50 and 70 cmH₂O for an inflow pressure equal to 30 cmH₂O, and lastly values equal to 40, 50, 60 and 80cmH₂O for an inflow pressure equal to 40cmH₂O.

Every height variations between the source reservoir and the drainage reservoir, has been repetead three time, paying attention to create the same testing conditions in order to obtain results comparable each orthers. Every time pressure data have been detected by the pressure sensors, the amount of fluid was weighed and the resultin flow-rate has been calculated.

Table 4.4 reports for each hydrostatic pressure value tested, obtained by adjusting the height of the source reservoir relative to the device and the height of the drainage reservoir relative to the device, the corresponding mean value and standard deviation of the flow-rate.

Qualitative test of the shunting device in a vertical position					
H_{inflow} [cm]	H_{outflow} [cm]	ΔH [cm]	$P_{\text{hydrostatic}}$ cmH ₂ O	Q_{mean} [$\frac{\text{ml}}{\text{min}}$]	STD [$\frac{\text{ml}}{\text{min}}$]
0	0	0	0	NO FLOW	
0	- 10	10	0	NO FLOW	
0	- 20	20	20	0.3867	0.025
0	- 40	40	40	3.225	0.035
10	0	10	10	NO FLOW	
10	- 10	20	20	0.965	0.036
10	- 20	30	30	2.178	0.103
10	- 40	50	50	5.217	0.094
20	0	20	20	0.838	0.035
20	- 10	30	30	2.094	0.077
20	- 20	40	40	3.685	0.149
20	-40	60	60	6.671	0.228
30	0	30	30	1.737	0.231
30	- 10	40	40	3.874	0.195
30	- 20	50	50	6.45	0.087
30	- 40	70	70	9.92	0.079
40	0	40	40	5.441	0.072
40	- 10	50	50	7.466	0.086
40	- 20	60	60	8.703	0.047
40	- 40	80	80	11.739	0.1510

Table 4.4: Qualitative data of the tests executed placing the shunting system in a vertical position. Table reports the mean values of the flow-rates and the corresponding standard deviations, for each hydrostatic pressure value tested. For each height variations, thus for each hydrostatic pressure value, the amount of fluid across the valve has been weighed three time, ensuring for each measurement the same testing conditions. From the fluid amounts (expressed in g) collected during the three test repetitions, the mean values of the flow-rate in $\frac{\text{ml}}{\text{min}}$ and the standard deviation have been calculated.

Figure 4.17 shows the pressure-flow curves of the shunting device, in vertical position, obtained at four different levels of outflow pressure.

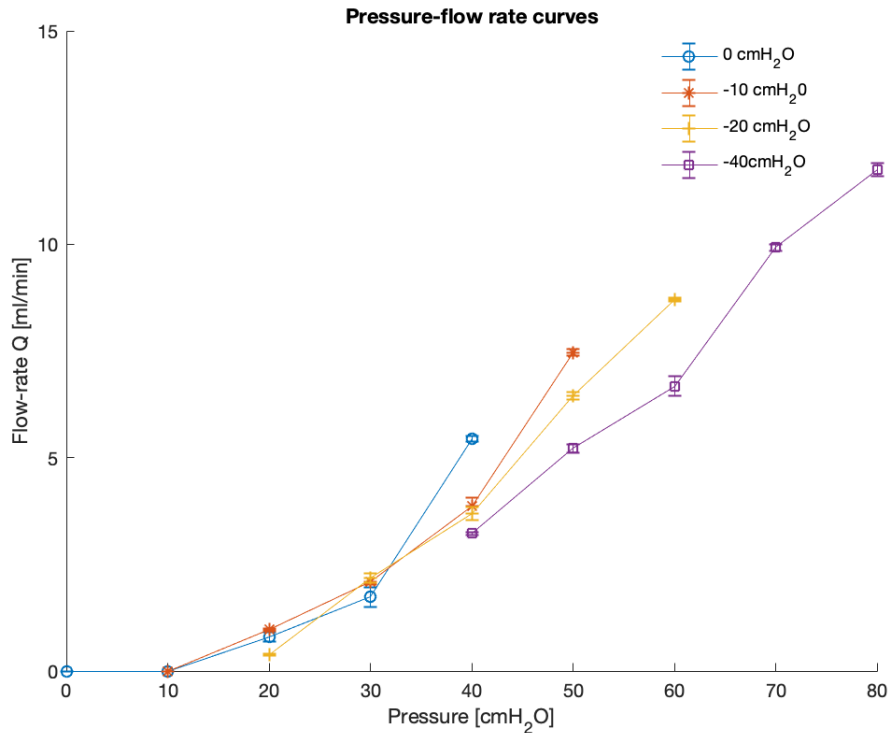


Figure 4.17: Pressure-flowrate curves of the shunting system in vertical position, obtained at four different levels of outflow pressure: blue curve for an outflow pressure equal to 0 cmH₂O; orange curve for an outflow pressure equal to -10 cmH₂O; yellow curve for an outflow pressure equal to -20 cmH₂O and lastly violet curve for an outflow pressure equal to -40 cmH₂O

Additionally, to understand when the gravitational valve moves from an open state to a closed state, the drainage reservoir has been placed at different heights in relation to the device, while the source reservoir was maintained at the same level of the device. In addition, the device has been evaluated also by placing the source reservoir at different height, maintaining the drainage reservoir unchanged.

It was observed that when the source reservoir is placed above the device, the valve is open and it allows the fluid flow because between the source reservoir and the device, an inflow pressure higher than the opening pressure of the valve is formed. While, when the reservoir is moved far below the device, a very negative pressure level create (even if not physiological) and the valve close, in order to preserve the hypo-pressure condition and to avoid the structure collapse.

Table 4.5 reports some examples of pressure values detected upstream and downstream the valve and the resulting state of the shunting device in vertically, when the geodetic height of the drainage reservoir is changed at different levels, maintaining the source reservoir at the same level of the device.

ΔH [cm]	P_1 [cmH ₂ O]	P_2 [cmH ₂ O]	Shunting device state
50	-6.9	-22.1	ON
40	-6.8	-20.6	ON
30	-6.8	-9	ON
20	-6.5	-2.9	ON
15	-6.5	-1.2	OFF

Table 4.5: “Semaphore test” to evaluate the open and closed configuration of the valve in vertical position, when different outflow pressures have been generated while maintaining the source reservoir at the same level of the device

Table 4.6 reports some examples of pressure values detected upstream and downstream the valve, when the geodetic height of the reservoir above the shunting system has been changed at different levels while maintaining the drainage reservoir at the same level of the device even if does not correspond to a physiological condition, because the drainage site in vertical position could not place at the same level of the device. It is a experimental conditions allows to understand the functioning of the device.

ΔH [cm]	P_1 [cmH ₂ O]	P_2 [cmH ₂ O]	Shunting device state
-15	-19	3.3	OFF
-10	-13.4	3.3	OFF
-5	-7.7	3.2	OFF
0	-7.1	3.3	OFF
10	1.4	3.5	ON
20	7.7	3.6	ON
30	14.9	3.6	ON
40	21.3	3.7	ON

Table 4.6: “Semaphore test” to evaluate the open and closed configuration of the valve in vertical position, when different inflow pressures have been generated while maintaining the drainage reservoir at the same level of the device (even if this condition is not physiological)

Chapter 5

Discussions

Physiologically, a shunting device works like a mechanical valve, exploiting a differential pressure between the ventricle's pressure and the peritoneal's pressure (in the most cases); it allows the drainage of the accumulated CSF in one direction from the cerebral ventricle system or from others CSF-filled compartments, like the arachnoid cysts, to the peritoneal cavity. Shunt system permits to minimize the increase of the ICP in the brain, due to the accumulated CSF.

The device works like a switch, moving from a closing state to an open state according to the differential pressure ΔP : if ΔP exceeds the opening pressure of the valve, the shunt opens and it allows CSF to flow, otherwise it remains in a closed configuration, maintaining the ICP level.

CSF's flow across the valve is influenced by several factors like the intraventricular pressure (IVP) that determines the ICP level according to the external atmospheric pressure, the hydrostatic pressure ($P_{\text{hydrostatic}}$), the opening pressure that characterizes the valve ($P_{\text{opening of the valve}}$), the pressure of the drainage site like the intra-abdominal pressure (IAP), the resistance of the valve (R_{valve}), the resistance of the system tubing ($R_{\text{system tubing}}$) etc.

The hydrostatic pressure is calculated by the equation:

$$P_{\text{hydrostatic}} = \rho g H \quad (5.1)$$

where ρ is the density of the CSF, g is the acceleration of gravity and H is the water column height in the system tubing; it acts only when patient moves in an upright position.

CSF, the gradient pressure between the ventricle system and the abdominal cavity and the system resistance are linked each others through the equation:

$$Q_{\text{CSF}} = \frac{\Delta P}{R_{\text{system}}} = \frac{\Delta P}{R_{\text{valve}} + R_{\text{system tubing}}} \quad (5.2)$$

The shunt valve resistance is described by a simple equation:

$$R_{\text{valve}} = \frac{\Delta P}{Q_{\text{CSF}}}. \quad (5.3)$$

While the system tubing resistance could be calculated through Poiseuille's law which describes the tubing resistance as the resistance offered by a tube to a laminar flow, and it represents a constant parameter due to the circuit geometry :

$$R_{\text{system tubing}} = \frac{8\mu L}{\pi r^4} \quad (5.4)$$

where μ is the CSF's viscosity, L is the system tubing length (length of the proximal and the distal catheters) and r is the radius of the catheters.

For determining ΔP , ICP and IAP play an important role according to the patient position.

Discussion of the tests results obtained for the valve in a horizontal position

In a horizontal position, the difference in height between the inlet of the shunting system (a CSF-filled brain compartment) and its outlet (peritoneum for example) is approximately zero because by convention the upper point of the abdomen surface of a patient is assumed as the zero level. $P_{\text{hydrostatic}}$ is null and the intra-abdominal pressure depends on the state of health of the patient, his nutritional condition, his daily routine etc.

So when patient is lying down (Figure 5.1) the ICP is calculated as:

$$ICP = P_{\text{opening of the valve}} + IAP. \quad (5.5)$$

On average IAP assumes in horizontally low values, so the greater pressure contribution moving CSF across the shunt valve is given by the intracranial pressure.

The opening pressure is a constant parameter for a fixed DP shunt valve, otherwise it can be externally adjusted, according to the clinical conditions and symptoms of patient, for a programmable DP shunt valve.

For our shunt system, the opening pressure in a horizontal position is determined only by the opening pressure of the adjustable DP unit, that is adjusted at a value of 0 cmH₂O. This low value of P_{opening} means that the valve offers to fluid flow the minimum resistance; since the gravitational unit does not work in this position, the valve principally works like a simple tube without valve, where the resistance to fluid flow is mainly offered by the tubing system, proximal and distal.

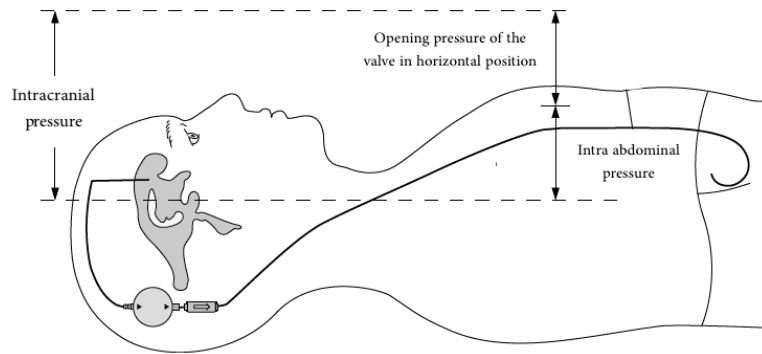


Figure 5.1: Pressures involved in the shunting system functioning when patient is in a recumbent position: $ICP = P_{\text{opening of the valve}} + IAP$. In this position, the upper surface of the patient's abdomen is considered the reference level, where pressure is at the atmospheric pressure and IAP is usually assumed equal to 0 mmHg. So the opening pressure of the shunt valve, determined by the only opening pressure of the adjustable DP unit, depends on the ICP; when ICP exceeds the opening pressure, shunting system opens and allows CSF to flow [19].

After the physical basics that characterize these devices, an experimental set-up has been designed with the aim to in-vitro replicate the simplified functioning of a cyst-peritoneal shunt system; these tests allowed to hydrodynamically analyze the device, (provided by the Regina Margherita Hospital in Turin) after being removed from a patient, to assess its fundamental pressure and flow characteristics and to verify that the performance of the device is within the manufacturer's stated functional range.

For the experimental tests about the shunting system in a horizontal position,

the device, the pressure sensors and the end of the distal catheter have been placed at the same height, in order that all these elements were at the same pressure, that is the atmospheric pressure.

Through this testing configuration, we tried to simulate a shunted patient in a recumbent position: ICP is simulated by the peristaltic pump upstream the shunt system that provides a source of pressure and allows to distilled water (simulating CSF because the CSF's viscosity at 37° is approximately 0.7 [mPa · s], similar to the water viscosity at the same temperature that is equal to 0.691 [mPa · s]) to flow across the shunt valve in a closing system (the CSF-filled compartment and the peritoneal cavity are represented by the same reservoir in the test rig).

By the infusion of distilled water at different flow-rates provided by the peristaltic pump (50, 40, 30, 20 and 10.44 $\frac{ml}{h}$) the pressure drop across the shunt system has been detected through pressure sensors.

The differential pressure readings ($\Delta P = P_2 - P_1$) provided by the sensors correspond to the “real” pressure drop of the valve, even if some assumptions have been made. P_1 signals assume higher values than values of the pressure signals detected downstream the valve (P_2); P_1 detects the pressure exerted by the distilled water to overcome the opening pressure of the shunt in horizontally, determined by the only opening pressure of the adjustable DP unit, equal to 0 cmH_2O .

The fluid dynamic Bernoulli's equation relates the sliding velocity, the pressure and the density of a fluid within a tube with the different sections and heights that characterize the tube itself. Considering two collection points within the system tubing, one upstream the shunting valve (equation's elements with subscript 1) and the other downstream the shunting valve (equation's elements with subscript 2), it is possible to write the Bernoulli's equation for our testing circuit as:

$$P_1 + \rho gh_1 + \frac{1}{2}\rho v_1^2 = P_2 + \rho gh_2 + \frac{1}{2}\rho v_2^2 + \Delta P_{valve} \quad (5.6)$$

where P_1 and v_1 are the fluid pressure and the fluid velocity upstream the shunting valve respectively; ρ is the fluid density (approximately 1000 $\frac{kg}{m^3}$ for the distilled water); P_2 and v_2 are the fluid pressure and the fluid velocity downstream the shunting valve respectively; ΔP_{valve} is the valve pressure drop and $h_1 - h_2$ is the difference between the collection points.

The sliding velocity of the distilled water within the system tubing has been neglected since the flow-rates permitting the correct shunting device functioning are very low (the highest flow-rate is equal to $0.833 \frac{ml}{min}$ and the smallest is equal to $0.174 \frac{ml}{min}$); furthermore, the hydraulic pump head¹ has been ignored since we tried to minimize the difference in height between the shunting device, the tubes and the water source within the reservoir, placing them at the same level. After these simplifications, the Bernoulli's equation becomes:

$$P_1 + \rho gh_1 = P_2 + \rho gh_2 + \Delta P_{valve} \quad (5.7)$$

The equation can be further reduced because the collection points lie on the same height; thus the pressure drop of the shunting valve

$$\Delta P_{valvola} = P_1 - P_2 = -\Delta P_{sensors} \quad (5.8)$$

corresponds to the differential pressure detected by the pressure sensors inserted upstream and downstream the valve, respectively.

A functioning range has been obtained (Figure 4.14), in the form of flow-pressure curve, with differential pressure values ΔP very similar and comparable with the flow-pressure curves provided by the manufacturer within the device data sheet. The flow-rate for this test is the independent variable while the resulting pressure drop, or the differential pressure across the valve is the dependent variable.

Good results has been achieved despite the guidelines reported by the device regulations has not been totally respected, about the testing modality to be performed by a manufacturer or a researcher, in order to obtain the hydrodynamic properties of the device.

The functioning range of the device has been obtained through non-destructive tests, thus without dividing the DP adjustable unit from the gravitational unit and by characterizing the totally shunting device.

The resulting graph (Figure 5.2) is comparable with the functioning range provided by the manufacturer; differential pressure values ($\Delta P = P_2 - P_1$) are included in

¹It is the increase of the mechanical energy that fluid per kg mass receives between the inlet section and the outlet section of the pump, expressed in [m].

the range 0-5 cmH₂O, as the device manufacturer states but higher values, for the same flow-rates set, has been obtained. Only a device has been tested and this could be the reason why a slightly different and greater values have been acquired, during testing the device; generally, in a testing conditions, it would be more appropriate to consider and to test, a sufficient number of times, a population of shunt valves constituted by several devices of the same model, in order to establish a statistical confidence level for the reproducibility of the flow-pressure response.

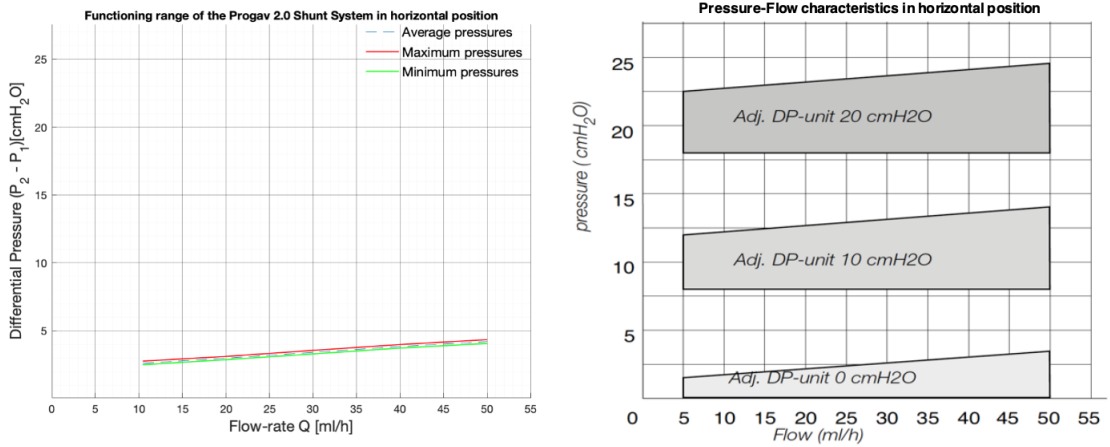


Figure 5.2: Comparison between the functioning range obtained after the hydrodynamical characterization of the shunting system in horizontal position and the functioning range provided by the manufacturer within the device data-sheet. Graphs shows a similar curve, but the first is characterized by higher pressure drop values across the valve, for the same flow-rates set.

All the flow-pressure curves obtained during different testing days and also the final curve, show an approximately linear relation between the flow-rate (Q) and the differential pressure ΔP : to increasing the flow-rate set through the peristaltic pump, the pressure drop across the shunt valve increases.

The linear regression of the resulting curve and the corresponding *coefficient of determination*, r^2 have been calculated, and a best fit line has been obtained. Coefficient r^2 is a good measure of the adequacy of the regression model and it is calculated through

$$r^2 = \frac{\sum(ax_i + b - y_1)^2}{\sum(y_1 - \bar{y})^2} \quad (5.9)$$

where the numerator, in this case, is the sum of the squares deviations of the differential pressure mean values from the best fit, previously calculated; the denominator is the sum of the squares of the variation of the differential pressure mean values about the mean, \bar{y} , which is the average of differential pressure data. We obtained $r^2=0.994$ and for a good fit, it should be close to unity; thus, it is possible to claim that the relation between the pressure drop across the valve, so the differential pressure $\Delta P=P_2-P_1$, depending on the flow-rates could be considered linear with good approximation, as shown in Figure 5.3

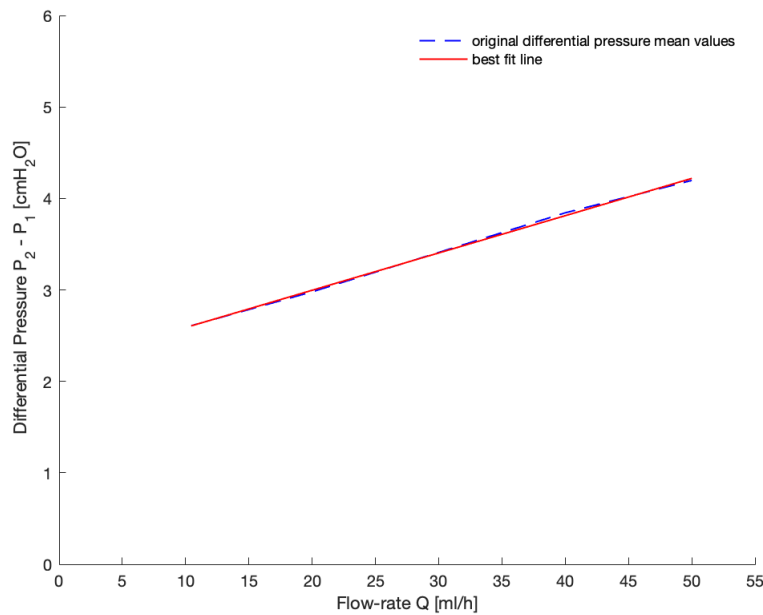


Figure 5.3: Least-squares line with the original differential pressure mean values from the functioning range

This behavior could be explained through the equation describing the simple relation between ΔP , Q and the total resistance to the fluid flow offered by the valve $R = \frac{\Delta P}{Q}$ expressed in this specific case in $\frac{[cmH_2O]}{[ml/h]}$.

Figure 5.4 shows the curve of the total fluid dynamic resistance offered by the valve to fluid flow, depending on the flow-rate.

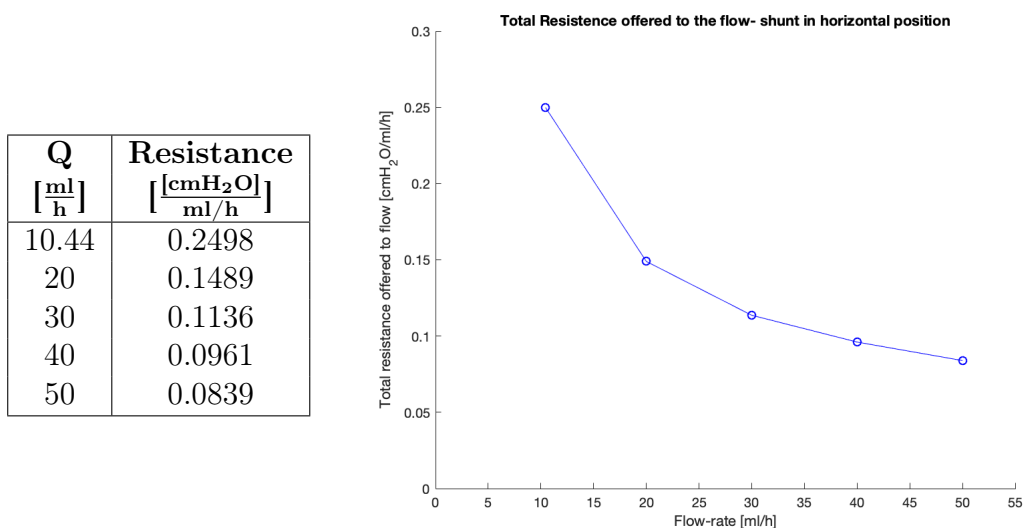


Figure 5.4: Graph of the total fluid dynamic resistance offered by the valve to fluid flow, against the flow-rate

The total fluid dynamic resistance is determined by two contributions, for the same flow-rate: one is given by the opening pressure of the valve and the other by the valve geometry and shape.

The first has only been evaluated from the “real” opening pressure of the valve. The device, in horizontal position, is characterized by an opening pressure value nominally stated by the manufacturer equal to 0 cmH₂O; actually, through the graph representing the differential pressure mean values depending on the flow-rate, this opening pressure value assumes a value greater than 0 cmH₂O.

From the linear regression ($y = 0.0408x + 2.1807$), previously calculated, a value slope of $0.0408 \frac{\text{cmH}_2\text{O}}{\frac{\text{mL}}{\text{h}}}$ and a constant term equal to 2.1807 cmH₂O have been obtained. We considered the constant term of the best fit line, calculated for a null flow-rate value, as the “real” opening pressure of the shunting valve; in fact if pressure fluid does not exceed the opening pressure value, flow-rate across the valve is null.

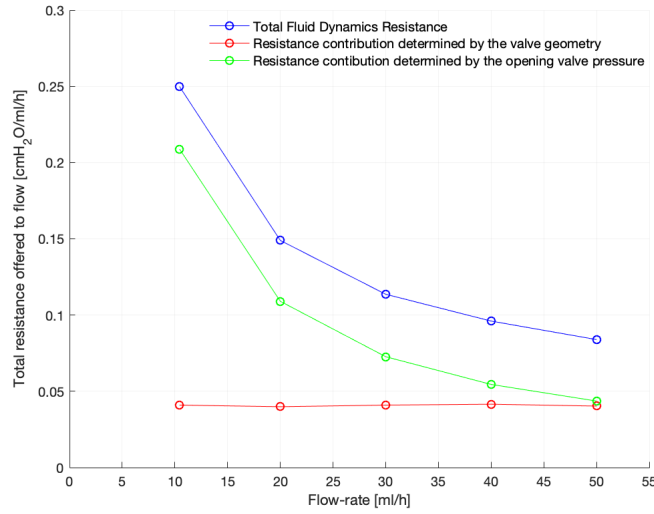


Figure 5.5: Graph shows all the resistance calculated from differential pressure mean values and flow-rate values: the equivalent total fluid dynamics resistance offered by the valve to fluid flow, the resistance contribution given by the opening pressure value of the valve and the resistance contribution given by the valve shape and geometry.

Since the opening pressure is a constant value, the resulting relation between this pressure and the flow-rate, calculated through the equation $R = \frac{\Delta P}{Q}$, will be characterized by a decreasing trend, in particular at branch of hyperbole (green line with circle markers in Figure 5.5). Thus, when fluid exerts a lower pressure that does not exceed the valve opening pressure, the device remains closed, flow-rate across it is null and resulting resistance will be infinite.

The second contribution determining the total fluid dynamic resistance has been calculated by subtracting the “real” opening pressure value (2.1807 cmH₂O) from the mean values of the differential pressure detected by the pressure sensors. The corresponding resistance will be approximately constant (red line with circle markers in Figure 5.5) as suggested by the linear trend of the flow-pressure graph (Figure 5.3), when the valve is open.

The total resistance of the valve is obtained from the differential mean pressure values, calculated as arithmetic average of the all differential pressure detected for the same flow-rate during different testing days.

It is characterized by a curve with a decreasing trend (blue line with circle markers

in Figure 5.5), tending (by extrapolating flow-rate toward infinite) to the value of the fluid dynamic resistance determined by the valve shape.

Thus, the higher the flow that crosses the valve and the lower the resistance, the greater is the difference of pressure across the valve.

The resistance offered by the valve to flow of distilled water decreases with increasing flow-rate values and Figure 5.4 shows the curve trend of the resistance against flow-rate: with lower flow-rate values, the sliding velocity of the fluid within the valve is low, thus it exerts against the ball-in cone mechanism a small pressure. So the outlet section of the adjustable DP unit is significantly reduced, providing to fluid a greater resistance and introducing a smaller pressure drop. On the contrary, when higher flow-rate values are generated, fluid flows with a greater velocity and it has an increase outlet section to cross, so the resistance offered to flow decreases.

The pressure data obtained during the different testing days are comparable each others, as table in the appendix section report ; this means that every time the same test conditions have been replicated. Actually compared to the first pressure readings, the height of the support, where the shunting system was placed, has been improved in order that the pressure sensor downstream the valve could detected a lower pressure value, closer to the atmospheric pressure assumed as relative pressure.

Furthermore an error bar (Figure 4.15) has been constructed where pressure mean values and the corresponding standard deviations, calculated from the mean values of the differential pressure signals detected at each flow-rate during different days, have been plotted. This type of graph depicts the data variability: standard deviation explains how sample data (in this case the data of the differential pressure signals) are distributed compared to the average value. So it allows to determine if the average is reliable to significantly represent data.

For each average value, not excessively high values of the standard deviations have been obtained: these results mean that data are not so dispersed compared to the corresponding average values and that the error bars are coherent compared to the pressure values of the functioning range stated by the manufacturer; however other acquisitions of the pressure signals, a greater number of testing devices and repeatable testing conditions would be required in order to try to minimize this data variability.

Actually, only during the first two testing days, greater values of standard deviations have been achieved; these results could be due to the test rig and to the components placement compared to the shunting device.

The results of the experimental tests about the shunting system in a horizontal position confirm that the Miethke ProGAV 2.0 Adjustable Shunt System continues to work despite it was removed from a patient.

Discussion of the tests results obtained for the valve in a vertical position

When a shunted patient moves in an upright position, the difference in height, thus in pressure, between the CSF-filled space and the drainage site increases; this is due to the hydrostatic effect of the vertical length of the catheter from the ventricles to the drainage site. The physics within the abdominal cavity change because of the variation of the gravity direction and the zero level, where pressure is assumed equal to the atmospheric pressure, moves toward the diaphragm.

Thus, the height between the Foramen of Monro and this new reference level is approximately 30-40 cm but it depends on the shunted patient age and height.

In vertical position ICP becomes slightly negative and the increased difference in height corresponds to a hydrostatic pressure that will provoke the CSF's flow.

Because of this increased difference in height, an excessive, rapid and non-physiological CSF's flow from the ventricle system to the peritoneum occurs; a hydrostatic valve, like a gravitational device, is inserted in line with an existing shunting system in order to counterbalance the greater contribution provided by the hydrostatic pressure, to regulate the CSF's flow, whose average rate of production is assumed equal to around $20 \frac{ml}{h}$ and lastly, to preserve the negative pressure level within the brain.

In this orientation (Figure 5.6), the ICP is calculated as

$$ICP = P_{hydrostatic} - P_{opening\ of\ the\ valve} - IAP \quad (5.10)$$

The valve opening pressure, in vertical position, increases compared to the horizontal position and it is determined both by the opening pressure of the adjustable DP unit and by the opening pressure of the fixed gravitational unit. In this case the first is equal to 0 cmH₂O and the second is equal to 25 cmH₂O; so the totally opening pressure provided by the device in vertically is 25 cmH₂O.

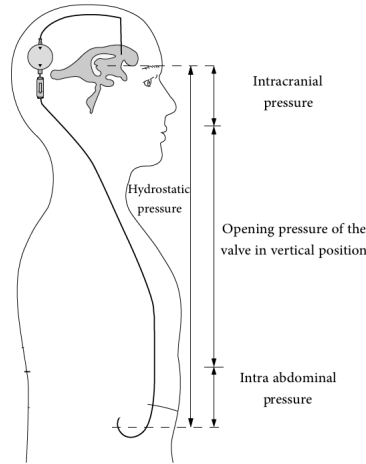


Figure 5.6: Pressures involved in the shunting system functioning when patient is in an upright position: $ICP = P_{Hydrostatic} - P_{opening\ of\ the\ valve} - IAP$. In this position, the shunted patient diaphragm is considered the reference level, where pressure is at the atmospheric pressure. The opening pressure of the shunt valve in this position is higher and it is determined by the opening pressure of the adjustable DP unit and the opening pressure of the fixed gravitational unit; when ICP exceeds the opening pressure, shunting system opens and allows CSF to flow [19]

The gravitational unit offers to fluid flow a higher resistance in order to prevent an excessive drainage of CSF compared to its rate of production, event known as “over-drainage”; this resistance is determined by the weight of the biggest ball that pushes the smallest sapphire ball into the valve seat with the aim to close the valve outlet section. In this position the gravitational unit opens and allows fluid to flow only when pressure difference exceeds the opening pressure of the valve. Instead, the valve will close and avoid the CSF’s flow when ICP is sufficiently negative to offset the hydrostatic pressure difference [40].

For the shunting device in vertical position, we performed only a qualitative tests without obtaining repeatable numerical results because some problems have emerged during the test bench implementation; we could not hydrodynamically characterize the device and obtain reliable pressure-flow characteristics. These tests only allowed to understand the functioning of the device, especially of the gravitational unit that acts only when patient moves from the supine position to an upright position.

A test rig (Figure 4.16) has been designed that replicates a simplified model of the shunting system.

For the test procedure we were inspired by the research study carried out by Freimann et al. [39]; they tested several type of hydrostatic valves including the Miethke shunt assistant that characterizes our testing device.

As mentioned in the chapter 4, we decided to replicate their same testing conditions and their same testing procedure despite we had a shunting system constituted both by an adjustable DP unit and a gravitational unit; we could replicate their tests because our adjustable DP unit is characterized by an opening pressure of 0 cmH₂O and offers to fluid flow the minimum resistance.

Through these tests we tried to simulate both the ICP increase, thus the conditions of high CSF's flow, and the siphoning effect, physiologically due to the physics variation within the abdominal cavity because of the change of the gravity direction.

The ICP variations have been simulated by adjusting the height of the source reservoir in relation to the device while, the IAP variation by adjusting the height of the drainage reservoir in relation to the device.

Graph represents four pressure-flow curves, obtained at four different levels of the outflow pressure simulating the siphoning effect, when the shunting device is vertically oriented.

The blue sample's curve has been obtained exploiting the flow-rate data calculated for an inflow pressure values of 0, 10, 20, 30 and 40 cmH₂O respectively, and for an outflow pressure value equal to 0 cmH₂O, kept unchanged. The device has been tested at an overall hydrostatic pressure equal to 0, 10, 20, 30 and 40 cmH₂O.

The orange sample's curve has been obtained exploiting the flow-rate data calculated for an inflow pressure values of 0, 10, 20, 30 and 40 cmH₂O respectively, and for an outflow pressure value equal to -10 cmH₂O, kept unchanged. In this case, the device has been tested at an overall hydrostatic pressure equal to 10, 20, 30, 40 and 50 cmH₂O. The other sample's curve have been obtained by defining the same inflow pressure values (0, 10, 20, 30 and 40 cmH₂O) and an outflow pressure of -20 cmH₂O for the yellow curve and an outflow pressure of -40 cmH₂O for the violet curve. Thus the testing device has undergone hydrostatic pressure equal to 20, 30, 40, 50, 60 cmH₂O and 40,50,60,70 and 80 cmH₂O respectively.

All the pressure-flow curves show a similar trend: the flow-rate across the device rises with increasing the difference in height between the reservoir upstream the device and the reservoir downstream the device, thus with increasing the pressure difference.

For this testing type, the defined pressure difference is the independent variable while the flow-rate is the dependent variable.

The flow measured in total, with the valve in vertical position, is in the range of 0-11.74 $\frac{mL}{min}$. Graph reports the mean values of the flow-rate, that it has been calculated three time for each difference in height set, and the corresponding standard deviations. We noted that standard deviations assume oscillating values; this means that, for certain differences in height defined between the two reservoirs, the testing conditions have not faithfully been replicated during the three consecutive measurements. For this reason, we decided to consider these tests as qualitative tests.

Figure 5.7 shows a comparison between our results and the results reported by the research article.

Despite the Miethke gravitational unit, tested by Freimann, is characterized by an opening pressure (20 cmH₂O) lower than the opening pressure of the unit included in our device (25 cmH₂O), the trend of the pressure-flow curves depicted in both graphs is comparable and very similar, thus flow-rate increases with increasing difference pressure; instead our numerical values obtained for the same pressure differences defined between the two reservoirs, are slightly lower. Additionally, compared to their procedure, we tested the shunting device also at an outflow pressure of -10 cmH₂.

Lower flow-rate values has been obtained probably because of the greater opening pressure of the our gravitational unit; a greater value means that the valve offers to fluid's flow a higher resistance so, on equal testing conditions, lower flow-rate values have been acquired. To obtain higher flow-rate values, a greater hydrostatic pressure should be defined.

When both the reservoir have been placed at the same level of the device ($\Delta H = 0\text{cm}$), no flow across the device has been detected because no force caused the fluid movement from the upepr region to the lower region. The same result has been obtained with an inflow pressure of 0 cmH₂O and an outflow pressure of -10 cmH₂O and for an inflow pressure of 10 cmH₂O and an outflow pressure of 0 cmH₂O.

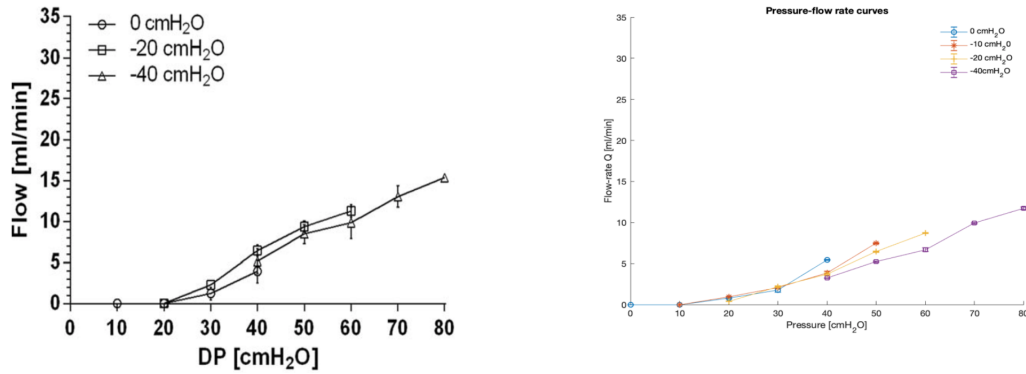


Figure 5.7: Comparison between the pressure-flow curves trend obtained by reference article and the qualitative pressure-flow curves trend obtained by testing the device in vertical position. Graphs show a comparable trend, but lower flow-rate value for the same differential pressures applied has been obtained.

Water began to flow when an overall hydrostatic pressure of 20 cmH₂O has been applied between the two reservoirs. Furthermore, the devices allowed fluid to flow toward the collection site even without inflow pressure but only with greater negative pressures that generate a greater siphoning effect, that sucks fluid if tubes are water-filled due to the gravity.

Additionally, the shunting device, especially the gravitational unit, provides a lower flow-rate to increasing of the siphoning effect and to decreasing inflow pressure: for the same overall hydrostatic pressure defined, obtained with different inflow and outflow pressure values, the resulting amount of fluid measured was lower for a greater outflow pressure and for a lower inflow pressure values than for a lower outflow pressure and for a greater inflow values. For example an overall hydrostatic pressure of 20 cmH₂O can be obtained through an inflow pressure of 0, 10 and 20 cmH₂O and for an outflow pressure of -20, -10 and 0 cmH₂O, respectively. For the first case, the measured flow-rate was equal to $1.737 \frac{ml}{min}$, for the second case $0.965 \frac{ml}{min}$ and for the last case $0.386 \frac{ml}{min}$.

This results could confirm the functioning of the gravitational unit: when lower pressure values upstream the device produces, gravitational unit responds reducing the increase fluid drainage due to siphoning, since it tries to counterbalance it.

Additionally some qualitative “semaphore tests” has been performed. Shunting device has been, firstly, tested by modifying the geodetic height of the drainage

reservoir at different levels, maintaining the source reservoir at the same level of the device. Subsequently, the device has been tested by modifying the geodetic height of the source reservoir, maintaining the drainage reservoir at the same level of the device (this testing condition is not physiological).

These tests highlight that gravitational unit closes when the position of the reservoir below the device produces a lower outflow pressure value; otherwise it remains open because gravity sucks the fluid. Furthermore, the device does not permit the fluid drainage also when the source reservoir has been placed below the device, in order to create a very negative inflow pressure.

Chapter 6

Conclusions and Future Works

A hydrodynamic study of the shunting system in horizontal position allowed to obtain the functioning range of the device, in terms of flow-pressure curve.

The resulting curve is characterized by a trend that similarly follows the curve trend of the functioning range provided by the manufacturer, despite slightly higher values have been obtained.

In this orientation, the Miethke proGAV 2.0 shunt system in-vitro tests revealed that it continues to work properly, despite it was removed from a patient and they did not highlight any type of problems or limitations.

In vertical position, criticality have emerged in the testing implementation; a qualitative study, in terms of pressure-flow curve, allowed to understand the functioning of the gravitational unit. For the testing procedure, reference was made to an in-vitro study, present in literature, about the performance and principles of some anti-siphoning devices. The resulting pressure-flow curves show a comparable trend with the curve trend reported in the research article, despite lower flow-rate values for the same differential pressure applied to the device, have been obtained. These qualitative tests revealed that the gravitational is strongly influenced by the differential pressure applied (hydrostatic pressure); additionally, they showed that the gravitational unit, with very negative inflow pressure or without outflow pressure, closes and does not allow fluid to flow, confirming its effective role in a shunting system.

Some problems have emerged during the bench test realization for testing the device in vertically, thus future works could consider the possibility to improve the bench test, required to hydrodynamically characterize the shunting device.

Figure 6.1 depicts an example of an in-vitro test bench [41] more complete, that allows to mimic the postural changes of a shunted patient in terms of trunk and head orientation. It is constituted by a reservoir upstream the device simulating the ICP level, a reservoir downstream the valve simulating the IAP level, a flow meter to measure flow-rate and some reclining supports (with specific lengths) that permit to change the valve orientation, with the aim to simulate a shunted patient in a supine (0°) and upright position (90°) and consequently to hydrodynamically characterize the shunting system in both the positions.

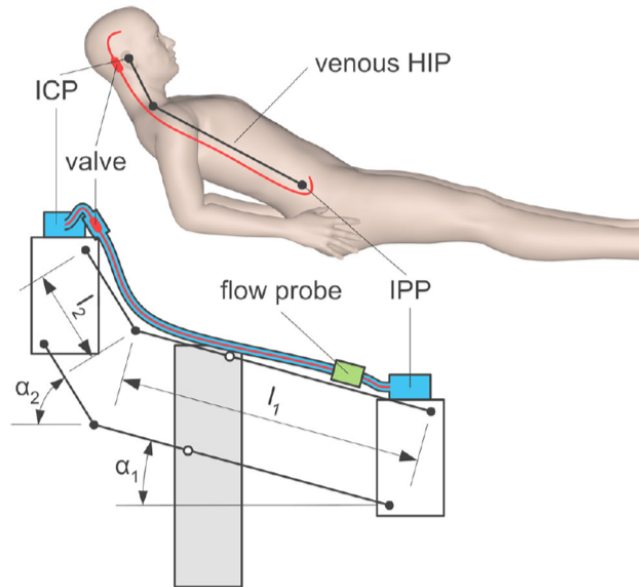


Figure 6.1: Schematic draw of a test bench to consider in future works, in order to improve the hydrodynamic characterization of the shunting device both in horizontal and vertical position.

In horizontally, test bench should position the source reservoir, the shunting system and the drainage reservoir at the same height, replicating the same testing conditions implemented in the test bench of this work; in vertical position it should rotate by 90° the valve, while maintaining the device at the same level of the source reservoir. In the last testing conditions a difference in height between the reservoir

above the device and the fluid collection point will create, simulating the hydrostatic pressure that develops in a shunted patient when he stands up and that causes the fluid drain.

This improved configuration would permit to study the effects of the gravitational devices on CSF dynamics and to obtain pressure-flow data more reliable, since all the elements can assume a specific height that keeps unchanged during the several testing procedure.

Finally, the improved test rig could be exploited to characterize both the shunting system at different opening pressure values of the adjustable DP unit (from 0 cmH₂O to 20 cmH₂O) and the single units (adjustable DP unit and fixed gravitational unit) of the device, separately.

The functioning range of the device, for each adjustment values, could be obtained and a more complete comparison between the resulting curve with the overall functioning range provided by the manufacturer could be performed.

Testing the shunting system, in particular the gravitational unit through a functional test, confirmed what has already been highlighted in some scientific articles: it is not enough to correctly choose a shunting system to ensure its functioning compared to the clinical specific case (clinically). Other factors play an important role about the device performance and, consequently, about the life quality of the patient: for example the periodic valve adjustments, the shunting system parameters, the physician experience, the clinical history of the patient, the interpretation of the clinical evidences and the interpretation of the results of the medical exams (MRI, CT, optical investigations etc.).

Actually the effective ICP's value depends on the device and its adjustments, but also on the valve pressure drop and the pressure drop across the distal and proximal catheters and on some patient physiological parameters, like the height, the state of health, the intra-abdominal pressure; in addition, some of these parameter cannot be changed by the neurosurgeon and they could not directly detected.

All of these considerations refer to the necessity, that kicked off this thesis work, of measuring in a continuous way and non-invasively the ICP value or other related parameters.

Appendix A

Numerical results of the shunting system test in a horizontal position

In this section the results of the experimental tests of the shunt system in a horizontal position, executed in different days, have been reported.

1° testing day								
Q [$\frac{ml}{h}$]	P _{mean} [cmH ₂ O]				Standard Deviation [cmH ₂ O]			
	1° cycle		2° cycle		1° cycle		2° cycle	
	↓ Q	↑ Q	↓ Q	↑ Q	↓ Q	↑ Q	↑ Q	↓ Q
50	4.7424	4.4854	4.6381	5.1954	0.0309	0.0309	0.0458	0.0768
40	4.5215	4.0861	4.3652	4.5722	0.0350	0.0346	0.0312	0.0706
30	4.1590	3.5019	3.8447	3.8897	0.0330	0.0318	0.0306	0.0381
20	3.8078	3.9628	3.4158	3.2847	0.0327	0.0377	0.0306	0.0474
10.44	3.2399	3.2399	2.8823	2.8823	0.0340	0.0340	0.0379	0.0379

Table A.1: Pressure mean values and standard deviations of the differential pressure signals detected at decreasing flow-rates (↓ Q) and increasing flow-rates (↑ Q) for each cycle respectively, during the first day

1° testing day								
	P_{\max} [cmH ₂ O]				P_{\min} [cmH ₂ O]			
	1° cycle		2° cycle		1° cycle		2° cycle	
Q [$\frac{ml}{h}$]	$\downarrow Q$	$\uparrow Q$	$\downarrow Q$	$\uparrow Q$	$\downarrow Q$	$\uparrow Q$	$\uparrow Q$	$\downarrow Q$
50	4.8464	4.6314	4.7991	5.3958	4.6593	4.3394	4.5319	4.9868
40	4.7321	4.1973	4.4614	4.7726	4.4085	3.9791	4.2901	4.3873
30	4.2929	3.6052	3.9475	4.0170	4.0796	3.4218	3.7674	3.7810
20	3.9061	4.0832	3.5451	3.4166	3.7240	3.8711	3.3199	3.1004
10.44	3.3430	3.3430	3.0087	3.0087	3.1397	3.1397	2.7884	2.7884

Table A.2: The maximum and the minimum pressure values of the differential pressure signals detected at decreasing flow-rates ($\downarrow Q$) and increasing flow-rates ($\uparrow Q$) for each cycle respectively, during the first day

Averaged pressure values 1° testing day				
Q [$\frac{ml}{h}$]	P_{mean} [cmH ₂ O]	Standard Deviation [cmH ₂ O]	P_{\max} [cmH ₂ O]	P_{\min} [cmH ₂ O]
10.44	3.0611	0.2065	3.1759	2.9641
20	3.6178	0.3198	3.7378	3.5039
30	3.8488	0.2697	3.9657	3.7625
40	4.3862	0.2186	4.5409	4.2662
50	4.7653	0.3055	4.9182	4.6293

Table A.3: Average and standard deviation of the mean values of the differential pressure for evaluating the functioning range of the shunt device, for the first day

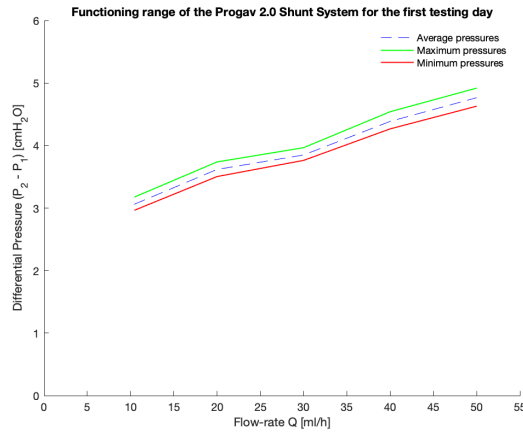


Figure A.1: Graph of the functioning range of the ProGav 2.0 Shunt System for the first testing day: it depicts the differential pressures mean values (blue dotted line), the differential pressures maximum values (red line) and the differential pressures minimum values (green line) for each flow-rate. Each value in the graph has been calculated as the average of the corresponding values obtained for each test in the test cycles.

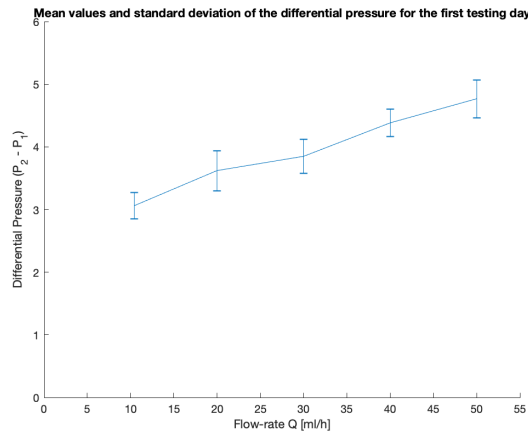


Figure A.2: Graph representing the differential pressure mean values and the corresponding standard deviations, calculated for each flow-rate, for the first day. Each value in the graph has been calculated as the average of the corresponding values obtained for each test in the test cycles.

2° testing day								
	P_{mean} [cmH ₂ O]				Standard Deviation [cmH ₂ O]			
	1° cycle		2° cycle		1° cycle		2° cycle	
Q [$\frac{\text{ml}}{\text{h}}$]	$\downarrow Q$	$\uparrow Q$	$\downarrow Q$	$\uparrow Q$	$\downarrow Q$	$\uparrow Q$	$\uparrow Q$	$\downarrow Q$
50	3.7106	4.4498	4.6141	6.0492	0.0335	0.0335	0.0487	0.0713
40	3.5216	3.9396	4.4180	5.5194	0.0308	0.066	0.0369	0.0739
30	3.2773	3.4263	4.0875	4.7227	0.0319	0.0456	0.036	0.0835
20	2.6316	2.9234	3.6952	3.7268	0.1179	0.0472	0.0381	0.0882
10.44	2.4395	2.4395	3.2714	3.2714	0.079	0.079	0.0651	0.0651

Table A.4: Pressure mean values and standard deviations of the differential pressure signals detected at decreasing flow-rates ($\downarrow Q$) and increasing flow-rates ($\uparrow Q$) for each cycle respectively, during the second day

2° testing day								
	P_{max} [cmH ₂ O]				P_{min} [cmH ₂ O]			
	1° cycle		2° cycle		1° cycle		2° cycle	
Q [$\frac{\text{ml}}{\text{h}}$]	$\downarrow Q$	$\uparrow Q$	$\downarrow Q$	$\uparrow Q$	$\downarrow Q$	$\uparrow Q$	$\uparrow Q$	$\downarrow Q$
50	3.8342	4.6738	4.8080	6.2087	3.6084	4.1148	4.4920	5.8394
40	3.6225	4.1241	4.5628	5.6906	3.4262	3.7759	4.3365	5.3505
30	3.3963	3.5506	4.2056	4.9319	3.1861	3.2983	4.0125	4.5049
20	2.8790	3.0478	3.8154	3.9103	2.3620	2.7810	3.5957	3.5009
10.44	2.6557	2.6557	3.4598	3.4598	2.2897	2.2897	3.124	3.124

Table A.5: The maximum and the minimum pressure values of the differential pressure signals detected at decreasing flow-rates ($\downarrow Q$) and increasing flow-rates ($\uparrow Q$) for each cycle respectively, during the second day

Averaged pressure values 2° testing day				
Q [$\frac{ml}{h}$]	P _{mean} [cmH ₂ O]	Standard Deviation [cmH ₂ O]	P _{max} [cmH ₂ O]	P _{min} [cmH ₂ O]
10.44	2.8554	0.4803	3.05775	2.7069
20	3.2443	0.5521	3.4131	3.0599
30	3.8784	0.6639	4.0211	3.7504
40	4.3497	0.8615	4.5	4.2223
50	4.7059	0.9779	4.8812	4.5137

Table A.6: Average and standard deviation of the mean values of the differential pressure for evaluating the functioning range of the shunt device, for second day

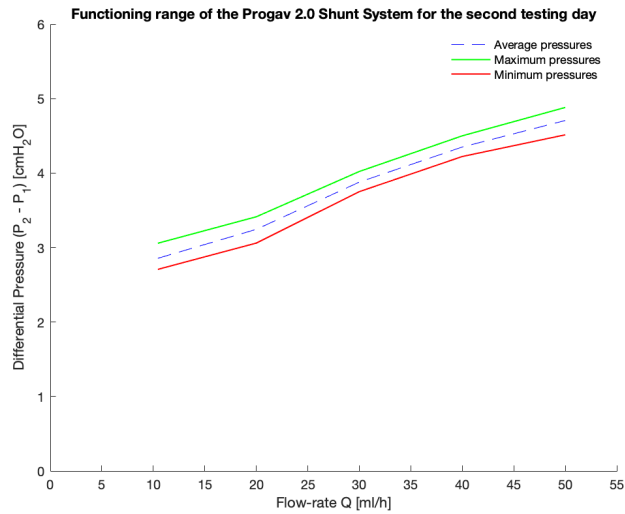


Figure A.3: Graph of the functioning range of the ProGav 2.0 Shunt System for the second day: it depicts the differential pressures mean values (blue dotted line), the differential pressures maximum values (red line) and the differential pressures minimum values (green line) for each flow-rate. Each value in the graph has been calculated as the average of the corresponding values obtained for each test in the test cycles.

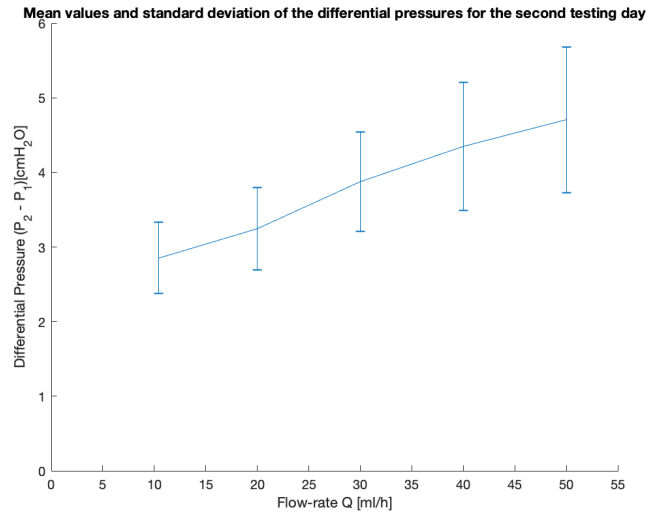


Figure A.4: Graph representing the differential pressure mean values and the corresponding standard deviations, calculated for each flow-rate, for the second day. Each value in the graph has been calculated as the average of the corresponding values obtained for each test in the test cycles.

3° testing day								
Q [$\frac{ml}{h}$]	P _{mean} [cmH ₂ O]				Standard Deviation [cmH ₂ O]			
	1° cycle		2° cycle		1° cycle		2° cycle	
	↓ Q	↑ Q	↓ Q	↑ Q	↓ Q	↑ Q	↑ Q	↓ Q
50	3.8974	3.9806	4.1878	3.9806	0.0354	0.0354	0.0692	0.0338
40	3.5739	3.6975	3.8406	3.6975	0.0347	0.0436	0.0571	0.0436
30	3.1560	3.3366	3.3356	3.5573	0.0390	0.1170	0.0473	0.117
20	2.8317	2.8608	2.9858	2.8172	0.0286	0.0492	0.0428	0.0492
10.44	2.5507	2.5507	2.6520	2.65207	0.0419	0.0419	0.0583	0.0583

Table A.7: Pressure mean values and standard deviations of the differential pressure signals detected at decreasing flow-rates (↓ Q) and increasing flow-rates (↑ Q) for each cycle respectively, during the third day

3° testing day								
	P _{max} [cmH ₂ O]				P _{min} [cmH ₂ O]			
	1° cycle		2° cycle		1° cycle		2° cycle	
Q [$\frac{ml}{h}$]	↓ Q	↑ Q	↓ Q	↑ Q	↓ Q	↑ Q	↑ Q	↓ Q
50	4.0299	4.1099	4.3898	4.1099	3.7922	3.8936	4.0187	4.0187
40	3.6755	3.8949	4.0060	3.8449	3.4636	3.5795	3.6865	3.6865
30	3.3745	3.4921	3.4921	3.8144	3.0560	3.2288	3.2288	3.2683
20	2.9302	2.9666	3.1285	2.9683	2.7591	2.7700	2.8910	2.8910
10.44	2.7095	2.7095	2.8331	2.8331	2.4510	2.4510	2.5454	2.5454

Table A.8: The maximum and the minimum pressure values of the differential pressure signals detected at decreasing flow-rates (↓ Q) and increasing flow-rates (↑ Q) for each cycle respectively, during the third day

Averaged pressure values 3° testing day				
Q [$\frac{ml}{h}$]	P _{mean} [cmH ₂ O]	Standard Deviation [cmH ₂ O]	P _{max} [cmH ₂ O]	P _{min} [cmH ₂ O]
10.44	2.6014	0.0585	2.7713	2.4982
20	2.8739	0.0768	2.9984	2.8278
30	3.3466	0.1642	3.5433	3.1955
40	3.7024	0.1090	3.8428	3.6040
50	4.0116	0.1238	4.1599	3.9308

Table A.9: Average and standard deviation of the mean values of the differential pressure for evaluating the functioning range of the shunt device, for the third day

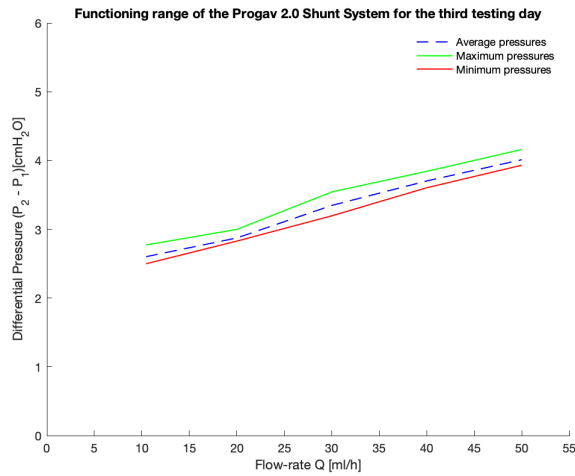


Figure A.5: Graph of the functioning range of the ProGav 2.0 Shunt System for the third day: it depicts the differential pressures mean values (blue dotted line), the differential pressures maximum values (red line) and the differential pressures minimum values (green line) for each flow-rate. Each value in the graph has been calculated as the average of the corresponding values obtained for each test in the test cycles.

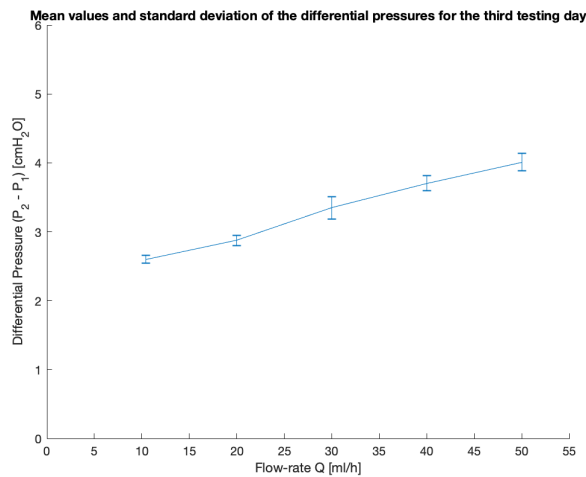


Figure A.6: Graph representing the differential pressure mean values and the corresponding standard deviations, calculated for each flow-rate, for the third day. Each value in the graph has been calculated as the average of the corresponding values obtained for each test in the test cycles.

4° testing day								
	P_{mean} [cmH ₂ O]				Standard Deviation [cmH ₂ O]			
	1° cycle		2° cycle		1° cycle		2° cycle	
Q [$\frac{\text{ml}}{\text{h}}$]	$\downarrow Q$	$\uparrow Q$	$\downarrow Q$	$\uparrow Q$	$\downarrow Q$	$\uparrow Q$	$\uparrow Q$	$\downarrow Q$
50	3.1119	3.3312	3.3719	3.3983	0.0251	0.0251	0.0271	0.0719
40	2.8460	2.8927	3.0388	2.9494	0.0273	0.0357	0.0314	0.0956
30	2.5148	2.4992	2.6983	2.5424	0.0254	0.0286	0.0322	0.0543
20	2.1993	2.0866	2.2475	2.1821	0.0373	0.0245	0.0324	0.0439
10.44	1.8615	1.8615	1.9689	1.9689	0.0328	0.0328	0.0510	0.0510

Table A.10: Pressure mean values and standard deviations of the differential pressure signals detected at decreasing flow-rates ($\downarrow Q$) and increasing flow-rates ($\uparrow Q$) for each cycle respectively, during the fourth day

4° testing day								
	P_{max} [cmH ₂ O]				P_{min} [cmH ₂ O]			
	1° cycle		2° cycle		1° cycle		2° cycle	
Q [$\frac{\text{ml}}{\text{h}}$]	$\downarrow Q$	$\uparrow Q$	$\downarrow Q$	$\uparrow Q$	$\downarrow Q$	$\uparrow Q$	$\uparrow Q$	$\downarrow Q$
50	3.2021	3.4451	3.4646	3.5555	3.0446	3.2013	3.2803	3.2123
40	2.9446	3.0048	3.1543	3.1302	2.7745	2.8023	2.9470	2.7146
30	2.6859	2.5914	2.8077	2.6719	2.4375	2.4091	2.6132	2.3807
20	2.3255	2.1626	2.3612	2.3145	2.1144	2.0134	2.1649	2.0566
10.44	1.9594	1.9594	2.1316	2.1316	1.7743	1.7743	1.8599	1.8599

Table A.11: The maximum and the minimum pressure values of the differential pressure signals detected at decreasing flow-rates ($\downarrow Q$) and increasing flow-rates ($\uparrow Q$) for each cycle respectively, during the fourth day

Averaged pressure values 4° testing day				
Q [$\frac{ml}{h}$]	P _{mean} [cmH ₂ O]	Standard Deviation [cmH ₂ O]	P _{max} [cmH ₂ O]	P _{min} [cmH ₂ O]
10.44	1.9152	0.062	2.0455	1.8171
20	2.1794	0.0665	2.2909	2.0873
30	2.5637	0.0915	2.6892	2.4601
40	2.9317	0.083	3.0585	2.8096
50	3.3033	0.1360	3.4168	3.1846

Table A.12: Average and standard deviation of the mean values of the differential pressure for evaluating the functioning range of the shunt device, for the fourth day

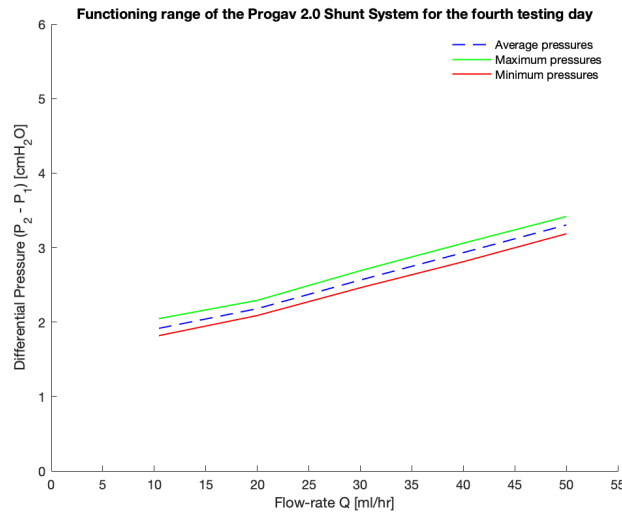


Figure A.7: Graph of the functioning range of the ProGav 2.0 Shunt System for the fourth day: it depicts the differential pressures mean values (blue dotted line), the differential pressures maximum values (red line) and the differential pressures minimum values (green line) for each flow-rate. Each value in the graph has been calculated as the average of the corresponding values obtained for each test in the test cycles.

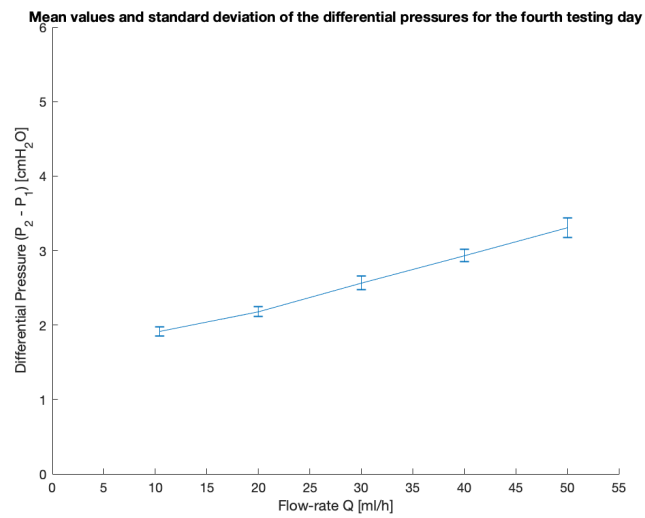


Figure A.8: Graph representing the differential pressure mean values and the corresponding standard deviations, calculated for each flow-rate, for the fourth day. Each value in the graph has been calculated as the average of the corresponding values obtained for each test in the test cycles.

Bibliography

- [1] C Logan et al. “Arachnoid cysts-common and uncommon clinical presentations and radiological features”. In: *Journal of neuroimaging in psychiatry & neurology* 1.2 (2016), pp. 79–84.
- [2] National Organization for Rare Disorders (NORD) 55 Kenosia Avenue Danbury. *Arachnoid Cysts Information Page*. URL: <https://www.ninds.nih.gov/Disorders/All-Disorders/Arachnoid-Cysts-Information-Page>.
- [3] Fatima Mustansir, Sanaullah Bashir, and Aneela Darbar. “Management of Arachnoid Cysts: A Comprehensive Review”. In: *Cureus* 10.4 (2018).
- [4] Hiroji Miyake. “Shunt devices for the treatment of adult hydrocephalus: recent progress and characteristics”. In: *Neurologia medico-chirurgica* 56.5 (2016), pp. 274–283.
- [5] Lina Momani, Abdel Rahman Alkharabsheh, and Waleed Al-Nuaimy. “Intelligent and Personalised Hydrocephalus Treatment and Management”. In: *Biomedical Engineering*. InTech, 2009.
- [6] Wajd N Al-Holou et al. “Prevalence and natural history of arachnoid cysts in adults”. In: *Journal of neurosurgery* 118.2 (2013), pp. 222–231.
- [7] Jeremy C Wang, Linda Heier, and Mark M Souweidane. “Advances in the endoscopic management of suprasellar arachnoid cysts in children”. In: *Journal of Neurosurgery: Pediatrics* 100.5 (2004), pp. 418–426.
- [8] FDA. *Cerebral Spinal Fluid (CSF) Shunt Systems*. <https://www.fda.gov/medical-devices/implants-and-prosthetics/cerebral-spinal-fluid-csf-shunt-systems>. [Online; accessed 09-July-2019]. 2018.

- [9] Garrett J. Soler et al. “A Review of Cerebral Shunts, Current Technologies, and Future Endeavors”. In: *The Yale Journal of Biology and Medicine* 91 (Sept. 2018), pp. 313–321.
- [10] Barry R Lutz, Pranav Venkataraman, and Samuel R Browd. “New and improved ways to treat hydrocephalus: pursuit of a smart shunt”. In: *Surgical neurology international* 4.Suppl 1 (2013), S38.
- [11] Hydrocephalus Association. *Fact Sheet: Shunt Systems for the Management of Hydrocephalus*. <https://www.hydroassoc.org/factsheets/>. [Online; accessed 09-July-2019]. 2012.
- [12] A Chakraborty, J Drake, and B Warf. *Methods for Cerebrospinal Fluid Diversion in Pediatric Hydrocephalus: From Shunt to Scope*. July 2016. URL: <https://neupsykey.com/methods-for-cerebrospinal-fluid-diversion-in-pediatric-hydrocephalus-from-shunt-to-scope/>.
- [13] G Smith et al. “Shunt Devices for Neurointensivists: Complications and Management”. In: *Neurocritical care* 27.2 (2017), pp. 265–275.
- [14] Su-Ho Kim et al. “Shunt Overdrainage Caused by Displacement of the Pressure Control Cam after Pressure Adjustment”. In: *Korean journal of neurotrauma* 12.2 (2016), pp. 163–166.
- [15] SS Lollis et al. “Programmable CSF shunt valves: radiographic identification and interpretation”. In: *American journal of neuroradiology* 31.7 (2010), pp. 1343–1346.
- [16] Integra LifeSciences Corporation. *Codman Hakim Programmable Valve System for Hydrocephalus*. <https://www.integralife.com/file/general/1533585515.pdf>. [Online; accessed 09-July-2019]. 2018.
- [17] Hashimoto Masaaki, MukaiI Hironobu, and Tsukada Toshiyuki. *Using the Codman Hakim Programmable Valve with SiphonGuard*. 2004. Sept. 2004.
- [18] Marek Czosnyka and Zofia H Czosnyka. “Overdrainage of cerebrospinal fluid and hydrocephalus shunts”. In: *Acta neurochirurgica* 159.8 (2017), pp. 1387–1388.

- [19] Christoph Miethke GMBH and CO.KG. *ProGav 2.0 Instruction Use*. https://www.miethke.com/fileadmin/user_upload/Produkte/Downloads/proGAV2.0/Gebrauchsanweisung___Instruction_for_use.pdf. [Online; accessed 09-July-2019].
- [20] Sait Ozturk et al. “Smartphones and Programmable Shunts: Are These Indispensable Phones Safe and Smart?” In: *World neurosurgery* 102 (2017), pp. 518–525.
- [21] Satoshi Utsuki et al. “Alteration of the pressure setting of a Codman-Hakim programmable valve by a television”. In: *Neurologia medico-chirurgica* 46.8 (2006), pp. 405–407.
- [22] Ali Nawaz Khan. *Arachnoid Cyst Imaging: Overview, Radiography, Computed Tomography*. URL: <https://emedicine.medscape.com/article/336489-overview>.
- [23] Bahram Mokri. “The Monroe–Kellie hypothesis: applications in CSF volume depletion”. In: *Neurology* 56.12 (2001), pp. 1746–1748.
- [24] W David Freeman. “Management of intracranial pressure”. In: *CONTINUUM: Lifelong Learning in Neurology* 21.5, Neurocritical Care (2015), pp. 1299–1323.
- [25] Chiara Robba. *Chapter 1 - Intracranial Pressure Monitoring*. Ed. by Heman-shu Prabhakar. 2018. URL: <http://www.sciencedirect.com/science/article/pii/B9780128099155000012>.
- [26] Mary Abraham and Vasudha Singhal. “Intracranial pressure monitoring”. In: *Journal of Neuroanaesthesiology and Critical Care* 2.03 (2015), pp. 193–203.
- [27] Maya Harary, Rianne Dolmans, and William Gormley. “Intracranial pressure monitoring—review and avenues for development”. In: *Sensors* 18.2 (2018), p. 465.
- [28] Xuan Zhang et al. “Invasive and noninvasive means of measuring intracranial pressure: a review”. In: *Physiological measurement* 38.8 (2017), R143.
- [29] M Gelabert-Gonzalez et al. “The Camino intracranial pressure device in clinical practice. Assessment in a 1000 cases”. In: *Acta neurochirurgica* 148.4 (2006), pp. 435–441.

- [30] Sebastian Antes et al. “Telemetric intracranial pressure monitoring with the Raumedic Neurovent P-tel”. In: *World neurosurgery* 91 (2016), pp. 133–148.
- [31] Sebastian Antes et al. “Intracranial Pressure–Guided Shunt Valve Adjustments with the Miethke Sensor Reservoir”. In: *World neurosurgery* 109 (2018), e642–e650.
- [32] Matthew Murray and Jared Shimada. “Intracranial Pressure Sensor”. In: *Bio-engineering Senior Theses* (2016). URL: https://scholarcommons.scu.edu/bioe_senior/46.
- [33] David D Limbrick et al. “The baric probe: a novel long-term implantable intracranial pressure monitor with ultrasound-based interrogation”. In: *Journal of Neurosurgery: Pediatrics* 10.6 (2012), pp. 518–524.
- [34] SC Mitchell et al. “Snap-valve cerebral shunt design for intracranial pressure operation and ultrasound visualization”. In: *Medical engineering & physics* (Apr. 2019).
- [35] József Klespitz and Levente Kovács. “Peristaltic pumps—A review on working and control possibilities”. In: *2014 IEEE 12th International Symposium on Applied Machine Intelligence and Informatics (SAMII)*. IEEE. 2014, pp. 191–194.
- [36] D Ninarello and L. Menna. *Design and development of an experimental system for the characterization of biological tissue and scaffold’s permeability, for regenerative medicine*. 2019.
- [37] Anthony J Wheeler and Ahmad Reza Ganji. *Introduction to engineering experimentation*. Prentice Hall New Jersey, 1996.
- [38] ISO 7197:1997. *Neurosurgical implants — Sterile, single-use hydrocephalus shunts and components*. Tech. rep. International Organization for Standardization, 1997.
- [39] Florian Baptist Freimann et al. “In vitro performance and principles of anti-siphoning devices”. In: *Acta neurochirurgica* 156.11 (2014), pp. 2191–2199.

- [40] Paul H Chapman, Eric R Cosman, and Michael A Arnold. “The relationship between ventricular fluid pressure and body position in normal subjects and subjects with shunts: a telemetric study”. In: *Neurosurgery* 26.2 (1990), pp. 181–189.
- [41] Manuel Gehlen et al. “Comparison of anti-siphon devices—how do they affect CSF dynamics in supine and upright posture?”. In: *Acta neurochirurgica* 159.8 (2017), pp. 1389–1397.
- [42] ASTM F 647-94(reapproved 2014). *Standard Practice for Evaluating and Specifying Implantable Shunt Assemblies for Neurosurgical Application*. Tech. rep. ASTM, 2014.
- [43] Marek Czosnyka and John D Pickard. “Monitoring and interpretation of intracranial pressure”. In: *Journal of Neurology, Neurosurgery & Psychiatry* 75.6 (2004), pp. 813–821.
- [44] Yurdal Serarslan et al. “Use of programmable versus nonprogrammable shunts in the management of normal pressure hydrocephalus: A multicenter retrospective study with cost–benefit analysis in Turkey”. In: *Medicine* 96.39 (2017).
- [45] Matheus Fernandes de Oliveira, Renan Muralho Pereira, and Fernando Gomes Pinto. “Updating technology of shunt valves”. In: *MedicalExpress* 1.4 (2014), pp. 166–169.
- [46] Antonino Germanò et al. “The treatment of large supratentorial arachnoid cysts in infants with cyst-peritoneal shunting and Hakim programmable valve”. In: *Child’s Nervous System* 19.3 (2003), pp. 166–173.
- [47] Garrett J Soler et al. “Focus: Medical Technology: A Review of Cerebral Shunts, Current Technologies, and Future Endeavors”. In: *The Yale Journal of Biology and Medicine* 91.3 (2018), p. 313.
- [48] Sophie Taillibert, Emilie Le Rhun, and Marc C Chamberlain. “Intracranial cystic lesions: a review”. In: *Current neurology and neuroscience reports* 14.9 (2014), p. 481.
- [49] Mahjouba Boutarbouch et al. “Management of intracranial arachnoid cysts: institutional experience with initial 32 cases and review of the literature”. In: *Clinical neurology and neurosurgery* 110.1 (2008), pp. 1–7.

BIBLIOGRAPHY

- [50] J-U Choi, Dong-Seok Kim, and Ryoong Huh. “Endoscopic approach to arachnoid cyst”. In: *Child’s Nervous System* 15.6-7 (1999), pp. 285–291.